surface fluxes
and boundary layer scaling

models and applications

Promotor   : dr.ir. L. Wartena,
              hoogleraar in de landbouwweerkunde
              en de omgevingsnatuurkunde

Co-promotor: dr. H.A.R. de Bruin,
              universitair hoofddocent

STELLINGEN

1. In een belangrijk deel van de stabiele grenslaag kunnen wind- en temperatuurprofielen beschreven worden met gelijkvormigheidsparameters van de oppervlaktelaag.

   (Dit proefschrift)

2. In de Pasquill-classificatie van de stabiliteit van de atmosferische oppervlaktelaag wordt impliciet een vochtigheidstoestand van het aardoppervlak aangenomen.

3. Het schatten van de verdamping overdag van begroeide landoppervlakten kan vaak geschieden zonder expliciet het vochtdeficit van de lucht in rekening te brengen.

   (H.A.R. de Bruin, A.A.M. Holtslag, J. Appl. Meteor., 21, 1982, 1610-1621 en H.A.R. de Bruin, J. Clim. Appl. Meteor., 22, 1983, 572-578)

4. De jaarlijkse energieopbrengst van grote windmolens met een ashoogte van 30 m of meer, wordt aanzienlijk onderschat wanneer men hiervoor de windsnelheid op 10 m hoogte extrapoleert met het logaritmisch windprofiel.

   (A.J.M. van Wijk, A.A.M. Holtslag, W.C. Turkenburg, Proceedings European Wind Energy Conference and Exhibition, Hamburg, 22-26 Oct. 1984)

5. In stedelijke gebieden voldoen concentraties van zwaveldioxide per windrichtingssector goed aan een lognormale frequentieverdeling.

   (G.J. Cats, A.A.M. Holtslag, Atmospheric Environment 14, 1980, 255-258)

6. De kwaliteit van de weersverwachting is in de afgelopen vijftien jaar niet alleen voor de middellange termijn significant verbeterd, maar ook voor de verwachting van 18 tot 30 uur vooruit.

   (Gebaseerd op een tijdreeksanalyse van recente "prestatie-indices" in combinatie met gegevens van H. Daan, Proceedings 9th AMS Conference on Weather Forecasting and Analysis, 1982, 166-168)

7. Korte termijn verwachtingen van grenslaagbewolking en mist zijn
    voor Nederland van groot belang. Voor de modelmatige beschrijving
    hiervan biedt een "luchtmassatransformatiemodel" goede perspec-
    tieven.

        (J. Reiff, A.G.M. Driedonks, A.A.M. Holtslag, KNMI weten-
        schappelijk rapport WR 86-4, 1986)

8. Toegang tot de academische promotie dient niet in eerste
    instantie op vooropleiding gebaseerd te zijn, maar op de
    bekwaamheid van de promovendus in het verrichten van zelfstandig
    wetenschappelijk onderzoek.

9. De betekenis van vormgeving voor wetenschappelijke publikaties
    wordt vaak onderschat.

10. Om het conflict tussen spelende kinderen en automobilisten niet
    onnodig te verscherpen verdient het aanbeveling de toegangswegen
    tot woonerven niet te asfalteren.

11. De kleuren van het meubilair in overheidsgebouwen kunnen vaak als
    al te grijs worden aangemerkt.

12. Op het platteland leidt het mestoverschot tot verzuring van de
    bodem, terwijl in de stad de mens dreigt te verzuren door een
    soortgelijk overschot op de stoep.

Stellingen behorend bij het proefschrift:
Surface fluxes and boundary layer scaling;
models and applications.
A.A.M. Holtslag, 16 juni 1987.

ISN 488137

a.a.m. holtslag

surface fluxes
and boundary layer scaling

models and applications

ISN 488137

CONTENTS   PAGE

CONTENTS (Continued)   PAGE

VOORWOORD

Zonder steun en hulp van anderen was dit proefschrift niet tot stand gekomen. Daarvoor wil ik graag alle betrokkenen bedanken.

In de eerste plaats bedank ik het KNMI voor de mogelijkheden die ik heb gekregen, om mijn onderzoek van de afgelopen jaren in deze vorm te presenteren. Daarbij bedank ik met name Aad van Ulden, Fons Baede en Henk Tennekes voor de speelruimte die zij mij gaven.

Mijn promotor, Bert Wartena, wil ik vooral bedanken voor zijn stimulerende rol en zijn van meet af aan grote vertrouwen in mijn capaciteiten om deze klus te klaren. Bert, ik hoop dat we ook hierna nog menig "achterhoeks" woordje kunnen spreken.

Mijn co-promotor, Henk de Bruin, wil ik graag bedanken voor zijn kritische begeleiding en zijn kennisoverdracht van de "energiebalans". Henk, bedankt voor alle tijd die je aan mijn verhalen hebt besteed en de vele discussies daaromtrent. Ook stel ik het op prijs dat we samen hoofdstuk IV opsturen als publikatie, na ons vorige artikel dat in jouw proefschrift verscheen.

Frans Nieuwstadt en Aad van Ulden, mede-auteurs van artikelen waarop respectievelijk hoofdstuk II en III gebaseerd zijn, ben ik erkentelijk voor hun bijdragen en stimulerende discussies.

I would also like to thank Sven-Erik Gryning, John Irwin and Bjarne Sivertsen for their co-operation in a working group on a "meteorological preprocessor for air pollution dispersion models", and their permission to adopt our article as chapter VI of this thesis. The draft of this chapter has been written during my stay at Risø National Laboratory in Denmark during the summer of 1985, for which Risø is gratefully acknowledged.

Verder ben ik mijn collega's zeer erkentelijk voor de vele discussies, suggesties en voor de prettige samenwerking. Naast bovengenoemden denk ik daarbij met name aan Anton Beljaars, Fred Bosveld, Han van Dop, Ad Driedonks, Peter Duynkerke, Hans Reiff, Wouter Slob, Stephen Tjemkes, Herman Wessels en Joan Wieringa.

In een groot gedeelte van mijn werk heb ik gebruik gemaakt van metingen te Cabauw, zonder zelf hierin bij te dragen. Ik dank alle medewerkers van het KNMI die hierbij wel betrokken zijn geweest.

Daarnaast wil ik graag de medewerkers van de bibliotheek bedanken voor hun prettige medewerking en adviezen.

Tot slot ben ik bij de grafische vormgeving van dit rapport veel dank verschuldigd aan mijn vriendin Monique Roest voor haar adviezen en omslagontwerp, aan Birgit Kok voor haar snelle en perfecte typewerk, aan Cees van Stralen voor het maken van de vele tekeningen, en aan de heer Wittebol met zijn medewerkers van de drukkerij voor hun enthousiaste medewerking.

Allen van harte bedankt!

Bert Holtslag

SAMENVATTING

Deze studie behandelt enkele aspecten van de atmosferische grenslaag. Deze laag wordt gedefinieerd als de onderste laag van de atmosfeer, waarin interaktie met het aardoppervlak plaatsvindt. De interaktie geschiedt voornamelijk door turbulente (wervelende) bewegingen. Deze wervelingen transporteren warmte, waterdamp en impuls tussen het aardoppervlak en de zogenaamde vrije atmosfeer.

Het doel van deze studie is het beschrijven van de grenslaag voor praktische toepassingen. In het bijzonder komen hierbij de oppervlaktefluxen van warmte, waterdamp en impuls aan de orde. Dit geschiedt in samenhang met de temperatuur- en windprofielen in de grenslaag. Tevens wordt een methode gepresenteerd voor het beschrijven van de verspreiding van luchtverontreiniging in de grenslaag.

In hoofdstuk I wordt de doelstelling van deze studie nader uitgewerkt. Daarbij wordt achtergrondinformatie gegeven over de oppervlaktefluxen en de grenslaaghoogte. Daarnaast wordt besproken hoe deze grootheden samenhangen met de energiehuishouding van het aardoppervlak. De belangrijkste componenten van de energiebalans komen aan de orde. Ten gevolge van de dagelijkse opwarming en de nachtelijke afkoeling van het aardoppervlak boven land, vertonen de componenten in de energiehuishouding een sterke variatie binnen een etmaal. Door deze dagelijkse gang blijkt ook de grenslaaghoogte sterk te variëren. Dit wordt in hoofdstuk I geïllustreerd voor een heldere zomerse dag.

In hoofdstuk II wordt een overzicht gegeven van een methode waarmee turbulente grootheden in de grenslaag beschreven kunnen worden. Deze methode staat bekend als "schaling". Bij het schalen van turbulente grootheden, worden deze met enkele karakteristieke parameters gecombineerd in dimensieloze groepen. Vervolgens worden vanuit theoretisch en experimenteel oogpunt, relaties gezocht tussen de dimensieloze groepen. Zulke relaties blijken onder bepaalde voorwaarden een universele geldigheid te hebben. Dit noemt men gelijkvormigheid.

In de atmosferische grenslaag kan men verschillende gebieden definiëren, waarvoor specifieke gelijkvormigheidsrelaties blijken te gelden. In hoofdstuk II worden deze gebieden geïllustreerd aan de

hand van diagrammen. Tevens worden de karakteristieke parameters voor
elk van de gebieden genoemd. Het blijkt dat de oppervlaktefluxen van
warmte en impuls, de grenslaaghoogte en de afstand tot het oppervlak
behoren tot de karakteristieke parameters.

Voor het praktisch toepassen van schaling zijn de oppervlakte-
fluxen dus van groot belang. Bovendien hangt de grenslaaghoogte sterk
samen met de oppervlaktefluxen. In het algemeen zijn de oppervlakte-
fluxen echter niet beschikbaar. Dit betekent dat de fluxen geparame-
triseerd moeten worden, dat wil zeggen uitgedrukt in bekende groot-
heden. In deze studie gaan we uit van routinematig beschikbare weer-
gegevens, zoals bedekkingsgraad van bewolking, luchttemperatuur en
specifieke vochtigheid op 2 m hoogte en de windsnelheid op 10 m
hoogte.

In de hoofdstukken III en IV worden schema's ontwikkeld voor de
bepaling van de oppervlaktefluxen uit de genoemde weergegevens. Hier-
voor worden uurlijkse parametrizaties ontwikkeld en getoetst aan
waarnemingen. Als zodanig komen alle belangrijke grootheden van de
stralings- en energiehuishouding van het aardoppervlak aan de orde.
In hoofdstuk III wordt het schema voor overdag behandeld, terwijl
hoofdstuk IV over het schema voor de nacht handelt. Dit laatste
schema wordt bovendien toegepast voor het bepalen van het tempera-
tuurprofiel in de stabiele grenslaag tot 80 m hoogte.

In hoofdstuk V worden de windprofielen te Cabauw tot 200 m hoogte
geanalyseerd, waarbij gebruik gemaakt wordt van schalingsresultaten
voor het beschrijven van de observaties. Bovendien wordt een uitbrei-
ding van de gangbare theorie voor zeer stabiele situaties onderzocht.
Ook wordt een analyse gegeven van het windrichtingsprofiel.

In hoofdstuk V wordt tevens gebruik gemaakt van de resultaten van
de hoofdstukken III en IV om het windprofiel tot 200 m hoogte te
schatten uit routinematige weergegevens. Deze schattingen komen goed
overeen met de direkte observaties. Toepassingen voor windenergie-
doeleinden komen aan de orde, zoals de simulatie van de frekwentie-
verdeling en de dagelijkse gang van de wind op 80 m hoogte.

Tot slot wordt in hoofdstuk VI een methode behandeld voor het
berekenen van de verspreiding van luchtverontreiniging in de grens-
laag. De methode bestaat uit een kombinatie van schalingstechnieken

voor de verschillende gebieden van de grenslaag, zoals die in hoofd-
stuk II worden besproken. Hierbij wordt de verspreiding van lucht-
verontreiniging direkt gekoppeld aan de turbulente toestand van de
atmosferische grenslaag.

Met behulp van de modellen van hoofdstuk VI kan men de grond-
concentratie berekenen ten gevolge van verontreinigingen uit een
continue puntbron (zoals een schoorsteen). De berekeningen worden
vergeleken met onafhankelijke waarnemingen uit de literatuur. Het
blijkt dat de berekeningen beter overeenkomen met de waarnemingen dan
de berekeningen met behulp van het praktisch veel gebruikte Gaussi-
sche pluimmodel.

In de verschillende hoofdstukken komen de toepassingen van de
modellen, methoden en parametrizaties aan de orde. In het algemeen
zijn de uitkomsten van deze studie van belang voor verschillende
toepassingen in de meteorologie en de hydrologie. Daarnaast zijn de
methoden van belang voor het schatten van windenergiemogelijkheden en
studies naar de verspreiding van luchtverontreiniging in de
grenslaag.

ABSTRACT

This study deals with applied modelling of some Atmospheric Boundary
Layer (ABL) features. We use scaling techniques for the description
of the turbulent structure in the ABL. A review is given on the dif-
ferent properties of the scaling techniques in stable and unstable
conditions. The essential role of the surface fluxes of heat and
momentum for the structure in the ABL is discussed.

Schemes are proposed for the estimation of the surface fluxes
from routine weather data over land. Both for day- and nighttime,
hourly values of the surface fluxes are modelled with the aid of the
surface radiation and energy balance. Models and parameterizations
for the individual components of these balances are compared with ob-
servations. During nighttime also the temperature profile up to 80 m
is simulated with the modelled surface fluxes. The output of the sur-
face flux schemes can be used for stability determination of the ABL.

Subsequently, diabatic wind profiles along the 200 m Cabauw tower
are analysed in terms of surface layer similarity. For stable condi-
tions an extension of the profile functions to strong stability is
evaluated. Besides, the turning of wind with height up to 200 m is
analysed. Together with the flux schemes, the wind speed profile can
be estimated from near surface weather data only. It is shown that
the agreement between estimates and observations is very good up to
at least ~100 m in generally level terrain. The methods are applied
to simulate the wind frequency distribution and the reversed diurnal
variation of the wind at 80 m.

Finally, a method for calculating the dispersion of non-buoyant
plumes in the ABL is presented. The method is based on the scaling
techniques of the ABL. Models are suggested for ground level con-
centrations of pollutants dispersed from continuous point sources.
These models are evaluated with independent tracer experiments over
land. The overall agreement between observations and predictions is
very good and shown to be better than the skill of the traditional
Gaussian plume model.

The proposed models and methods are intended for applications in
meteorology and hydrology, for wind energy assessment methods and for
air pollution dispersion studies.

Chapter I

GENERAL INTRODUCTION

1. Purpose and background

In this study we are dealing with some aspects of the Atmospheric
Boundary Layer (ABL). This layer can be defined as the lower region
of the atmosphere, which interacts with the earth's surface. As such
the ABL is dominated by the vertical transports of sensible heat,
humidity and momentum. These transports, between the surface and the
overlying (so-called) free atmosphere, are mainly characterized by
turbulence. For that reason, the surface fluxes[*] of heat and momentum
are of major importance for the description of turbulence in the ABL.

In the past decades much research has been done on the turbulent
structure of the ABL. It appears that often the structure can be des-
cribed with only a few characteristic parameters. These parameters
can be identified from the governing equations or by inspection of
the physics. It is practice to combine the characteristic parameters
with the relevant physical quantities into a reduced number of dimen-
sionless quantities. This approach is generally known as dimensional
analysis, but with respect to turbulence in the ABL it is often re-
ferred to as "Scaling".

Scaling of the ABL leads to similarity predictions of non-
dimensionalized quantities. A well-known result is the logarithmic
wind profile, which has been found to satisfy observations in the
lower atmosphere up to 100 m or more under certain conditions (see
chapter V).

The purpose of the present study is to use scaling of the ABL for
practical applications. In particular, we are dealing with the sur-
face fluxes of heat and momentum, the profiles of wind and tempera-
ture and the dispersion of air pollution in the ABL. As such we will

---

[*]In this study we use flux as a short for flux density, which denotes
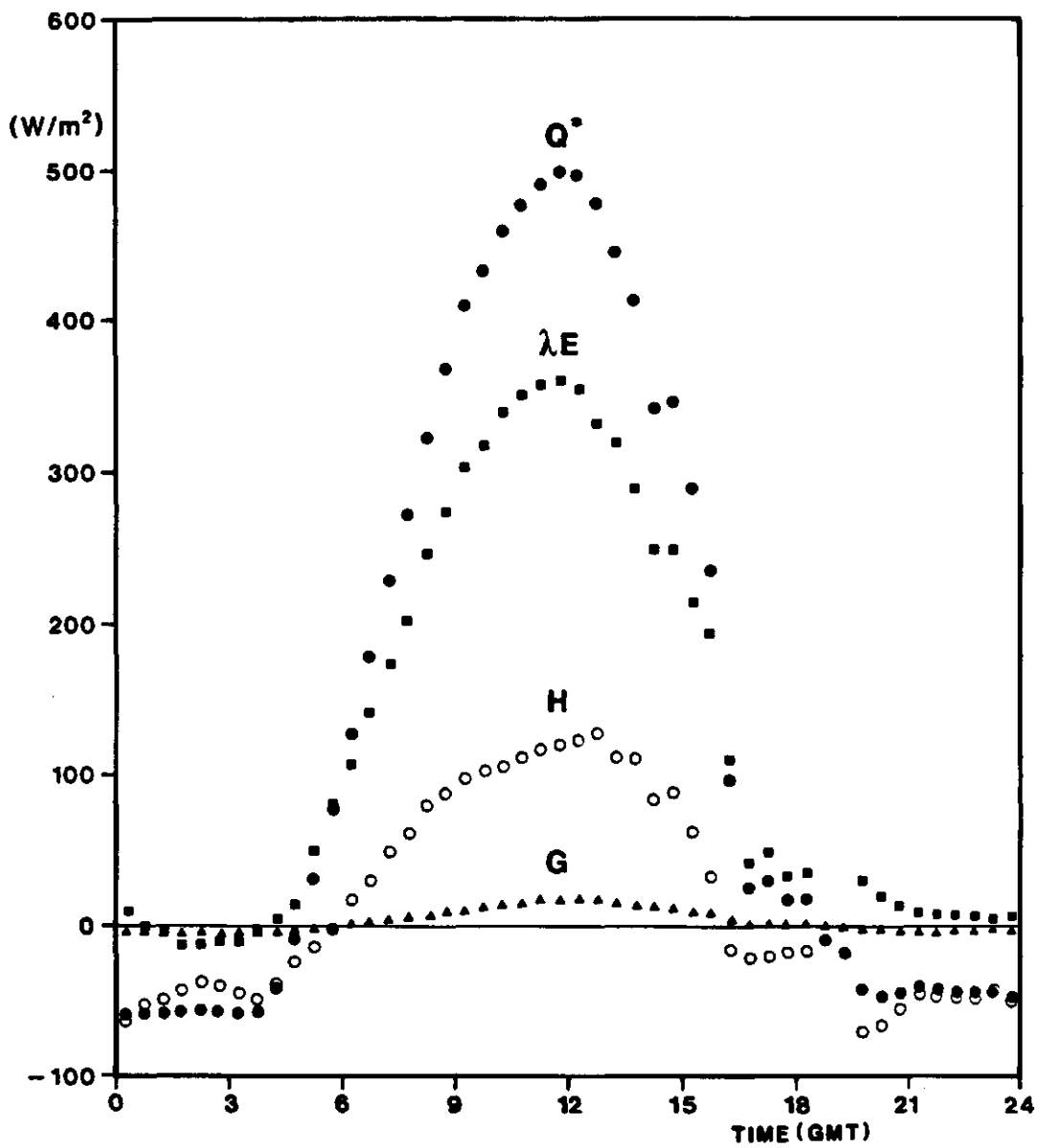the transport of a quantity per unit time and per unit area.

Fig. 1.

The observed diurnal variation of the components in the surface
energy balance, at Cabauw on a cloudless day in summertime
(May 31, 1978). Here Q^* is net radiation, λE is flux due to
evaporation ($\lambda E > 0$) or condensation ($\lambda E < 0$) at the surface,
H is surface sensible heat flux, and G is soil heat flux at the
surface.

2

restrict ourselves to conditions in which the turbulence is not directly influenced by the presence of fog or clouds. Moreover, we will restrict ourselves to generally level, but not necessarily homogeneous surfaces.

The surface fluxes of heat and momentum are among the characteristic scaling parameters and are, therefore, needed for the application of scaling results. Since these fluxes are normally not available, we will focus much of our attention to the parameterization of these fluxes from routine weather data. We will restrict our parameterizations to conditions over land with short vegetation e.g. grass coverages. For conditions above sea, practical methods for the estimation of the surface fluxes are discussed by e.g. Brutsaert (1982) and Large and Pond (1982).

2. Surface fluxes and boundary layer height

The surface fluxes of sensible and latent heat are part of the surface energy balance. Other major terms of the energy balance are the net radiation and the soil heat flux. The net radiation Q^* is the net amount of radiant energy supplied to or lost by the surface. The supply originates partly from the sun (shortwave contribution) and from the atmosphere (longwave contribution). From the sun's radiation a part is reflected at the surface. Due to infra-red radiation of the surface also radiant energy is lost. The soil heat flux G is the amount of energy connected to heating (G > 0) or cooling (G < 0) of the upper soil layer.

Generally, the terms of the surface energy balance above land show a diurnal cycle. This is illustrated in Fig. 1, which shows a typical example for the observed diurnal cycle in summertime on a cloud less day at Cabauw. The data of Fig. 1 are discussed in De Bruin and Holtslag (1982). In Fig. 1, H is the surface flux of sensible heat. For H > 0 the atmosphere is heated from below (daytime), while for H < 0 the atmosphere near the surface is cooled (nighttime). This leads to unstable and stable stratifications of the lower atmospheric layers, respectively. Furthermore, λE is the
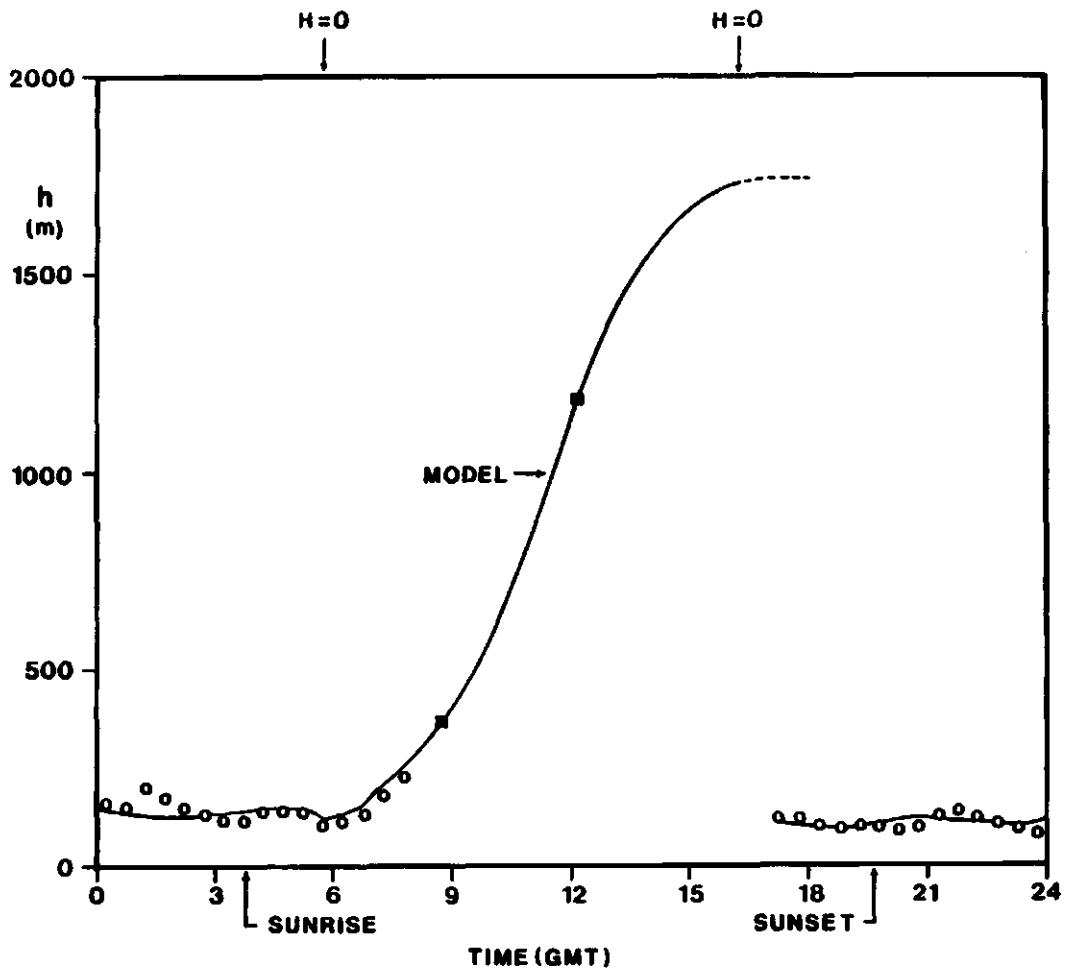
Fig. 2.

The diurnal variation of turbulent boundary layer height h for the period in Fig. 1. Indicated are the moments of sunrise, sunset and H = 0. Dots indicate observations of h with an acoustic sounder, squares are estimates of h obtained from temperature profiles. The indicated line is based on calculations. Further explanation is in the text.

surface flux of latent heat (or water vapour flux), which is connected to evaporation ($\lambda E > 0$) or condensation ($\lambda E < 0$) of water at the surface. Due to the high value of the latent heat of vapourization, λE is often a large term in the surface energy budget during daytime. During nighttime stable conditions $|\lambda E|$ is generally small compared with the other terms.

The magnitude and the diurnal cycle of the sensible heat flux has important consequences on the height and the structure of the turbulent ABL. During unstable conditions the air adjacent to the surface is heated and will rise. This rise continues as long as the air is warmer then the surroundings (up to an inversion layer). This process is known as convection, which is accompanied with the production of convective turbulence in the ABL. Besides of convective turbulence, mechanical turbulence is formed by friction of the flow at the surface. This leads to a downward flux of momentum directed to the surface.

During unstable conditions mechanical and convective turbulence are both present, which leads to efficient mixing of heat, moisture, contaminants and momentum in the ABL. In such conditions profiles of temperature and wind are relatively flat in a major part of the boundary layer. During stable conditions, however, turbulence of mechanical origin is suppressed by a downward heat flux H. This leads to a relatively thin turbulent layer and less vertical exchange, as compared with the unstable ABL. As a consequence, a stable boundary layer is characterized by larger gradients in the profiles of wind and temperature.

In Fig. 2 we have given the diurnal cycle of the turbulent boundary layer height h for the period of Fig. 1. The data of this figure are taken from Nieuwstadt (1981) during stable conditions and Driedonks (1981) during unstable conditions. The indicated line is based on model calculations, of which the surface fluxes of heat and momentum are important input parameters (Van Ulden and Holtslag, 1985). In Fig. 2 it is seen that during stable conditions h is generally small, typically 100 m even after sunrise. However, once the solar heating is strong enough to create a positive heat flux H,
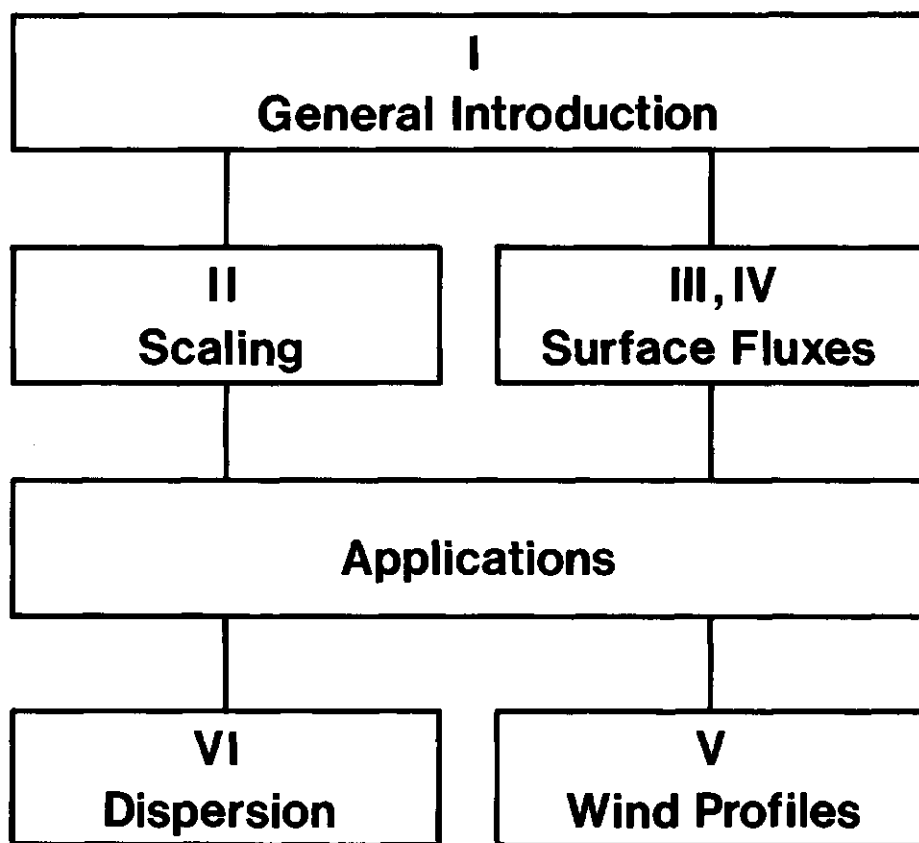
Fig. 3.
Summary of the chapters in this report and their connection.

the stable boundary layer is heated from below. This leads to a turbulent layer, which gradually increases in time. Besides of the time history of the surface fluxes, the height of the layer depends among other effects on the stratification of the air aloft (Driedonks, 1981; Reiff et al., 1984).

At the end of the afternoon, but before sunset, the deep tur- bulent layer disappears and a stable layer is formed near the surface. We note that the diurnal variation of Fig. 2 is only representative for conditions in summertime at clear skies. For cloudy skies and also in wintertime, the diurnal variation of h is much less (as it is for the sensible heat flux H).

3. A survey of the present study

In Fig. 3 the contents of this thesis is briefly summarized and the connection of the individual chapters is shown. From this figure also the title of the present study might be clear.

In chapter II a review is given on scaling of the ABL. The ABL is divided into a number of scaling regimes. Each of the regimes is characterized by distinct scaling parameters. The results are pre- sented at the hand of diagrams for unstable and stable conditions. With these diagrams the scaling regimes are illustrated as a function of the major boundary layer parameters, e.g. the surface fluxes and the boundary layer height.

In chapters III and IV schemes are presented for the estimation of the surface fluxes from routine weather data e.g. total cloud cover, and air temperature, specific humidity and wind observations at a single height. Hourly parameterizations are given for the quantities in the surface radiation and energy budget over land, during daytime (chapter III) and nighttime (chapter IV) respectively. As a part of the nighttime scheme we describe the temperature profile up to 80 m in terms of the model quantities.

The parameterizations of chapters III and IV are compared with observations of the Cabauw facilities and data from literature. The proposed schemes can be used to replace the traditional Pasquill

classification of stability in the atmospheric surface layer (e.g. Pasquill and Smith, 1983). The methods are also relevant for application in short range weather forecast models (Reiff et al., 1984; Driedonks et al., 1985) and air pollution dispersion models (Van Dop et al., 1982; Van Ulden and Holtslag, 1985). Besides the methods might be relevant for other applications in meteorology and hydrology (De Bruin, 1982).

In chapter V we are dealing with Cabauw wind profiles up to 200 m in the ABL. We use scaling techniques to analyse the observations as a function of stability, both during daytime and nighttime. Extension of the usual wind speed profile to very stable conditions is discussed. Also the wind direction profile is analysed. With the flux schemes of the preceeding chapters, the theory is applied to the simulation of the wind frequency distribution at 80 m. Also the diurnal variation of wind at a height substantially above normal observation level is simulated. As such the methods are relevant for wind energy assessment studies (Van Wijk et al., 1985; Petersen and Troen, 1986) and analyses of surface layer wind (e.g. Cats, 1980; Wieringa, 1986). Moreover, the methods may replace the use of empirical power "laws", the use of which has no physical foundation and only little practical advantage (Wieringa, 1981).

In chapter VI a method is given for calculating the dispersion of non-buoyant plumes in the ABL. The method consists of a combination of scaling techniques for the different regions in the ABL, as has been reviewed in chapter II. As such the dispersion of air pollution is related directly to the turbulent state of the ABL. In this chapter, we suggest models for ground level concentrations of pollutants dispersed from continuous point sources. The models are evaluated with independent tracer experiments over land adopted from literature. The method may replace the traditional Gaussian plume model (e.g. Pasquill and Smith, 1983). In combination with the surface flux schemes and the wind profile, the method can be used to update regulatory dispersion studies for urban planning (Holtslag et al., 1986).

Let us finally give some editorial comments. The chapters II-VI are based on individually published or submitted journal articles. Some redundancy of the subject matters in the chapters is therefore unavoidable, but the advantage is that each chapter can be read independently. The general line through the study should be apparent from this chapter.

Chapter II

SCALING THE ATMOSPHERIC BOUNDARY LAYER[*]

Abstract

In this chapter we review scaling regimes of the idealized
Atmospheric Boundary Layer. The main emphasis is given on recent
findings for stable conditions. We present diagrams in which the
scaling regimes are illustrated as a function of the major boundary
layer parameters. A discussion is given on the different properties
of the scaling regimes in unstable and stable conditions.

11

1. Introduction

Scaling is a well-known approach to describe turbulence in the atmospheric boundary layer (ABL). Its basic assumption is that the structure of the ABL can be described in terms of only a few characteristic parameters. A well-known example is the surface layer for which Monin-Obukhov similarity theory is well established (e.g. Businger, 1973; Wyngaard, 1973). Scaling has been also applied to the unstable ABL. Its validity in this case has been confirmed both by experiments (Kaimal et al., 1976; Caughey et al., 1979; Nichols and Readings, 1979) and by numerical simulations (Deardorff, 1974, Moeng, 1984). Only recently progress has been made with the scaling of the stable boundary layer (Nieuwstadt, 1984a).

In all scaling approaches the boundary layer is subdivided into various regions each characterized by different scaling parameters. For someone not familiar with scaling of the ABL it is frequently not clear in which regions certain scaling assumptions apply and under what conditions these are valid. Our purpose, therefore, is to review the scaling of the ABL and to present it in terms of diagrams in which the scaling regions are illustrated as a function of the major boundary layer parameters. Although such a diagram is not new for the unstable boundary layer (e.g. Nichols and Readings, 1979, Van Dop et al., 1980), we believe that it is new for the stable case. We nevertheless present diagrams for both boundary layers because it facilitates a comparison between both types.

Our discussion is limited to the horizontally homogeneous and clear ABL, so all cases with active clouds or fog are excluded. These processes introduce additional scaling parameters. Their incorporation in a more generalized description of the ABL will be the next challenge of boundary layer meteorology.

We start with a description of the unstable boundary layer and subsequently discuss the stable boundary layer.

2. The unstable ABL

An unstable ABL is generally formed due to an upward (virtual) sensible heat flux H at the surface (H > 0). The latter is a result of a positive (virtual) temperature difference between the surface and the overlying air . For dry air we can write $H = \rho\, C_p\, \overline{w\theta}_o$, where $\overline{w\theta}_o$ is the kinematic surface heat flux. It appears that $\overline{w\theta}_o$ is one of the basic scaling parameters for the turbulence in the unstable ABL (Panofsky, 1978; Caughey, 1982).

The other basic scaling parameters in the unstable ABL are the surface flux of momentum τ_o, the height above the surface z and the mixing height h (e.g. Tennekes, 1982). Here τ_o defines the friction velocity u_* by $\tau_o = u_*^2$ (kinematic units). The mixing height h is defined as the mean height to which turbulence extends. Generally, scalar quantities are well-mixed to this height in very unstable conditions.

The surface fluxes of heat and momentum define the Obukhov length scale L as (Obukhov, 1946)

$$L = \frac{-\, u_*^3}{k\, \frac{g}{T}\, \overline{w\theta}_o} ,$$

(1)

where g/T is the buoyancy parameter and $k(\approx 0.4)$ is the Von Kármán constant. Together with the already introduced length scales z and h we can form two independent dimensionless parameters for the turbulent structure in the ABL. Here we choose the non-dimensional height z/h and the stability parameter $h/|L|$. For small $h/|L|$ the stratification is close to neutral, while for increasing $h/|L|$ stability effects become more important.

Figure 1 shows a plot of z/h against a typical range of -h/L for the unstable ABL. In this diagram five regions can be distinguished, which were mentioned by e.g. Panofsky (1978), Nichols and Readings (1979), Caughey (1982) and Driedonks and Tennekes (1984). This diagram resembles the ones presented by Nichols and Readings (1979), Van Dop et al. (1980) and Olesen et al. (1984). However, these
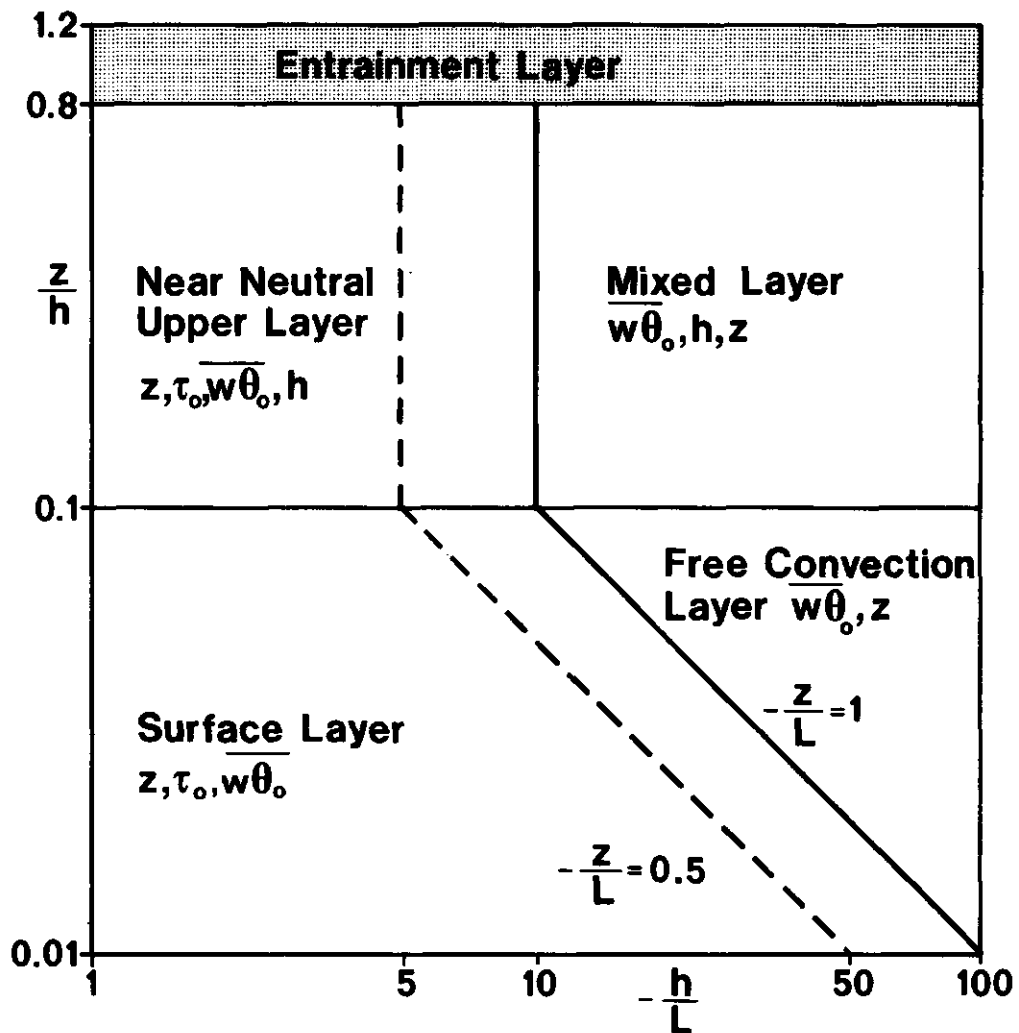
Figure 1.
Definition of scaling regions in the unstable ABL (L < 0). Basic
scaling parameters for the turbulence are indicated.

authors use z/h and z/L as independent parameters instead of z/h and -h/L in our case. In Figure 1 we have indicated that a value of -h/L ≈ 5 may be already sufficient to drive the ABL in the so-called convective state (Deardorff, 1974). In that case the top of the surface layer is -z/L = 0.5.

In Figure 1 we have listed the basic scaling parameters for the surface layer (SL), the free convection layer (FCL) and the mixed layer (ML). Each of these regions is characterized by a reduction in the number of the basic scaling parameters z, τ_0, $\overline{w\theta_0}$ and h. In each region we can form scales for velocity, temperature and length. For instance, in the SL the velocity scale is given by $u_* = \tau_0^{1/2}$, in the FCL we have (Deardorff, 1970; Tennekes, 1970)

$$w_f = (\frac{g}{T} \overline{w\theta_0} z)^{1/3} , \qquad (2)$$

and in the ML it is convenient to define

$$w_* = (\frac{g}{T} \overline{w\theta_0} h)^{1/3} . \qquad (3)$$

It turns out that scaling of turbulent quantities in the different scaling regions leads to similarity predictions of the behaviour of non-dimensionalized quantities. These predictions are to a large extent supported by observations (e.g. Businger, 1973; Wyngaard, 1973; Caughey, 1982). We note that for the mixed layer some dimensionless quantities do vary with relative height z/h (such as standard deviation of vertical velocity), while profiles of scalars are often found to be uniform. For the latter cases, therefore, z is of less importance in the mixed layer (e.g. Caughey, 1982).

In Figure 1, also a near neutral upper layer (NNUL) is indicated (z/h > 0.1 and -h/L < 5 to 10). This layer will be found over land only with low solar insolation or strong winds. Above the sea the NNUL is found more often (Nichols and Readings, 1979). The latter authors showed that in addition to h, the scaling parameters for the SL are also relevant for this region. For neutral conditions the turbulent structure might be influenced by the effect of Coriolis force on the mixing height h (e.g. Tennekes, 1982).

Finally, the entrainment layer (EL) of Figure 1 illustrates the zone in which air with different properties from above the ABL influences the turbulent structure (Deardorff et al., 1980). At present the structure of the EL is not well understood and no scaling parameters can be given (Driedonks and Tennekes, 1984). Tentatively we have situated the EL for $0.8 \leq z/h \leq 1.2$ (if $h/|L| > 1$).

3. The stable ABL

A stable ABL is formed during nighttime over land when the surface is cooled by longwave emission of radiation. Over sea a stable ABL is generally formed by warm air advection. In stable conditions turbulence of mechanical origin is suppressed by a downward heat flux H (H < 0). As a result the layer in wich turbulence can be maintained is typically an order of magnitude smaller than that under unstable conditions.

The stable stratification in the ABL leads to small eddies. As a consequence the structure of the stable ABL is completely different from that of the unstable ABL. Nevertheless, the turbulence in the SL can be treated in terms of Monin-Obukhov similarity theory with z, τ_0 and $\overline{w\theta}_0$ as scaling parameters. Just above the SL the turbulence scales with z and the local values of the fluxes τ and $\overline{w\theta}$. This is known as local scaling, a similarity approach recently developed by Nieuwstadt (1984a).

In the local scaling regime the non-dimensionalized turbulent variables can be described as a function of z/Λ (Nieuwstadt, 1984a). Here Λ is called the local Obukhov length, which is defined as

$$\Lambda = - \frac{\tau^{3/2}}{k \frac{g}{T} \overline{w\theta}} .$$

(4)

For large values of z/Λ we expect that the dependence on z must disappear. The background is that vertical motion is inhibited due to the stable stratification and that turbulent eddies no longer feel

16

the presence of the surface. This is called z-less stratification (Wyngaard, 1973, Nieuwstadt, 1984a). Consequently, z-less scaling means that dimensionless quantities approach a constant value for large z/Λ. For instance, the Richardson number Ri approaches a constant value of Ri = 0.2. The latter value and thus z-less stratification are already achieved by the Cabauw data at $z/\Lambda \approx 1$ (Nieuwstadt, 1984a).

To delineate the regimes in the ABL where local scaling and z-less scaling are valid we need profiles of τ, $\overline{w\theta}$ and Λ. Let us express such profiles as

$$\tau/\tau_o = (1 - z/h)^{\alpha_1} \tag{5}$$

with $\tau_o = u_*^2$,

$$\overline{w\theta}/\overline{w\theta}_o = (1 - z/h)^{\alpha_2} \tag{6}$$

and

$$\Lambda/L = (1 - z/h)^{\alpha_3} . \tag{7}$$

Here h is the mean height of the turbulent ABL, which is generally smaller than the height to which the surface temperature inversion extends. Further, $\alpha_1 - \alpha_3$ are positive coefficients, which are related by $\alpha_3 = 3/2 \, \alpha_1 - \alpha_2$.

There is no theoretical justification for profiles such as (5)-(7) and therefore they should only be interpreted as convenient approximations and not as generalized turbulence profiles for the stable ABL. As a matter of fact such profiles would be in contradiction with local scaling, because they depend on surface values of turbulent quantities and they adopt h as a scaling height. Moreover, observations do not lead to a single value for the exponents α_1 and α_2 (Caughey et al., 1979; Nieuwstadt, 1984a). Nevertheless, in the case of horizontally homogeneous and steady conditions when the cooling rate of the ABL is constant, Nieuwstadt (1984a) was able to derive Eqs. (5)-(7) with $\alpha_1 = 3/2$, $\alpha_2 = 1$ and $\alpha_3 = 5/4$. This was done

$\dfrac{z}{h}$

1

Intermittency

Near Neutral Upper Layer

$\dfrac{h-z}{\Lambda}=10$

z-less
Scaling
$\tau,\overline{w\theta}$

0.5

$\dfrac{z}{\Lambda}=1$

Local
Scaling
$z,\tau,\overline{w\theta}$

0.1

Surface Layer $z,\tau_o,\overline{w\theta}_o$

0

1   5 $\dfrac{h}{L}$ 10
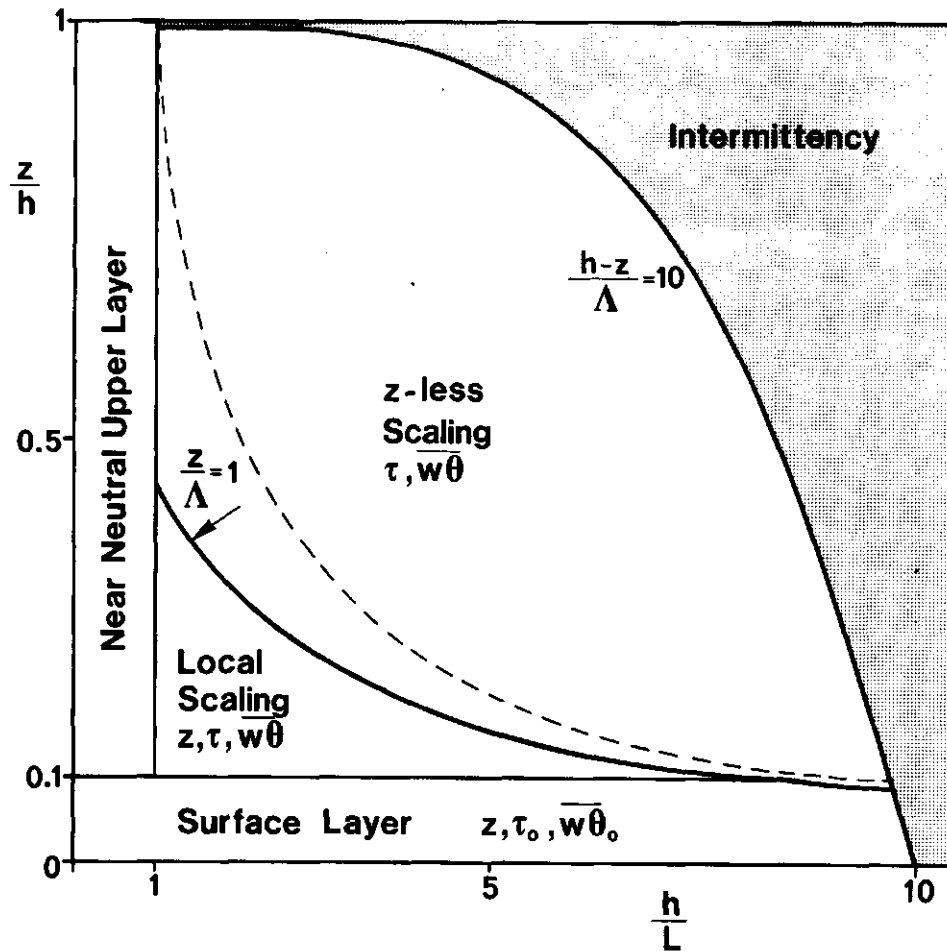
Figure 2.

As Figure 1 for the stable ABL (L > 0). The dashed line is given by
z/L = 1. (see section 4).

by applying the closure hypothesis $Ri = Ri_f = 0.2$ on the equations of motion for the stable ABL, where Ri_f is the flux Richardson number. In the following we will use the latter value of α_3 to estimate the size and shape of the scaling regions.

In Figure 2 we have summarized the above scaling regions. Here conditions with $h/L < 1$ are considered to be near neutral (Nieuwstadt, 1984b). The SL is taken up to $z/h = 0.1$ as in the near-neutral unstable case. The local scaling region is defined up to $z/\Lambda \approx 1$, because z-less scaling already applies for $z/\Lambda \geq 1$ as indicated by Nieuwstadt's results. Again the basic scaling parameters for the turbulence are indicated in the diagram. Note that for the z-less region the only possible length scale is given by Λ, which according to Eq. (7) is in general a decreasing function of height.

In Figure 2 we have indicated also an intermittency region, in which turbulence is very weak and sporadic and, therefore, no longer continuous in time and space. This means that the turbulence is confined to isolated patches, which develop and disappear as a function of time. No satisfactory theory for the intermittent stable ABL has been developed at present. We expect that intermittency extends to the surface for low wind speed or large stability.

In the upper part of the ABL we may expect intermittent turbulence as well. This intermittency is connected to fluctuations in the height of the turbulent layer around its mean height h, as can be seen from acoustic sounder height-time charts (e.g. Crease et al., 1977). Let δ denote the maximum deviation around h. Then turbulence is continuous and scaling is applicable for $z \leq h - \delta$ or $\delta \leq h - z$. To make a first guess we assume here that δ is connected to the local length scale at the top of the z-less scaling region Λ. Somewhat arbitrarily we take $\delta = a\,\Lambda$, where we assume that δ is large compared with Λ, e.g. $a \gg 1$.

From $\delta = h - z$ and $\delta = a\Lambda$ we obtain $(h - z)/\Lambda \approx a$. This equation describes the border line between the z-less scaling and intermittency region. In Fig. 2 we have indicated this line with $a \approx 10$. It is seen that the region of continuous turbulence exists only for relatively small h/L, in accordance with observations (Nieuwstadt, 1984b). Nevertheless, we stress that the relationship $\delta = a\Lambda$ is a

19

drastic simplification of the processes near the top of the stable turbulent boundary layer. The situation is even more complicated when internal waves are present in the vicinity of h (De Baas and Driedonks, 1985).

4. Discussion

In Figures 1 and 2 we show the several scaling regions of the unstable and stable ABL. In the best understood regions we have listed the basic parameters which characterize the turbulent quantities. Here it is noted that for the scaling of a scalar (e.g. humidity or concentration of contaminants) a flux $\overline{wc}$ can be formed, which has the same function as $\overline{w\theta}$ for temperature. For unstable conditions, however, the statistics of fluctuating horizontal velocity components (σ_u, σ_v) are influenced by the large eddies throughout the unstable ABL (Panofsky et al., 1977; Højstrup, 1982) so that these variables do not obey SL scaling. Moreover, in the figures we have neglected the presence of the viscous sublayer very close to the surface. For the latter we refer to Brutsaert (1982).

In Figures 1 and 2 a fixed value of the stability parameter h/L may be represented by a straight vertical line. Such a line illustrates a certain turbulent state of the whole ABL. When we move along such a line, we observe the change in vertical ABL structure. Dependent on the value of h/L we encounter the different scaling regimes.

The range of values for h/L is different for unstable and stable conditions. In fact, for unstable conditions $h/|L|$ may increase to infinity (In the case of no wind and strong insolation above land). For stable conditions, however, no fully turbulent ABL's are observed in the Cabauw data beyond $h/L \approx 6$ (Nieuwstadt, 1984b). For $h/L \leq 6$ Figure 2 shows indeed a small intermittency region near the top of the ABL. For larger values of h/L the intermittency region increases very strongly.

The different range of values for $h/|L|$ in unstable and stable conditions has a large influence on the appearance of Figures 1

and 2. In unstable conditions a free convection layer (FCL) enters above the surface layer for $h/|L| > 5$ to 10 and for increasing values of $h/|L|$ the FCL layer becomes relatively more important than the surface layer. This reflects the fact that with increasing instability, the buoyant production of turbulence dominates over an increasing part of the boundary layer. The relative thickness of the mixed layer (ML), however, is unaffected by the value of $h/|L|$. In fact it has been shown that the existence of the ML and its characteristic structure becomes independent of $h/|L|$, once the ABL is driven in the convective state (Deardorff, 1974).

In stable conditions Figure 2 shows that the local scaling region decreases for increasing h/L. This is caused by the fact that with increasing stability the height z becomes less important as a scaling parameter because the eddies reduce in size. As a result the z-less region increases with h/L up to $h/L - 5$. For larger values of h/L this region decreases as well, while at the same time the intermittency region extends further downwards. However, it should be remembered that the actual curves in Figure 2 depend on the numerical value of the constant α_3.

In Figure 2 we have indicated the line $z/L = 1$ (dashed). Comparison of this line with the line $z/\Lambda = 1$ shows that in a large part of the stable ABL $\Lambda - L$ (see also Eq. (7)). This means that a formulation of z/Λ as required by local scaling is almost equivalent to the surface layer similarity in terms of z/L. This latter result may explain why often the SL results of Monin-Obukhov theory are valid up to $z/L - 1$ (Wyngaard, 1973). Holtslag (1984a; Ch. V) showed a good agreement between observed stable wind profiles and an extended SL description, even for $z/L > 1$.

The dividing lines between the regions in Figure 1 are commonly accepted in the literature (e.g. Caughey, 1982; Olesen et al., 1984). In fact the latter authors give a plot of z/h against z/L, which gives similar results as our Figure 1 for the unstable side. For stable conditions, however, a plot of z/h against z/L introduces a not well-defined region in the diagram. Olesen et al. (1984) call this "a poorly understood region" (see their Figure 1). The advantage of our plot given in Figure 2 is that we are able to interpret the scaling behavior of every region at the stable case.

From the discussions in this chapter we note the essential role of the surface fluxes of heat and momentum. Applied methods for the derivation of the surface fluxes are discussed in Chapters III and IV. In Chapters V and VI we apply the scaling techniques to the description of the wind profile and to the turbulent dispersion of contaminants in the ABL.

Chapter III

A SIMPLE SCHEME FOR DAYTIME ESTIMATES OF THE SURFACE FLUXES FROM
ROUTINE WEATHER DATA [*]

Abstract

In this chapter a simple empirical scheme is presented, which gives
hourly estimates of the surface fluxes of heat and momentum from
routine weather data during daytime. The scheme is designed for grass
surfaces, but it contains parameters which take account of the sur-
face properties in general. The required input weather data are no
more than a single wind speed, air temperature at screen height and
total cloud cover. The output of the scheme is in terms of the Monin-
Obukhov similarity parameters; it is obtained by using estimates for
the mean values of the surface radiation and energy budget. For the
climate of The Netherlands a good agreement is found between a full
year of observations and estimates made with the scheme. For all data
it appears that root mean square errors are 90 Wm^{-2} for the incoming
solar radiation, 63 Wm^{-2} for the net radiation, 34 Wm^{-2} for the sen-
sible heat flux, 0.01 ms^{-1} for the friction velocity and 0.67×10^{-3}
for the similarity ratio between the surface roughness length and the
Obukhov length scale. A discussion is given on the surface parameters
and coefficients of the scheme.

1. Introduction

The surface fluxes of heat, water vapour and momentum determine to a great extent the state of the atmospheric boundary layer. As such these fluxes are the principal boundary conditions for e.g. weather forecast models and air pollution dispersion models. In principle the fluxes can be measured. However, usually such measurements are not available, and in a forecast model the fluxes have to be parameterized in terms of variables predicted by the model. So in general there is a need to relate the surface fluxes to weather variables, either measured routinely of predicted by forecast models. It is the aim of this paper to establish such relations.

A scheme is developed that requires the following input data: total cloud cover, mean wind speed at one level and air temperature. Moreover estimates of the surface characteristics and of the solar elevation are used. If available, measurements of the global radiation can be included. The scheme provides estimates for the incoming solar radiation (K^+), the net radiation (Q^*), the flux of sensible heat (H), the evaporation rate (E), the surface stress in terms of the friction velocity (u_*) and the Obukhov stability parameter (L). As such the scheme can serve as an alternative for the traditional Pasquill stability classification (Pasquill and Smith, 1983).

The scheme consists of four parts which are described in the sections 2-5 (see also table 1). In section 2 we deal with the parameterization of the incoming solar radiation in terms of solar elevation and total cloud cover. We adopt the models by Collier and Lockwood (1974, 1975) and by Kasten and Czeplak (1980). We test these models on radiation data obtained in Cabauw and De Bilt.

In section 3 we present a model for the surface radiation budget which provides the net radiation. The model is a generalization of the model by Monteith and Szeicz (1961) and is tested against an independent data set. Section 4 describes the partitioning of the net radiation over the various heat fluxes at the earth's surface. We use the energy balance model by De Bruin and Holtslag (1982) with the net radiation estimated from the model of section 3. The calculated sensible heat flux is compared with the heat flux obtained from measured temperature and wind profiles (see appendix A).

Table 1

Summary of the methods in this paper which are used to obtain the output of the scheme with the necessary input data.

Section	Parameterized quantity	Method	Input data
2	Incoming solar radiation (K^+)	Parameterization of the transmissivity of the atmosphere	Solar elevation (ϕ; see appendix B) Total cloud cover (N) Turbidity coefficients (a_1, a_2) Cloudiness coefficients (b_1, b_2)
3	Net radiation (Q^*)	Parameterization of the terms in the surface radiation budget	Incoming solar radiation (K^+) Air temperature (T) Longwave radiation coefficient (c_1) Total cloud cover (N) Cloudiness coefficient (c_2) Surface albedo (r) Surface heating coefficient (c_3)
4	Sensible heat flux (H) Latent heat flux (λE)	Parameterization of the terms in the surface energy budget	Net radiation (Q^*) Air temperature (T) Surface moisture parameters (α and β)
5	Friction velocity (u_*) Obukhov length scale (L)	Monin-Obukhov similarity theory	Sensible heat flux (H) Wind speed (U_z) Surface roughness length (z_o)

Finally in section 5 we use the estimated heat flux in combination with a single wind speed to obtain the friction velocity (u_*) and the Obukhov length scale (L). We compare u_* and L with the values obtained directly from measured wind and temperature profiles (appendix A). In this section we use the Monin-Obukhov similarity theory for the atmospheric surface layer and the flux-profile relations by Dyer and Hicks (see Dyer, 1974 and Paulson, 1970).

In each section the output of the scheme is compared with meteo-
rological observations in Cabauw, The Netherlands. A description of
the Cabauw facilities can be found in Driedonks et al. (1978). For
our comparisons we have used from a full year of available daytime
data those, for which no instrumental or observational errors were
reported and for which no rain, snow of fog appeared. Therefore the
application of the scheme is restricted to neutral or unstable
weather conditions, when the flux of sensible heat is positive.

The scheme is designed for grass surfaces, but it contains para-
meters which take account of the surface properties in general. This
is discussed in section 6. Future refinements of the scheme are pos-
sible within the same general framework.

2. The incoming solar radiation

At many meteorological stations, incoming solar radiation is
measured. When such measurements are available, these can be used
directly to estimate the net radiation (see section 3). When no
measurements are at hand, observations of total cloud cover (N) and
knowledge of the solar elevation (ϕ) are needed to estimate the
incoming solar radiation. A simple procedure for the estimation of
ϕ from the geographical position on earth and the time is given in
appendix B. Here we present a method to determine the incoming solar
radiation.

2.1 Clear skies

The incoming solar radiation at ground level in clear skies (K_o^+)
depends to a very large extent on the solar elevation ϕ. A simple
parameterization for K_o^+ is (Kasten and Czeplak, 1980; Collier and
Lockwood, 1974)

$$K_o^+ = a_1 \sin\phi + a_2, \tag{1}$$

where a_1 and a_2 are empirical coefficients. These coefficients des-
cribe the average atmospheric attenuation of K_o^+ by water vapour and
dust for a given site.

In table 2 published values for the turbidity coefficients a_1 and a_2 are given for several locations. Also least square estimates of a_1 and a_2 are given for clear sky data in De Bilt in 1977. These data were obtained with a Moll-Gorczynski pyranometer for 504 hours with total cloud cover $N \leq 0.25$ and solar elevation $\phi \geq 10$ degrees.

It appears that for the same value of ϕ the coefficients of table 2 give a broad range of average K_o^+ values. This range can be attributed to climatological variations in the turbidity of the atmosphere. The coefficients of Collier and Lockwood (1975) give a fair average of all coefficients for $\phi > 20$ degrees. Therefore the latter coefficients can be used for a site where the turbidity coefficients are not known at beforehand, which is usually the case. Then we may expect systematic deviations for K_o^+ up to about 10% depending on the mean turbidity of the site. The accuracy of the mean solar radiation estimates at clear skies is also within about 10%.

Table 2
Comparison of the turbidity coefficients a_1 and a_2 of Eq. (1) for several locations.

$a_1 (Wm^{-2})$	$a_2 (Wm^{-2})$	Location	Reference
910	-30	Hamburg (53°38'N, 9°50'E)	Kasten and Czeplak (1980)
990	-30	Harrogate (54°N, 1°30'W)	Collier and Lockwood (1975)
1100	-50	North Atlantic (52°30'N, 20°W)	Lumb (1964), obtained from his Fig. 1a
1098	-65	Boston (42°13'N, 71°7'W)	Haurwitz (1945) obtained after expansion of his equation $K_o^+ = 1098 \sin\phi \exp(-0.059/\sin\phi)$
1041	-69	De Bilt (52°06'N, 5°11'E)	This study (correlation coefficient r = 0.98, root mean square error $\sigma = 40\ Wm^{-2}$, which is 9.5% of the observed average)

Table 3a

Comparison of hourly values of observed incoming solar radiation K^+ with calculated values of (1) and (2) for De Bilt in three classes of total cloud cover N. The data cover one year of measurements for solar elevation $\phi \geq 10$ degrees. The calculations are made with $a_1 = 990$ Wm^{-2}, $a_2 = -30$ Wm^{-2}, $b_1 = 0.75$ and $b_2 = 3.4$.

	N ≤ 0.25	0.25 < N < 0.75	N ≥ 0.75	all N
n	504	564	1944	3012
$\bar{x}$	438.3	430.4	232.9	304.2
$\bar{y}$	422.9	388.4	231.3	292.8
r	0.980	0.908	0.820	0.906
σ	46.7	91.9	86.3	82.2
$\sigma/\bar{y}$	0.110	0.237	0.373	0.281

Notes:

n	:	number of measurements
x	:	calculated value
y	:	observed value
$\bar{x}, \bar{y}$	:	averages of x, y respectively
σ	:	root mean square error $\{\overline{(y-x)^2}\}^{\frac{1}{2}}$
r	:	correlation coefficient

Table 3b

As table 3a, but here the comparison is made for 30-minute averages at Cabauw. Because there were no cloud observations available at Cabauw, we took the average of observations at four weather stations around Cabauw (within 40 km). See notes of table 3a.

	N ≤ 0.25	0.25 < N < 0.75	N ≥ 0.75	all N
n	252	568	923	1743
$\bar{x}$	470.9	421.8	231.4	328.1
$\bar{y}$	430.5	363.1	214.0	293.9
r	0.983	0.889	0.819	0.904
σ	54.8	105.1	88.3	90.3
$\sigma/\bar{y}$	0.130	0.289	0.413	0.307

28

Apart from mean deviations also random deviations will occur due to local variations in the turbidity. To get an impression of the total error which have to be expected we have made a comparison of (1) with observations of K_o^+ in De Bilt and Cabauw, The Netherlands. The calculations were made with the coefficients of Collier and Lockwood (1975) for cases with solar elevation $\phi > 10$ degrees. Results are given in tables 3a and 3b. Table 3a shows at the left hand side the comparison for De Bilt at clear skies (N < 0.25). It is seen that the agreement is good. The root mean square error $\sigma = 46.7$ Wm^{-2}, which is 11% of the observed average. When our adjusted values for De Bilt ($a_1 = 1041$ Wm^{-2} and $a_2 = -69$ Wm^{-2}) are used the agreement improves, of course ($\sigma = 40$ Wm^{-2}). From table 3b for the comparison at Cabauw we obtain $\sigma = 54.8$ Wm^{-2}, which is 13% of the observed average. In the following we will use (1) with the coefficients of Collier and Lockwood (1975). Then for our data in The Netherlands the total error in the incoming solar radiation at clear skies is within 13% on average.

2.2 The effect of clouds

In general the presence of clouds reduces the incoming solar radiation. Many publications have appeared on this subject. Often a distinction is made between the amount of higher and lower clouds and between the types of clouds (e.g. Davies and Uboegbulam, 1979). Other models use the total cloud cover only; e.g. Kasten and Czeplak (1980) propose

$$K^+ = K_o^+ (1 - b_1 N^{b_2}) , \qquad (2)$$

where N is total cloud cover, K_o^+ is the value from (1) and b_1 and b_2 are empirical coefficients, which may depend on the climate of the specific site. Kasten and Czeplak obtain for 10 years of observations at Hamburg $b_1 = 0.75$ and $b_2 = 3.4$ on the average. With b_1 and b_2 of Kasten and Czeplak, and a_1 and a_2 of (1) taken from Collier and Lockwood (1975), we have made a comparison of (2) with one year of pyranometer measurements of K^+ in De Bilt and Cabauw. We have used hourly and 30-minute averages for solar elevation $\phi \geq 10$ degrees. The
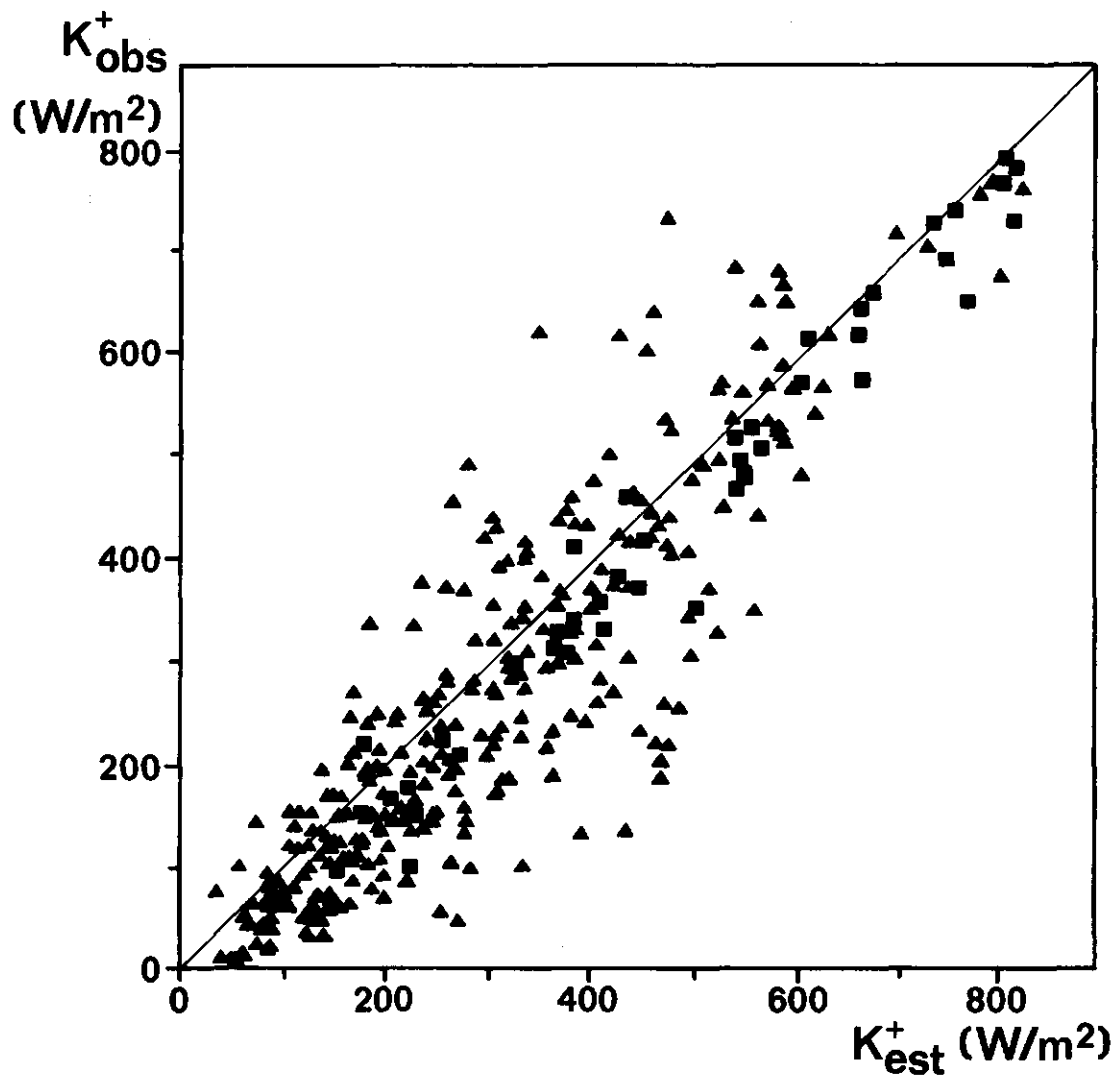
Fig. 1

Comparison of observed half-hourly averages of the incoming solar radiation (K^+_{obs}) with estimated values of (1) and (2) (K^+_{est}) at Cabauw.

Notes: In this figure a random selection is given of the whole data set. Squares refer to clear skies ($N \leq 0.25$) and triangles refer to other conditions.

results are summarized in tables 3a and 3b. In these tables we have
distinguished three classes of total cloud cover (N). In table 3a for
data at De Bilt, it is seen that the ratio between the root mean
square error and the observed average increases from 11% at clear
skies (N ≤ 0.25), and ~24% at intermediate cloud fractions (0.25 < N
< 0.75), up to ~37% for cloudy skies (N ≥ 0.75). These findings
reflect the problems by estimating shorttime values for K^+ from cloud
data, such as the possible overlap of different type of clouds, the
position of the clouds with respect to the direct solar beam, the
varying atmospheric turbidity, etcetera.

From table 3b for the data at Cabauw it is seen that the scatter
increases slightly compared with the results of table 3a. Probably
this is caused by the averaging of total cloud cover observed at four
weather stations around Cabauw, which was done because no local cloud
observations were available in Cabauw. In Fig. 1 a random selection
of the comparison for Cabauw is given. Here only two classes of cloud
cover are distinguished. From the skill of Fig. 1, which is repre-
sentative for the whole data set of table 3b, it is seen that large
deviations can occur between (1) and (2) and observations. However,
in general the simple estimates of (1) and (2) may still be useful in
practice, as will be shown in the following.

3.   The surface radiation budget.

To estimate the net radiation Q^* at the surface we parameterize
the components of the surface radiation budget. This reads:

$$Q^* = (1 - r)K^+ + L^+ - L^-, \qquad (3)$$

where r is the albedo of the surface, L^+ the incoming longwave radia-
tion from the atmosphere and L^- the outgoing longwave radiation from
the surface. K^+ is the incoming solar radiation that we have dis-
cussed in the former section. Of this radiation a fraction r is re-
flected by the surface. This fraction depends on the type of the sur-
face, the solar elevation and the shortwave spectrum (Paltridge and

Platt, 1976). From measurements in Cabauw over short grass we found r = 0.23 on the average. This is a normal value for short grass (Oke, 1978). We will use this constant value for r (see section 6.1). In the following we are dealing with the two longwave terms of (3), L^+ and L^-, to obtain finally Q^*.

3.1 The incoming longwave radiation L^+

A very simple parameterization of the incoming longwave radiation in the absence of clouds L_o^+ was proposed by Swinbank (1963). He related L_o^+ to the air temperature T at screen height (1-2 m) by

$$L_o^+ = c_1 T^6, \tag{4}$$

where $c_1 = 5.31 \times 10^{-13}$ $Wm^{-2}K^{-6}$ is an empirical constant. Arnfield (1979) tested this relation for several locations and concluded, that its estimate is within 5 percent on the average. We will adopt this relation for clear skies. To account for cloud cover (N), we employ the linear correction by Paltridge and Platt (1976). This reads:

$$L^+ = c_1 T^6 + c_2 N, \tag{5}$$

where $c_2 = 60$ Wm^{-2} is appropriate for mid-latitudes.
Other type of parameterizations of L^+ are discussed in Arnfield (1979) and Lind and Katsaros (1982).

3.2 The outgoing longwave radiation L^-

The outgoing longwave radiation L^- from the surface arises from the Stefan-Boltzmann law

$$L^- = \sigma T_s^4, \tag{6}$$

where the earth's surface is assumed to be a black body (Sellers, 1965), $\sigma = 5.67 \times 10^{-8}$ $Wm^{-2}K^{-4}$ is the Stefan-Boltzmann constant and T_s is the surface radiation temperature. Since the surface radiation temperature is not normally available we approximate L^- by

$$L^- = \sigma T^4 + 4\sigma T^3 (T_s - T). \qquad (7)$$

During unstable conditions the surface radiation temperature T_s exceeds the air temperature T. To obtain a suitable description of the correction term $4\sigma T^3$ (T_s - T) in (7) we made a comparison between measurements of this term and measurements of the incoming solar radiation K^+, the net radiation Q^* and the sensible heat flux H obtained with the Bowen's ratio method (see section 4 and Oke, 1978). For this comparison we use data of our micrometeorological field at Cabauw. This field is covered with short grass (kept at ~8 cm). The surface radiation temperature T_s was measured with a infra-red radiation thermometer (type Heimann). The air temperature is measured at 1.1 m.

Fig. 2 shows results of the comparison for four days in the summer of 1977, where we have used 30-minute averages. For these days the total cloud cover N varied between N = 0.25 and N = 1, while the average value was N ~ 0.5. Further the average wind speed at 10 m varied between U_{10} ~ 2.5 ms^{-1} and U_{10} ~ 6 ms^{-1}, with an average U_{10} ~ 4 ms^{-1}. From the comparison between $4\sigma T^3$(T_s - T) and K^+, Q^* and H no wind speed effect and no cloud cover effect could be detected. From Fig. 2 it is seen that a good estimate of the correction term in (7) can be obtained from Q^*, so that

$$4\sigma T^3 (T_s - T) = c_3 Q^*, \qquad (8)$$

is a good approximation. From the limited amount of data in Fig. 2b we obtained c_3 ~ 0.12. Since (8) and c_3 describe the relative increase of the surface radiation temperature with net radiation c_3 may be regarded as a heating coefficient for the surface (see also Monteith and Szeicz, 1961). In section 6.4 we will discuss the heating coefficient in more detail. With (7) and (8) we can approximate L^- by

$$L^- = \sigma T^4 + c_3 Q^*. \qquad (9)$$
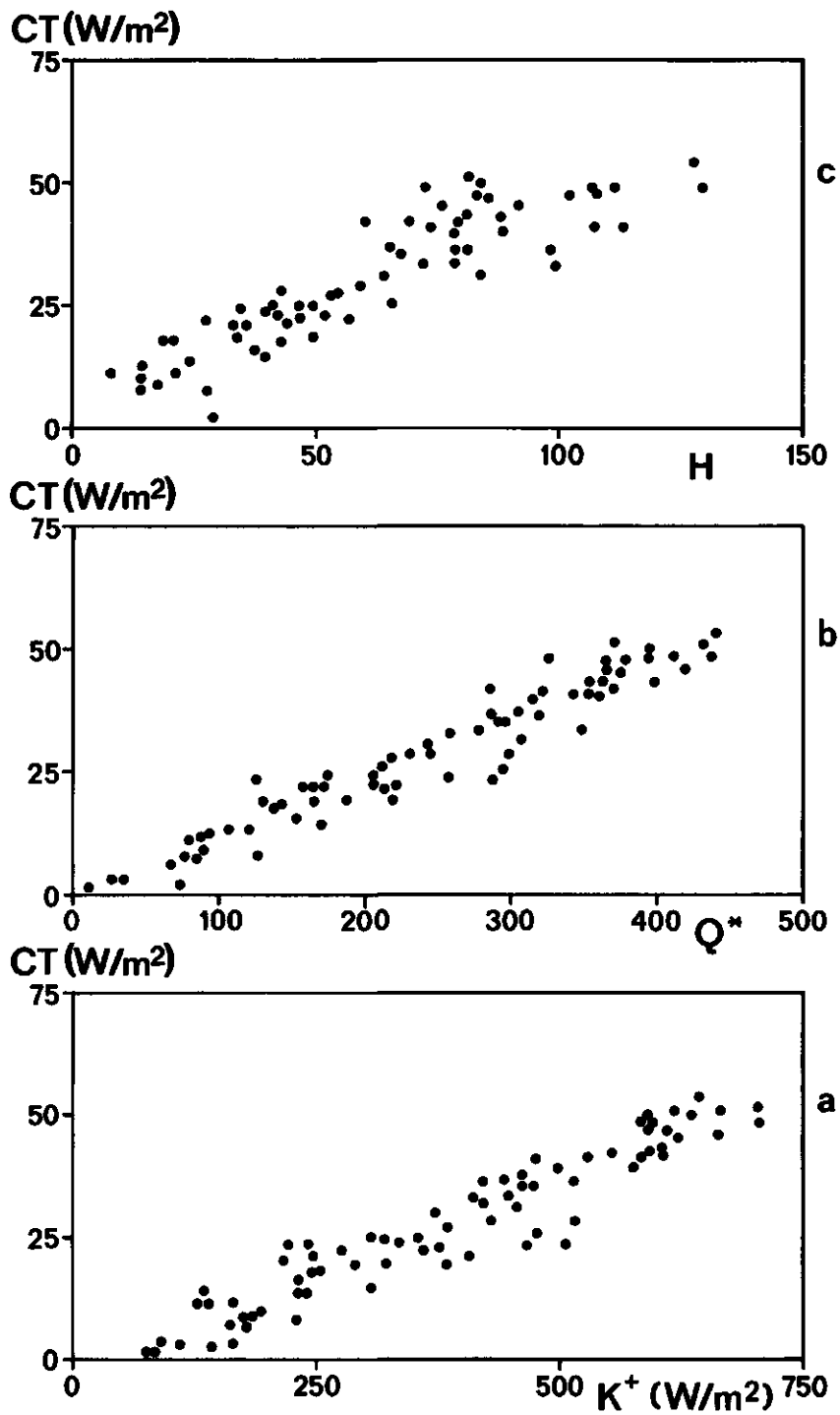
Fig. 2

Comparison of the correction term CT = $4\sigma T^3(T_s - T)$ of Eq. (7) with half-hourly observations of:

a. the incoming solar radiation K^+

b. the net radiation Q^*

c. the sensible heat flux H;

at a micrometeorological field in Cabauw for four summerdays in 1977.

34

Table 4a
Comparison of the observed net radiation Q^* at Cabauw with calculated
values using Eq. (11) and measured values of K^+ in unstable conditions.
Here N is total cloud cover. See notes of table 3a.

	N ≤ 0.25	0.25 < N < 0.75	N ≥ 0.75	all N
n	168	384	447	999
$\bar{x}$	271.3	241.7	181.8	219.9
$\bar{y}$	286.7	246.7	191.7	228.8
r	0.990	0.983	0.973	0.982
σ	28.4	24.3	23.7	24.8
$σ/\bar{y}$	0.099	0.099	0.124	0.086

Table 4b
As table 4a, but here the calculated values are obtained from Eq. (11) and
calculated values of K^+ using Eqs. (1) and (2).

	N ≤ 0.25	0.25 < N < 0.75	N ≥ 0.75	all N
n	168	384	447	999
$\bar{x}$	298.0	276.5	179.4	236.7
$\bar{y}$	286.7	246.7	197.7	228.8
r	0.973	0.870	0.714	0.857
σ	36.3	67.8	66.9	63.2
$σ/\bar{y}$	0.127	0.275	0.349	0.219

3.3 The net radiation Q^*

When we use (5) for the incoming longwave radiation L^+ and (6) for the outgoing longwave radiation L^-, we obtain for Q^* from the surface radiation budget (3)

$$Q^* = (1-r) \, K^+ + c_1 T^6 - \sigma T_s^4 + c_2 N. \qquad (10)$$

Here it is seen that Q^* is in general a function of K^+ and r as pointed out before. Moreover Q^* depends on the air temperature at screen height T, the surface radiation temperature T_s, the total cloud cover N and the coefficients c_1 and c_2. Because T_s is not a routine weather quantity, we approximate L^- by (9) instead of (6), which yields for Q^*

$$Q^* = \frac{(1-r) \, K^+ + c_1 \, T^6 - \sigma T^4 + c_2 \, N}{1 + c_3} . \qquad (11)$$

We have compared (11) with one year of 30-minute measurements of Q^* obtained with a Suomi net pyrradiometer in Cabauw. The estimates are made using $r = 0.23$ and $c_3 = 0.12$, both with measured values of K^+ and with K^+ estimated by means of (1) and (2). Table 4a shows the results for the calculation with measured K^+. Again a distinction is made in three classes of total cloud cover. It is seen that the root mean square error normalized by the observed average is within 10% for $N \leq 0.75$ up to 12.4% at cloudy skies. Fig. 3 shows, for a random sample of the data in table 4a, the good agreement for Q^*.

Table 4b shows the results for Q^* with calculated values of K^+ from (1) and (2). Thus only air temperature and total cloud cover are used as input weather data to obtain Q^*. For clear skies ($N \leq 0.25$) the scatter increases only slightly with respect to table 4a. But for larger cloud amounts the normalized error increases from ~28% at intermediate cloud covers ($0.25 < N < 0.75$) up to ~35% for cloudy skies ($N \geq 0.75$). This is caused by the errors in the estimation of K^+ with (1) and (2). However, the estimate of Q^* is still satisfactory, as illustrated in Fig. 4.

In the present model the properties of the surface are represented by two adjustable parameters. The first parameter is the albedo r, which describes the effect on the net incoming solar radiation. The

36
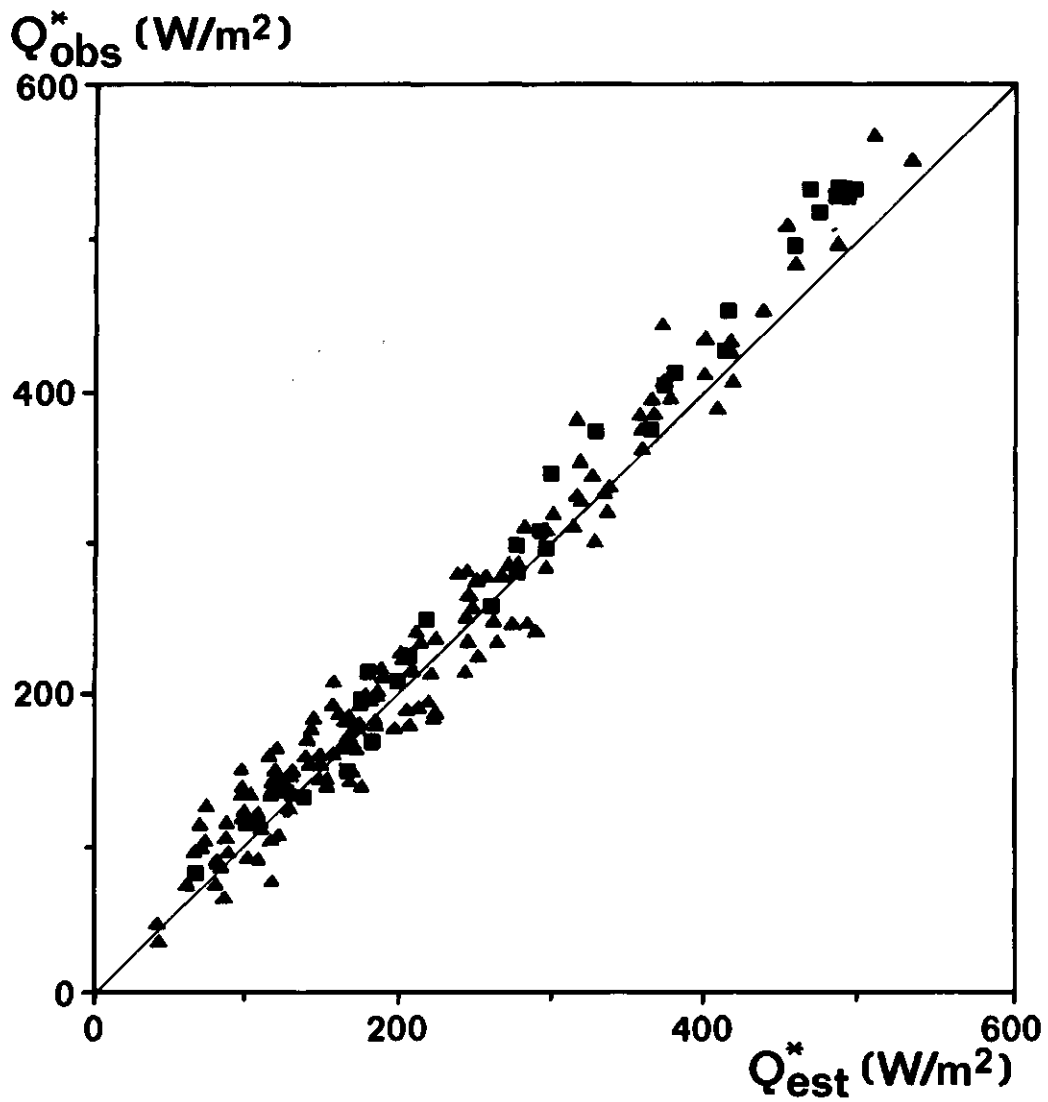
Fig. 3

Comparison of measured half-hourly averages of the net radiation at Cabauw (Q^*_{obs}) with estimated values (Q^*_{est}) of (11) using measured incoming solar radiation. See notes of Fig. 1.
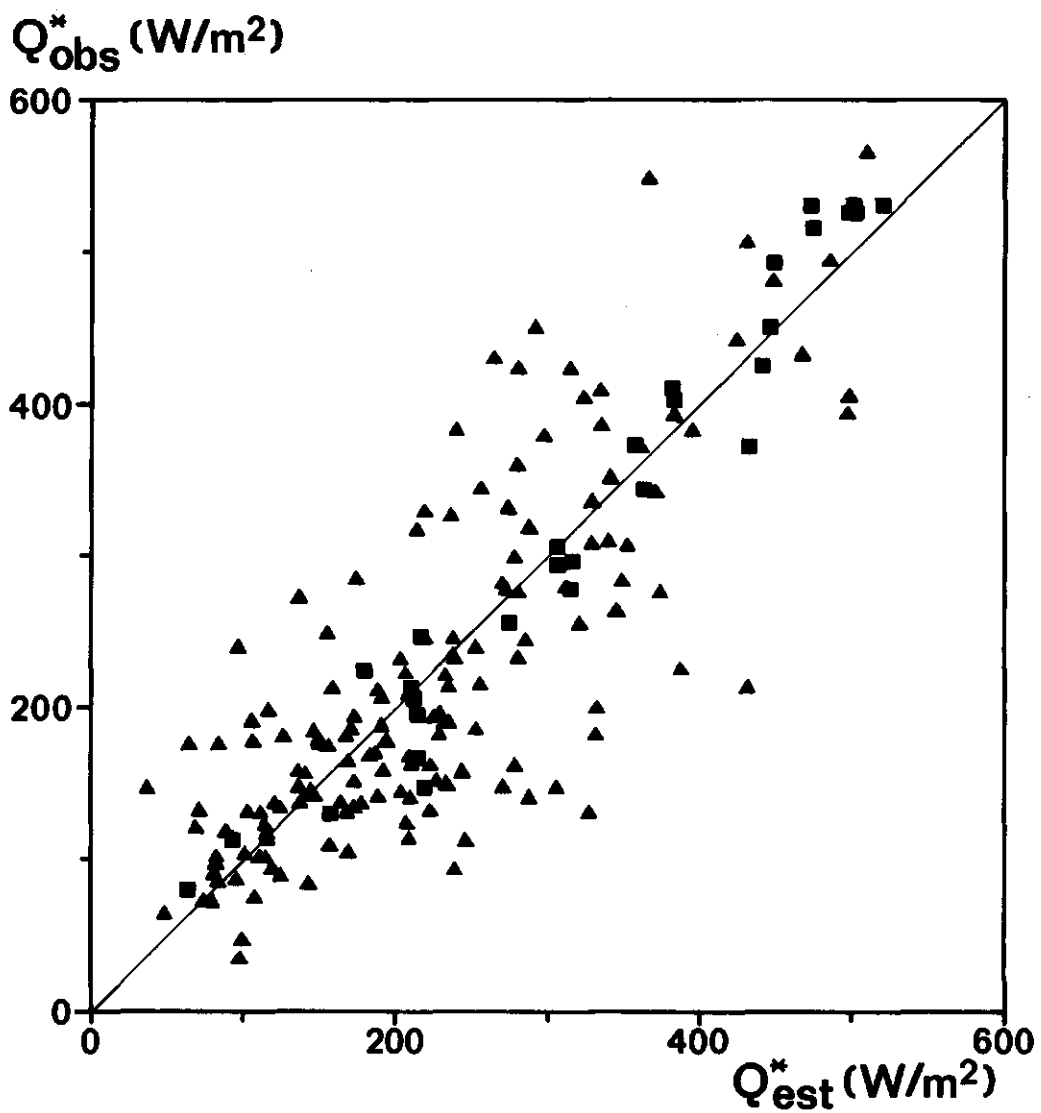
Fig. 4

As Fig. 3, but here Q^*_{est} is obtained with (11) and calculated values of K^+ using (1) and (2). See notes of Fig. 1.

second parameter c_3 characterizes the thermal properties of the surface. Thus the present approach is fairly general. It has the advantage that the basic physics of the surface radiation budget are still present in the final parameterization. This in contrast with the regression models used by Monteith and Szeicz (1961), Gay (1971) and Nielsen et al. (1980). In the latter models regressions are made between net incoming solar radiation $(1-r)K^+$ and the net radiation Q^*. In such an approach specific site effects are not so easy to recognize. In the present approach these can be dealt with in principle (see section 6.4).

4. The surface energy budget

The surface energy budget relates the net radiation Q^* of the former section to the various heat fluxes at the earth's surface. This reads (Oke, 1978):

$$H + \lambda E + G = Q^*, \tag{12}$$

where H is the sensible heat flux, λE the latent heat flux and G is the soil heat flux. For a land surface G is mostly small compared with Q^* during daytime. A good estimate for G is (De Bruin and Holtslag, 1982)

$$G = c_G Q^*, \tag{13}$$

where $c_G = 0.1$ is obtained for a grass covered surface in The Netherlands (see also section 6.2). Since net radiation can be evaluated from standard meteorological data (section 3), the partitioning of H and λE over the available energy $Q^* - G$ has to be dealt with.

4.1 The partitioning of H and λE

A physically realistic way to determine the partitioning of H and λE is the Penman-Monteith approach (Monteith, 1981). A problem with this approach is that several input parameters are needed which are difficult to obtain. For instance, the surface resistance for latent heat is needed. Several attempts are made in literature to evaluate this surface resistance by means of empirical rules (Smith and Blackall, 1979; Deheer-Amissah et al., 1981; Berkowicz and Prahm, 1982a). However, De Bruin and Holtslag (1982) show that the Penman-Monteith approach can be simplified in such a way that it becomes more suitable in the present context.

The simplified parameterization reads:

$$H = \frac{(1 - \alpha) + (\gamma/s)}{1 + (\gamma/s)} (Q^* - G) - \beta, \qquad (14)$$

and

$$\lambda E = \frac{\alpha}{1 + (\gamma/s)} (Q^* - G) + \beta. \qquad (15)$$

Here $s = \partial q_s/\partial T$, where q_s is the saturation specific humidity; $\gamma = C_p/\lambda$, where C_p is the specific heat of air at constant pressure and λ the latent heat of water vapourization; α and β are empirical parameters. The ratios γ/s and $(\gamma/s)/(1+\gamma/s)$ are tabulated as a function of temperature at standard pressure in table 5.

To evaluate H and λE by way of (14) and (15) we must specify α and β. The parameter α accounts for the (strong) correlation of H and λE with $Q^* - G$, while the parameter β accounts for the un-correlated part. For $\alpha=1$ and $\beta=0$, , Eq. (15) describes the so-called equilibrium evaporation rate (Priestly and Taylor, 1972). Monteith (1981) shows that this evaporation rate occurs, when the specific saturation deficit is constant with height (see also Chapter IV). Generally, however, both α and β may depend on the surface moisture condition. Preliminary estimates for a grass covered surface in The Netherlands are $\alpha \sim 1$ and $\beta \sim 20$ Wm^{-2} (De Bruin and Holtslag, 1982).

Table 5

The dependence of the ratios Y/s and (Y/s)/(1 + Y/s) on temperature for standard pressure P = 1000 mb.

T (°C)	Y/s	$\dfrac{Y/s}{1 + Y/s}$
-5	2.01	0.67
0	1.44	0.59
5	1.06	0.51
10	0.79	0.44
15	0.60	0.38
20	0.45	0.31
25	0.35	0.26
30	0.27	0.21
35	0.21	0.17

The latter values for α and β are obtained for normal summer conditions, when the surface is supplied with enough water to evaporate. When there is lack of water the value of α decreases (De Bruin and Holtslag, 1982). Since in The Netherlands the surface is normally not very dry, $\alpha = 1$ and $\beta = 20$ Wm^{-2} should be good enough for our practical scheme; we will use these values below. In section 6.3 we discuss values of α and β for other surface moisture conditions.

4.2 Estimation of the sensible heat flux

In this section we will compare the flux of sensible heat calculated with (11), (13) and (14) with the heat flux derived from measured wind and temperature profiles. The estimation of the heat flux has been performed both with measured incoming solar radiation K^+ (table 6a) and with the calculated value using (1) and (2) (table 6b). The "observed" heat flux was obtained from a full year of profile data in unstable conditions (30-minute averages) with the semi empirical flux-profile relations by Dyer and Hicks (see appendix A).

Table 6a

Comparison of the observed sensible heat flux H from profiles, using the calculated values of Eqs. (11), (13), (14) and measured values of K^+ in unstable conditions. Here N is total cloud cover. See notes of table 3a.

	N ≤ 0.25	0.25 < N < 0.75	N ≥ 0.75	all N
n	168	384	447	999
$\bar{x}$	67.7	60.4	42.9	53.8
$\bar{y}$	63.2	61.3	46.2	54.9
r	0.795	0.788	0.803	0.800
σ	27.3	29.1	22.3	26.0
$\sigma/\bar{y}$	0.432	0.475	0.483	0.474

Table 6b

As table 6a, but here the calculated values are obtained with Eqs. (11), (13), (14) and calculated values of K^+ with Eqs. (1) and (2). See notes of table 3a.

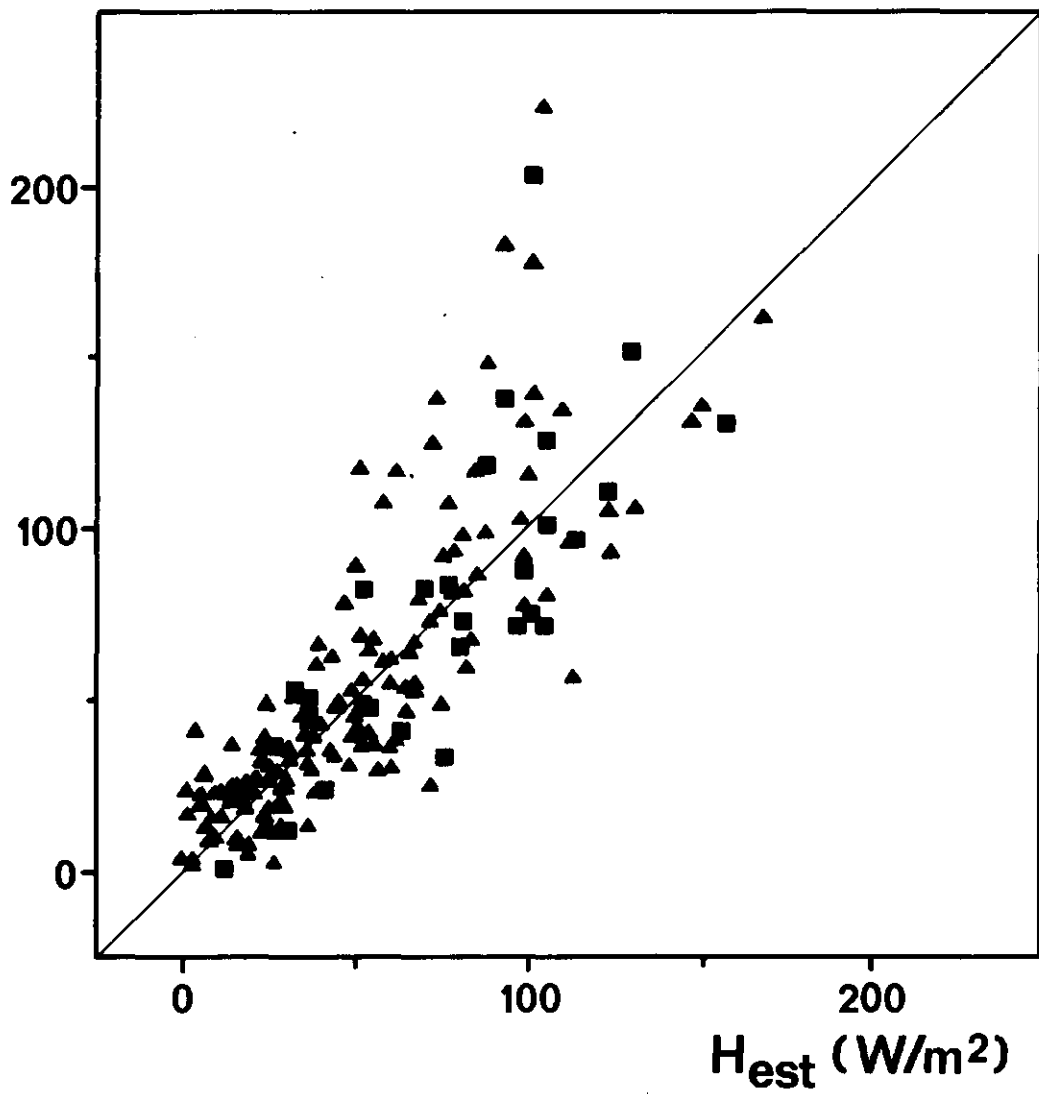|	N ≤ 0.25	0.25 < N < 0.75	N ≥ 0.75	all N
n	168	384	447	999
$\bar{x}$	76.0	71.9	41.5	59.0
$\bar{y}$	63.2	61.3	46.2	54.9
r	0.785	0.652	0.524	0.640
σ	30.3	37.2	32.1	33.9
$\sigma/\bar{y}$	0.479	0.607	0.695	0.617

42

Fig. 5

Comparison of the sensible heat flux obtained from profiles of wind
and temperature (H_{obs}) with the sensible heat flux estimated with
(11), (13) and (14) using measured incoming solar radiation (H_{est}).
See notes of Fig. 1.

43

From table 6a it is seen that the root mean square error normalized by the observed average increases slightly with total cloud cover from ~43% for clear skies (N ≤ 0.25) up to ~48% for N ≥ 0.75. Fig. 5 shows a random sample of the data in table 6a. From table 6b it is seen that the normalized error increases from ~48% for clear skies (N ≤ 0.25) up to ~70% for cloudy skies (N ≥ 0.75), when estimates of K^+ are used from (1) and (2). Fig. 6 shows a sample of the data in table 6b. From the tables and figures it is clear that with measurements of K^+ the estimates of H are improved.

The relative skill of H improves also with increasing instability. For 179 selected cases with $-100 ≤ L < -25$ m we obtain $σ = 40$ Wm^{-2}, which is 49% of the observed average. Here L is the Obukhov stability parameter (see section 5). When measurements of K^+ are used we obtain $σ = 34$ Wm^{-2} which is 42% of the observed average in the selected very unstable cases.

In the above calculations we have used $α = 1$ and $β = 20$ Wm^{-2} under all circumstances. The specific dependence of $α$ and $β$ on the moisture condition of the surface awaits further examination and should improve the performance of the scheme (see also section 6.3). Nevertheless, even with constant values for $α$ and $β$ the accuracy of the present scheme is quite satisfactory. This is illustrated in the following by a comparison between heat fluxes obtained from measurements using two different methods at two sites in Cabauw which are close to each other.

The first method is the Bowen's ratio method, in which measurements of the net radiation and the soil heat flux are used together with the ratio of the sensible heat flux to the latent heat flux (see Oke, 1978). The ratio between the fluxes is derived from observed profiles of temperature and humidity. The second method is the earlier mentioned flux-profile method of appendix A. The comparison between the two "observed" heat fluxes is shown in Fig. 7. The data of Fig. 7 were obtained during the summer of 1977. In general the agreement between the two methods in Fig. 7 is good, but the skill is only slightly better than of Fig. 5. This is due to measurement errors, to small scale terrain variations and to physical imperfections in the two methods. Fig. 7 shows the limited accuracy in

H_{obs} (W/m^2)
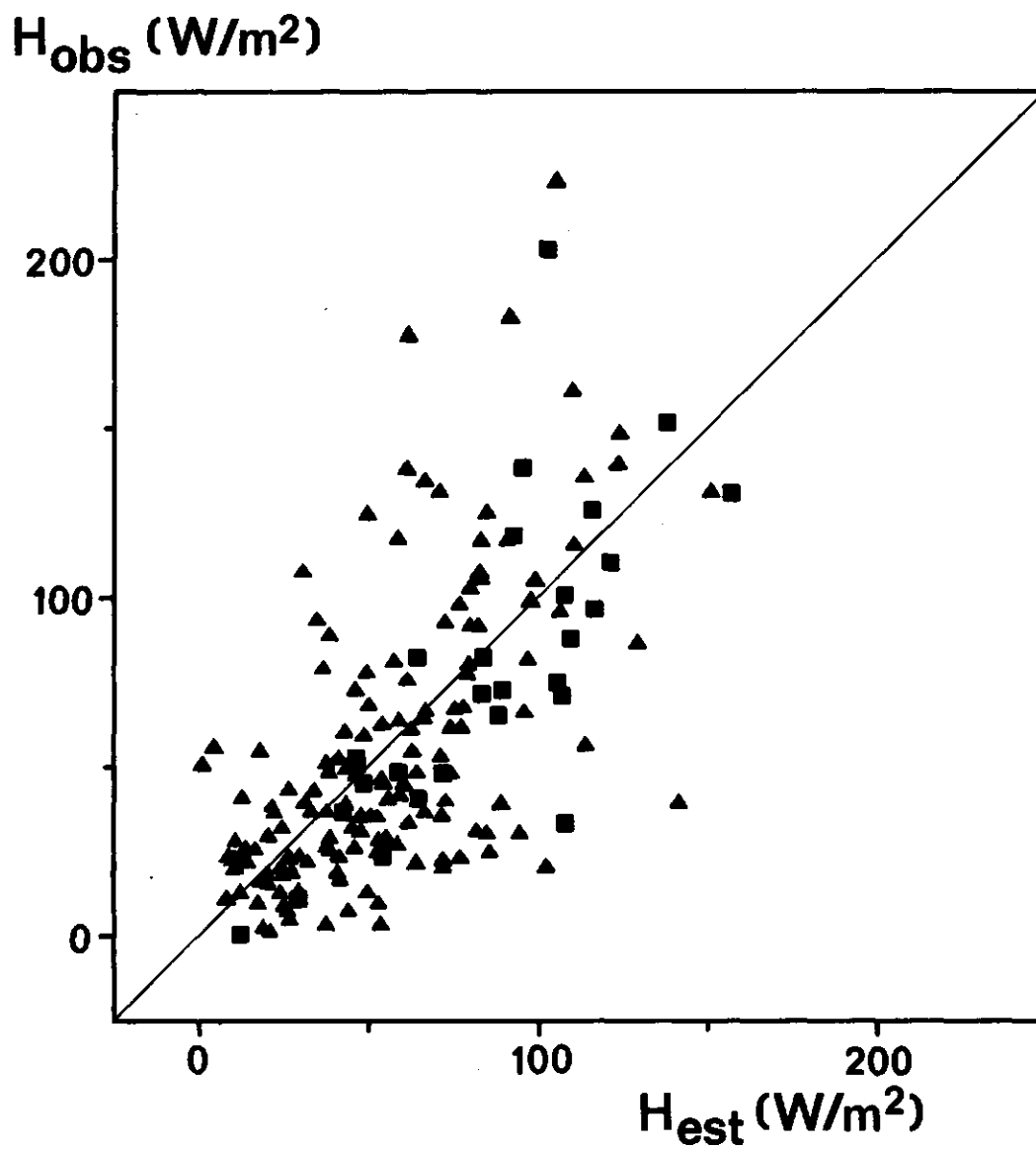
Fig. 6

As Fig. 5, but here H_{est} is obtained from (11), (13) and (14) with calculated values of K^+ using (1) and (2). See notes of Fig. 1.
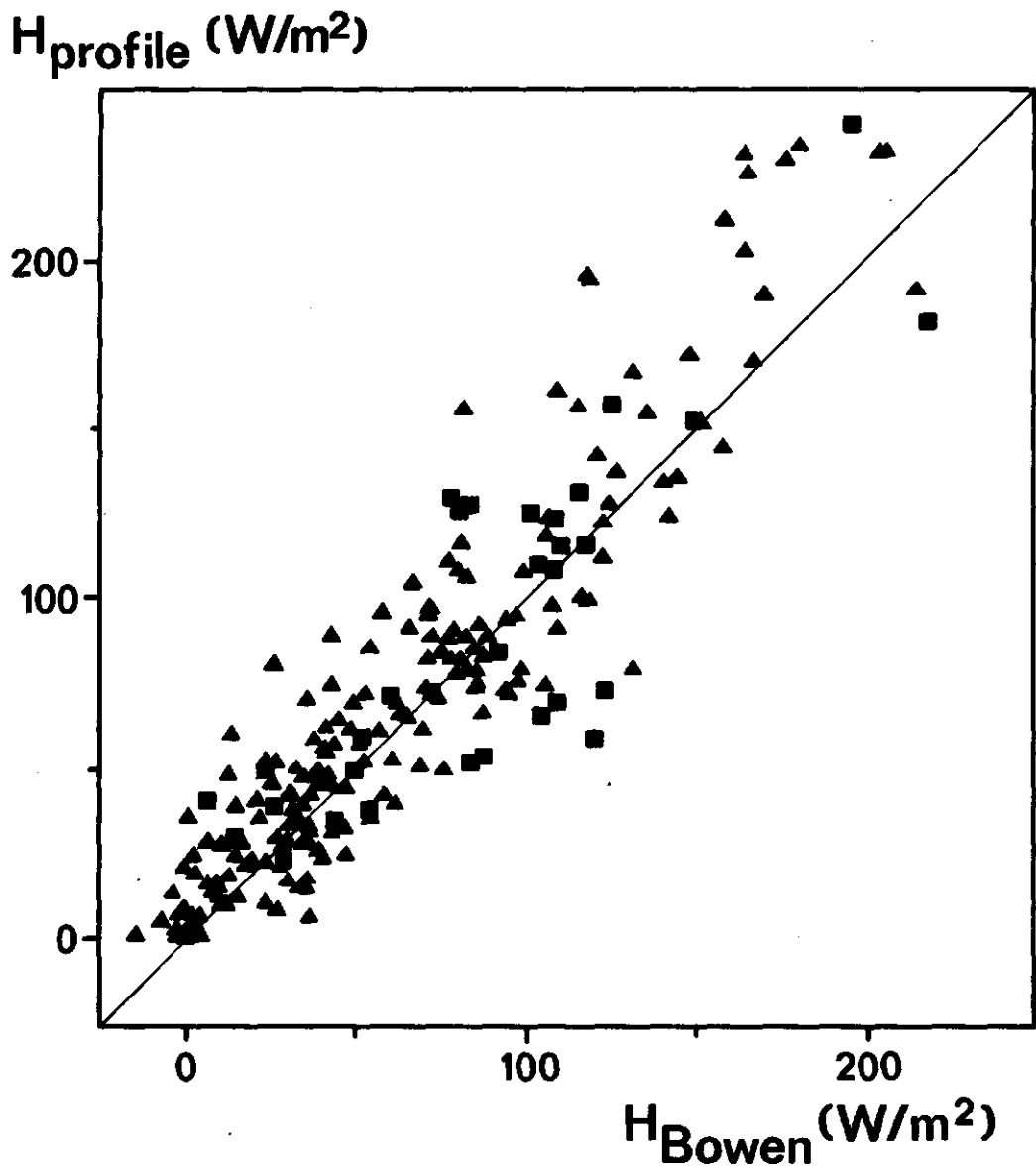
Fig. 7

Comparison of the sensible heat flux obtained from measurements using Bowen's ratio method (H_{Bowen}) with the sensible heat flux obtained from wind and temperature profiles ($H_{profile}$) during the summer of 1977. See notes of Fig. 1.

obtaining H from measurements. Therefore we conclude that (14) with $\alpha = 1$ and $\beta = 20$ Wm^{-2} produces in general rather good estimates for hourly values of H.

In appendix C an application of the scheme for H is given, by calculating the solar elevation for transition hours between stable and unstable conditions when H vanishes.

5. The momentum flux and the Obukhov stability parameter

Knowing the heat flux from the preceeding part of our scheme it is a small step to estimate the Obukhov length scale L and the surface momentum flux or shear stress. The latter quantity is here denoted by

$$\tau = \rho u_*^2, \tag{16}$$

where ρ is the density of air and u_* the friction velocity. Applying Monin-Obukhov similarity theory, u_* is related to the wind speed U_z at the height z by (see Dyer, 1974 and Paulson, 1970)

$$u_* = kU_z[\ln(z/z_0) - \psi_M(z/L) + \psi_M(z_0/L)]^{-1}, \tag{17}$$

where k is the Von Kármán constant (k = 0.41), z_0 the surface roughness length, ψ_M a stability function (defined in appendix A) and

$$L = - \frac{\rho \ C_p \ T \ u_*^3}{k \ g \ H}, \tag{18}$$

the Obukhov length scale. Here T is the air temperature, g the acceleration of gravity, ρ the density of air, C_p the specific heat at constant pressure, and H is the sensible heat flux. Principally, the virtual heat flux has to be used in Eq.(18), but the difference between this heat flux and H is small in our data set (see Busch, 1973).

From (17) and (18) u_* and L can be solved by iteration when T, H, z_0 and U_z are known. The surface roughness length (z_0) can be ob-

Table 7

Terrain classification by Wieringa (1980) in terms of aerodynamical
roughness length z_0

Class	Short terrain description	z_0 (m)
1	Open sea, fetch at least 5 km	0.0002
2	Mud flats, snow; no vegetation, no obstacles	0.005
3	Open flat terrain; grass, few isolated obstacles	0.03
4	Low crops; occasional large obstacles, $x/h > 20$	0.10
5	High crops; scattered obstacles, $15 < x/h < 20$	0.25
6	Parkland, bushes; numerous obstacles, $x/h \sim 10$	0.5
7	Regular large obstacle coverage (suburb, forest)	(1.0)
8	City center with high- and low-rise buildings	?-?

Notes: Here x is a typical upwind obstacle distance and h the height of
the corresponding major obstacles. Class 8 is theoretically not attractive
within the framework of boundary layer meteorology and can better be
modelled in a wind tunnel. For simple modeling applications it may be
sufficient to use only classes 1, 3, 5, 7 and perhaps 8.

tained from table 7 (see also section 6.5). To solve u_* and L we use
the following procedure. The sensible heat flux H is estimated with
(11), (13), (14) and measurements of K^+ or estimates of K^+ with (1)
and (2). The measured 10 m wind speed is used for U_z and for T the
air temperature at screen height (2 m) is used. The computation
starts with an estimate for u_* by way of (17), where we take in-
itially $\psi_M = 0$ ($L = \infty$). Then with (18) an estimate for L is obtained.
With this estimate again (17) is used to improve the estimate for u_*,
and so on. It appears that usually not more than three iterations are
needed to achieve an accuracy of 5% in successive values of L.

Using the above procedure we obtain very good results for the
friction velocity u_*. Notably the correlation coefficient between
estimates and values derived from profiles (see appendix A) $r = 0.99$
and the root mean square error $\sigma = 0.01$ ms^{-1}, which is 1.7% of the
observed average. The results for z_0/L are $r = 0.85$ and
$\sigma = 0.67 \times 10^{-3}$ which is 82% of the observed average. Here we have
used the estimated value for the incoming solar radiation K^+ with (1)
and (2) for the whole data set (number of observations n = 999). A
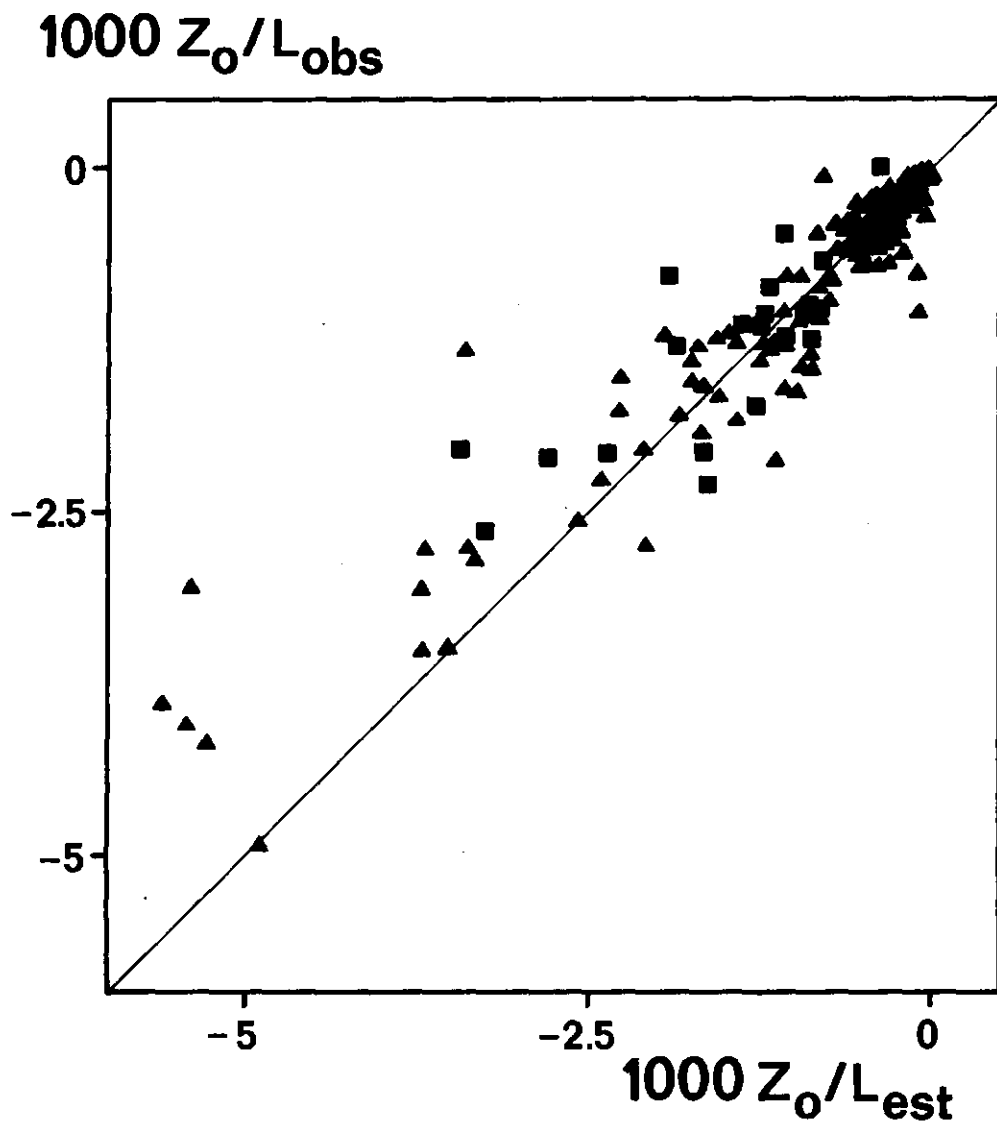
Fig. 8

Comparison of the similarity ratio z_0/L obtained from profiles of wind and temperature (z_0/L_{obs}) with the estimated value from the proposed scheme (z_0/L_{est}). See notes of Fig. 1.

random selection of the data for z_0/L is given in Fig. 8. It is seen that the agreement for clear skies and cloudy skies is comparable.

In section 4.2 we have seen that the relative skill for H improves with increasing instability. As a result also the relative skill of z_0/L improves. For the 179 very unstable cases with $-100 \leq L < -25$ or $-6 \times 10^{-3} < z_0/L \leq -1.5 \times 10^{-3}$ (see section 6.5) we obtain $\sigma = 1.02 \times 10^{-3}$, which is ~40% of the observed average. When measurements of K^+ are used in the scheme we obtain $\sigma \approx 0.83 \times 10^{-3}$, which is ~33% of the observed average.

Certainly there will be some bias in the above comparison, since in both measured values of u_* and L and estimated values of u_* and L the same wind speed data have been used (Hicks, 1981). However, it has been shown earlier that our profile measurements relate well to direct eddy correlation measurements of u_* (Nieuwstadt, 1978). With this in mind we can still conclude from the above comparisons, that with our scheme realistic estimates of u_* and L can be obtained.

6. Discussion on the surface parameters of the scheme

6.1 The surface albedo r

The albedo r describes the effect of the surface on the net incoming solar radiation, which is important in the surface radiation budget (3). In this study we have used a representative value for r of short grass. A more detailed evaluation of the albedo may take into account the dependence on solar elevation and the shortwave spectrum (Paltridge and Platt, 1976; Oke, 1978). In Oke (1978) and Burridge and Gadd (1977) values of r for other type of surface coverages can be found.

6.2 The ratio between soil heat flux and net radiation

The ratio between soil heat flux and net radiation c_G is small compared with 1 only during the day. We have used $c_G = 0.1$, which was obtained for a grass covered surface in The Netherlands (De Bruin and Holtslag, 1982). From measurements of the soil heat flux G and net radiation Q^* during the Prairie Grass experiment (Barad, 1958) we

have found that with $c_G = 0.1$ good results can be obtained. The root mean square error between measurements and estimates of G is $\sigma = 27$ Wm^{-2}, which is 7% of the observed average of $Q^* - G$ in the Prairie Grass experiment. Also, Burridge and Gadd (1977) use $c_G = 0.1$ for snow-free surfaces if $Q^* > 0$. For snow-covered surfaces Burridge and Gadd propose $c_G = 0$, which reflects the poor conductivity of snow. This subject certainly requires further investigation.

6.3 The surface moisture parameters α and β

In section 4 we have introduced the surface moisture parameters α and β. We have seen that with $\alpha = 1$ and $\beta = 20$ Wm^{-2} good results for the sensible heat flux H can be obtained for grass provided with enough water to evaporate. In this section we will discuss values for α and β for other surface moisture conditions.

For bare soil, for instance, we expect $\lambda E = 0$ when there is no water to evaporate. In (14) and (15) α and β are constants for given surface conditions. This can only be fulfilled by putting $\alpha = \beta = 0$ for $\lambda E = 0$. Taking these limits for α and β we may rewrite β of (14) and (15) as

$$\beta = \beta' \alpha, \tag{19}$$

where β' is the value for which $\alpha = 1$. Eq. (19) is in agreement with the value of β used in section 4 if $\beta' = 20$ Wm^{-2}. In general we may rewrite (15) for λE with the use of (19) as

$$\lambda E = \alpha\left[\frac{1}{1+\gamma/s} (Q^* - G) + \beta'\right]. \tag{20}$$

Here α can be computed by means of a regression analysis between observations of λE and $(Q^* - G)/(1+\gamma/s) + \beta'$. For instance for the Prairie Grass experiment (see Barad, 1958), we obtain $\alpha = 0.45$ if $\beta' = 20$ Wm^{-2} (correlation coefficient $r = 0.6$, root mean square error $\sigma = 56$ Wm^{-2} for λE, which is 40% of the observed average).

The advantage of (20) is that in principle only one parameter remains which depends on the surface moisture condition (notably α). The specific dependence of α on the moisture condition of the

surface awaits further examination. De Bruin (1983) presents a model for α in very unstable conditions. He shows that in these conditions α is primarily determined by the stomatal resistance. A further extension of De Bruin's approach is given by McNaughton and Spriggs (1986).

6.4 The surface heating coefficient

The surface heating coefficient c_3 of section 3.2 relates the difference between the surface radiation temperature T_s and the air temperature T to the net radiation Q^* as given in (8). On the other hand it is common practice to relate a surface temperature T_o and a air temperature T by (e.g. Monteith, 1981)

$$T_o - T = \frac{R}{\rho\ C_p}\ H\ .$$

(21)

Here R is the resistance for the flux of sensible heat H. In general R combines an atmospheric resistance and a surface resistance. The atmospheric resistance may depend on stability, wind speed, etcetera, as discussed by Thom and Oliver (1977). The surface resistance for sensible heat is still a matter of controversy (Garratt and Hicks, 1973).

The surface radiation temperature T_s of (8) may differ from the surface temperature T_o of (21). In the present context we need a relation between T_s - T and H. According to Fig. 2b it is seen that $4\sigma T^3(T_s - T) \approx 0$ for $Q^* = 0$, which with (13) and (14) yields $H + \beta = 0$. These findings suggest that (21) can be changed into

$$4\sigma T^3(T_s - T) = \frac{4\sigma T^3 R'}{\rho\ C_p}\ (H + \beta)\ ,$$

(22)

where R' is a modified resistance for sensible heat. In Fig. 2c we have compared $4\sigma T^3(T_s - T)$ with H. From this limited amount of data no possible wind speed influence could be detected. Apparantly R' is dominated by transfer processes in the surface vegetation layer.

When (22) is combined with (8), (13) and (14), we may write for the surface heating coefficient c_3

$$c_3 = \frac{4\sigma T^3 R'}{\rho C_p} (1 - c_G) (\frac{1-\alpha + \gamma/s}{1 + \gamma/s}) . \qquad (23)$$

This relation shows that c_3 may vary with the surface moisture parameter α. Further it is seen that soil properties are important (accounted for by R' and c_g) and the air temperature T. In section 3.2 we have used $c_3 = 0.12$, which was obtained from the data of Fig. 2b. With this value of c_3 very good results for Q^* were obtained, as shown in Fig. 3 and table 4a. Using our values for c_3, c_G, α and $T = 15°C$ (average temperature) we obtain $R' = 80$ ms^{-1}. The latter estimate is on the average in agreement with the data of Fig. 2c.

We finally compute values of the heating coefficient c_3 for other surface and climatic conditions. For the Prairie Grass experiment (Barad, 1958) we obtain $c_3 = 0.25$. This value is calculated with (23) using $\alpha = 0.45$ (section 6.2), $T = 27°C$ (average value for the Prairie Grass experiment), $c_G = 0.1$ and $R' = 80$ ms^{-1}. Further for bare soil we obtain $c_3 = 0.38$, using $\alpha = 0$, $c_G = 0.1$, $R' = 80$ ms^{-1} and $T = 27°C$.

The computed values of c_3 with (23) for the Prairie Grass experiment and bare soil agree surprisingly well with the values reported by Monteith and Szeicz (1961). Their values were obtained from a regression analysis between Q^* and $(1-r)K^+$ at clear skies. The above findings seem to indicate that (23) can be used for estimates of c_3 for short vegetation with $R' = 80$ ms^{-1}, $c_G = 0.1$ and varying values of α.

6.5 The surface roughness length z_0

The surface roughness length z_0 can be obtained from routine wind measurements with a method given by Wieringa (1976, 1980, 1983). This method relates z_0 either to the normalized standard deviation of wind speed, or to the ratio of the averaged wind speed observed in a given period and the maximum gust recorded during the same period. If no gustiness observations are available, a crude estimate of z_0 can be obtained from a visual terrain classification (table 7).

For our experimental site in Cabauw it appears that z_0 varies with wind direction between $z_0 = 0.06$ m and $z_0 = 0.25$ m, with a typical value of $z_0 = 0.15$ m on average.

7. Summary and conclusions

In this paper a simple empirical scheme is presented which relates the surface fluxes of heat and momentum to weather variables, either measured routinely or predicted by forecast models. The required input weather data are the air temperature, the total cloud cover and a single wind speed. The scheme is designed for a grass covered surface, but it contains parameters that can be adjusted to other coverages. An estimation scheme for the solar elevation is given which uses geographical position and time.

In the scheme the mean values of the surface radiation and energy budget are parameterized to obtain the sensible heat flux. From the sensible heat flux, a single wind speed and the surface roughness length, the flux of momentum in terms of the friction velocity is obtained, applying Monin-Obukhov similarity theory. The output of the scheme is compared with micrometeorological data, and finally the fluxes are compared with fluxes derived from profile data in unstable conditions.

For one year of observations at Cabauw, The Netherlands, we obtain a good agreement between observations and estimates. It appears that the root mean square error $\sigma = 90$ Wm^{-2} for the incoming solar radiation, $\sigma = 63$ Wm^{-2} for the net radiation, $\sigma = 34$ Wm^{-2} for the sensible heat flux, $\sigma = 0.01$ ms^{-1} for the friction velocity and $\sigma = 0.67 \times 10^{-3}$ for the similarity ratio between the surface roughness length and the Obukhov stability parameter (z_o/L). Moreover the scheme provides the latent heat flux. The results for the net radiation and the sensible heat flux are improved markedly when measured values for the incoming solar radiation are used.

Because of its simplicity and its fair agreement with observations we conclude that the scheme is useful for many applications in boundary layer meteorology. At present the scheme is applied in an air mass transformation model for short range weather forecasting (Reiff et al., 1984) and in a mesoscale air pollution transport model (Van Dop et al., 1982).

Appendix A
Fluxes and profiles

The fluxes of heat and momentum can be obtained from observed pro-
files of wind and temperature using the similarity relations for the
atmospheric surface layer (see Dyer, 1974). These relations are based
on Monin-Obukhov similarity theory, which assumes stationarity and
horizontally homogeneous conditions. The flux of momentum τ is re-
lated to the friction velocity u_* by

$$\tau = \rho \, u_*^2, \qquad (A1)$$

where ρ is the density of air. The flux of sensible heat H is related
to u_* and the temperature scale θ_* by

$$H = -\rho \, C_p \, u_* \, \theta_*, \qquad (A2)$$

where C_p is the specific heat at constant pressure. Nieuwstadt (1978)
gives a method based on least square estimates, which provides u_*
and θ_* from observed wind and temperature profiles. Then the fluxes
can be calculated from (A1) and (A2). However, this method is rather
complicated and time consuming on a computer.

In the following a simplified method is given of which the re-
sults are comparable to those from Nieuwstadt's method. We will use
the simplified method to compare the fluxes with the fluxes of the
proposed scheme in this paper. For the simplified method are needed:
a single wind speed U_z at level z, a surface roughness length z_o and
a temperature difference $\Delta\theta$ between the heights z_1 and z_2 in the
atmospheric surface layer. With these data u_* and θ_* can be calcu-
lated from the integrated flux-profile relations of Dyer and Hicks
(see Dyer, 1974 and Paulson, 1970)

$$u_* = k \, U_z [\ln(\frac{z}{z_o}) - \psi_M(\frac{z}{L}) + \psi_M(\frac{z_o}{L})]^{-1} \qquad (A3)$$

and

$$\theta_* = k \ \Delta\theta[\ln(\frac{z_2}{z_1}) - \psi_H(\frac{z_2}{L}) + \psi_H(\frac{z_1}{L})]^{-1}. \qquad (A4)$$

Here k is the Von Kármán constant, taken at $k = 0.41$, and L is the Obukhov stability parameter defined by

$$L = \frac{T \ u_*^2}{k \ g \ \theta_*}, \qquad (A5)$$

where g is accelaration of gravity and T is air temperature. For $L < 0$ (unstable) it reads:

$$\psi_M = 2 \ \ln(\frac{1+x}{2}) + \ln(\frac{1+x^2}{2}) - 2 \ \tan^{-1}(x) + \frac{\pi}{2}, \qquad (A6)$$

$$\psi_H = 2 \ \ln(\frac{1+x^2}{2}), \qquad (A7)$$

where

$$x = (1 - 16 \ \frac{z}{L})^{\frac{1}{4}}. \qquad (A8)$$

The fluxes H and τ can be obtained from the above equations starting with a prescribed value of the Obukhov stability parameter L. We have used $L = -36$. Then u_* and θ_* are calculated from (A3)-(A8). Using (A5), L is computed by using the estimated values of u_* and θ_*. The new value of L is substituted in (A3)-(A8) to obtain improved values for u_* and θ_*. This cycle is repeated until successive values of L do not change more than 5%. It appears that few cycles are needed (usually not more than 5) in order to achieve the required accuracy of 5% for L. Then H and τ are calculated with (A1) and (A2).

As input data we have used 30-minute averages of wind speed U_z at $z = 10$ m and the temperature difference $\Delta\theta$ between $z_2 = 10$ m and $z_1 = 0.6$ m from each second half hour of our data. The surface roughness length z_0 was obtained from gustiness, using a method by Wieringa (1976; see section 6.5).

It appears that this simplified method provides fluxes which are within a few percent to the results of Nieuwstadt (1978).

56

Appendix B

Procedure for estimating the solar elevation (ϕ)

The solar elevation (ϕ) for a given time and location may be calcu-
lated by simplifying well-known astronomical formulae. For a given
day the daynumber d may be crudely estimated from

$$d = 30 \ (M-1) + D, \qquad (B1)$$

where M is the number of the actual month (1-12) and D is the number
of the actual day in the month (1-31). From d the solar longitude
(SL) can be evaluated

$$SL = 4.871 + 0.0175 \ d + 0.033 \sin (0.0175 \ d), \qquad (B2)$$

where SL is in radians. The solar declination (δ) follows from

$$\delta = \text{arc} \sin (0.398 \sin (SL)). \qquad (B3)$$

Using the above estimates for d, SL and δ we can compute the hour
angle (h) through which the earth must turn to bring the meridian of
the given location directly under the sun

$$h = -\lambda_w + 0.043 \sin (2SL) - 0.033 \sin (0.0175 \ d)$$

$$+ 0.262 \ t - \pi, \qquad (B4)$$

where λ_w is the western longitude (in radians) of the location and t
is the universal time in hours. The solar elevation (ϕ) follows from
the above relations by applying (Sellers, 1965)

$$\sin(\phi) = \sin\delta \ \sin\psi + \cos\delta \ \cos\psi \ \cos h , \qquad (B5)$$

where ψ is the latitude of the location (in radians). With the above
scheme for the calculation of ϕ the accuracy for ϕ is within 0.05
radians, which is acceptable within the present context.

Appendix C

The solar elevation for which the surface heat flux vanishes

The solar elevation ϕ_O for which the atmospheric surface layer
changes from a stable to an unstable stratification can be calculated
from the proposed scheme. To this end H is taken zero in (14) and Q^*
is solved using (13). From the obtained value for Q^* we calculated K^+
from (11) and finally ϕ_O from (1) and (2). We have selected hours
with the actual solar elevation ϕ for which the absolute value of
$(\phi - \phi_O) \leq 5$ degrees and for which the sensible heat flux from
profiles (see appendix A) $H \leq 20$ Wm^{-2}.

Table 8 gives average results for the solar elevation ϕ_O and the
observed and calculated values of the sensible heat flux within each
class of total cloud cover (N). It is seen that the transition be-
tween stable and unstable conditions on the average takes place for
$\phi_O = 13$ degrees if $N \leq 0.75$, but that ϕ_O increases to 23 degrees for
overcast conditions (N = 1).

On the average ϕ should exceed the values of ϕ_O listed in table 8
to obtain an unstable atmospheric surface layer. For instance, during
wintertime in The Netherlands it is possible to have stable condi-
tions during the whole day if the sky is overcast.

Table 8

The dependence of the solar elevation in transition hours (ϕ_O) on total
cloud cover (N). H_1 and H_2 are the fluxes of sensible heat obtained from
profiles and calculated by way of the proposed scheme, respectively.

N	ϕ_O	$H_1(Wm^{-2})$	$H_2(Wm^{-2})$
0	13	-8	3
0.125	12	-4	1
0.25	12	-0	-1
0.375	12	-5	0
0.5	12	-7	4
0.625	13	-3	5
0.75	13	-3	1
0.875	15	-3	0
1	23	-2	-1

58

Chapter IV

APPLIED MODELLING OF THE NIGHTTIME SURFACE ENERGY BALANCE OVER LAND[*]

Abstract

In this chapter a semi-empirical scheme is proposed which relates the
nocturnal surface fluxes of sensible heat, latent heat and momentum
to routine weather data. The main components of the surface radiation
and energy balance over land are described on a (half-)hourly basis.
Observations over a grass-covered surface at Cabauw are used to
investigate proposals from literature and to develop new para-
meterizations. The input data of the scheme are total cloud cover,
and wind speed, air temperature and specific humidity deficit at
single heights in the atmospheric surface layer. A semi-empirical
expression is proposed for the estimation of the soil heat flux. Also
the relation between the surface radiation temperature and the tem-
perature at the level of the roughness length is described semi-
empirically. The output of the scheme is presented in terms of the
main forcing terms. On average, the agreement of the model quantities
with observations is reasonable. For instance, for clear skies with
total cloud cover $N \leq 0.25$, it appears that root mean square errors
are at best 9 W/m^2 for sensible heat flux, 6 W/m^2 for latent heat
flux, 9 W/m^2 for soil heat flux, 13 W/m^2 for net radiation and
1.8 K for surface radiation temperature. The temperature profile up
to 80 m is well described by the present scheme. A discussion is
given on the difference of the scheme with previous methods in
literature.

1. Introduction

The turbulent state of the nocturnal atmospheric boundary layer (NABL) is primarily determined by the surface fluxes of sensible heat and momentum. In NABL models, which are needed for e.g. air pollution studies and short term weather forecasts, the fluxes have to be parameterized in terms of routine weather data or in terms of output parameters of meteorological models.

It is the objective of this paper to present such a parameterization scheme for the surface fluxes of sensible heat, latent heat and momentum. For this, the complete surface radiation and surface energy budget are treated and parameterized. The scheme requires total cloud cover, and wind speed, air temperature and specific humidity deficit at single heights in the surface layer. The scheme can be regarded as the counterpart of the daytime scheme by Holtslag and Van Ulden (1983, Ch. III).

Venkatram (1980) proposed a very simple method for the evaluation of the surface flux of sensible heat. He showed that the turbulent temperature scale θ_* (for its definition see section 3) is more or less constant for clear sky conditions. Holtslag and Van Ulden (1982) generalized this approach and showed θ_* to be dependent on total cloud cover. Such a method appears to be suitable for the description of the nocturnal wind profile at Cabauw up to ~100m (Holtslag, 1984a; Ch. V) and the turbulent height of the NABL (Nieuwstadt, 1984b).

The drawback of Venkatram's approach and its variants, is that θ_* does not vanish at low wind speeds. The latter has to be expected for cases in which turbulence cannot be maintained, and is confirmed by observations (Van Ulden and Holtslag, 1983). Moreover, Venkatram's approach does not describe the entire energy balance at the surface.

Recently, Van Ulden and Holtslag (1983, 1985) presented a more complete model for the nocturnal energy budget. They showed that θ_* is approximately constant, within a certain range of wind speed. Moreover, the constant is directly related to the "isothermal" net radiation, which is primarily determined by total cloud cover. So, the model by Van Ulden and Holtslag can explain the empirical results of Venkatram (1980) and Holtslag and Van Ulden (1982).

The present study can be regarded as an extension of the work by Van Ulden and Holtslag (1983, 1985). Among other things, we modified their descriptions of soil heat flux and evaporation. Also the vertical water vapour transport within the soil layer is accounted for, which may cause dew at the surface (e.g. Monteith, 1963; Oke, 1978). Moreover, flux-profile relations are adopted and evaluated, leading to a better description of the nocturnal temperature profile in very stable conditions. For this, use has been made of the work by Hicks (1976) and others. In addition, we take into account that the sinks or sources of momentum, heat and radiation are at (apparent) different levels near the surface (e.g. Brutsaert, 1982).

In the last decades many micro-meteorological experiments have been carried out. Nevertheless, there are only few reliable observations of the surface fluxes during nighttime. The main reason for this is the fact that the absolute magnitude of the fluxes are often small and of the same order as the instrumental errors. Moreover, not all the quantities of the surface energy budget are completely understood (section 3). This means that large scatter is to be expected when model predictions and observations are compared.

In this study we will make use of a fairly complete data set collected at Cabauw (section 2). The set is used both for comparison and parameterization purposes. Therefore some of the proposed parameterizations need further verification at other sites. Nevertheless, we believe that the present methods will be useful for climatological studies, engineering design purposes, air pollution stability classification, etcetera.

Besides the different terms of the surface energy budget, also the surface radiation temperature is described by our model. The latter is defined as the temperature that determines the outgoing longwave radiation (see section 3.2). As such it is often used in remote sensing studies. Calculated values of this quantity are compared with direct observations of an infrared thermometer. Since, the entire temperature profile (inclusive the surface), is described by our approach, the model might be useful for agricultural studies as well (e.g. frost problems).

2. Data set

In this study we analyse observations from the 200 m tower and
the micro-meteorological field at Cabauw, The Netherlands. A
description of the Cabauw facilities can be found in Driedonks et al.
(1978). The Cabauw data sets are described by Wessels (1984), and
those collected at the micro-meteorological field by De Bruin and
Holtslag (1982). We use observations with optimum quality for the
period 1 March 1978 - 1 March 1979, with the sun below the horizon.

From the available data at the micro-meteorological field
(covered with short grass) we use net radiation, surface radiation
temperature and the soil heat flux. Net radiation Q^* is measured with
a "Funk"-pyrradiometer. The surface radiation temperature T_s is
obtained with a "Heimann"-infrared thermometer installed at about 2
meters above the grass surface. The soil heat flux is obtained from
heat flux plates and temperature differences in the soil top layer
using the method by Slob, as described by De Bruin and Holtslag
(1982). This method provides G_H at the surface due to conduction in
the soil and ignores the contribution by vapour movement within the
soil (G_v).

Along the main tower the temperature profile is available above
20 m. We have used the observations at the 40 m and 80 m level. Up to
20 m the temperatures were obtained from the auxiliary mast, as
reported by Wessels (1984). In our data set, total cloud cover N has
been taken as the average of four nearby synoptic stations. From the
available data at Cabauw we have taken 30 minute values around the
time of observation of N. Observational hours with rain or fog were
excluded from the present data set.

In the present data set the fluxes of sensible heat and momentum
are indirectly derived from observations at an auxiliary mast with
the profile method. This method is described by Holtslag (1984a, Ch.
V), except that here Eqs. (10) and (12) are used for the stability
functions of heat and momentum (see section 3.3). Below this method
is referred to as method 1. As input to method 1 we use a vertical
temperature difference between 10 m and 0.5 m; the 10 m wind speed
and an effective surface roughness length z_0. The latter is

determined with a method by Wieringa (1976). For the Cabauw surroundings typically $z_0 = 0.15$ m, which is substantially larger than values found for uniform grass. This is due to surface inhomogeneities. Nieuwstadt (1978) showed that the profile method using an effective roughness length, provided fluxes which are in good agreement with fluxes obtained from direct turbulence measurements.

The profile method 1 does not provide the latent heat flux λE. For the latter quantity we use data of the energy balance field. This is done with a profile method (method 2), using dry and wet bulb temperature differences between 0.45 m and 1.1 m, a wind speed at 2 m and the small scale roughness length of grass of - 1 cm (Wessels, 1984). Here it is assumed that the flux profile relations for sensible heat and water vapour transfer are equal. This method is thought to be more reliable than Bowen's ratio method (e.g. Oke, 1978), because of the generally low values of λE during nighttime and the large instrumental errors in e.g. Q^* and G_H.

A comparison between the two profile methods for the sensible heat flux H provides a rms difference $\sigma = 11.6$ W/m² on an average of - -31.5 W/m² for method 1 and -27.9 W/m² for method 2 (correlation coefficient $r = 0.74$, number of observations $n = 131$). This comparison refers to half hourly values for which the total cloud cover $N \leq 0.25$. The relatively large scatter between the two methods for the derivation of H from measurements, shows that its value cannot be determined very accurately. For that reason we will compare our model estimates with observations averaged in classes of the "forcing terms", e.g. total cloud cover, temperature at reference height, specific humidity deficit and wind speed.

In order to get an impression of the analysed data set, we have listed in table 1 the observed ranges and averages of the input parameters and some derived quantities. Here H from method 1 is listed and λE from method 2. The data are divided into classes of total cloud cover N. In this study we use data at "clear skies" ($N \leq 0.25$) and "cloudy skies" ($N \geq 0.75$) only.

Table 1
Observed ranges and averages of input parameters and model quantities
in the present data set. Upper case refers to clear skies (N ≤ 0.25)
and lower case to cloudy skies (N ≥ 0.75). The number of observations
are n - 193 and n - 312, respectively. For λE and T_s the numbers are
less (see tables 4a and 4b).

Quantity	Symbol	Unit	Range		Average
total cloud cover	N	-	0	0.25	0.13
			0.75	1.0	0.88
10 m wind speed	U_{10}	m/s	1.0,	8.0	3.0
			1.0,	9.7	4.0
air temperature at 2 m height	T_2	°C	1.6,	20.6	11.8
			0.8,	18.7	10.8
specific humidity deficit at 1.1 m in the air	δq_a	g/kg	0.3,	8	1.5
			0.2,	6	1.1
neutral estimate of friction velocity	u_{*N}	m/s	0.1,	0.8	0.3
			0.1,	1.0	0.4
isothermal net radiation	Q_i^*	W/m^2	-92,	-52	-83
			-49,	-18	-39
net radiation	Q^*	W/m^2	-85,	-14	-56
			-70,	0	-22
surface sensible heat flux	H	W/m^2	-100,	0	-25
			-88,	0	-23
surface latent heat flux	λE	W/m^2	-22,	28	- 6
			-24,	52	8
soil heat flux at the surface due to conduction only	G_H	W/m^2	-56,	12	-20
			-38,	14	- 8
surface radiation temperature	T_s	°C	-1.0,	15.7	7.9
			-4.0,	15.1	8.4
air temperature at 50m height	T_{50}	°C	3.5,	22.1	13.5
			1.3,	18.7	11.0

3. The model

3.1 General

The surface energy balance over land can be written as

$$H + \lambda E + G = Q^*,\qquad\qquad (1)$$

where H and λE are the fluxes of sensible and latent heat (defined positive upwards), G is the soil heat flux and Q^* is the net radiation. The latter two energy densities are defined positive downwards.

The net radiation Q^* reflects the net radiative heat loss, that cools the surface relatively to the air and soil layers beneath. So Q^* can be considered as the driving force of the energy balance at the surface (1). During nighttime Q^* is given by

$$Q^* = L^+ - L^-.\qquad\qquad (2)$$

Here L^+ denotes the incoming longwave radiation from the atmosphere, which is generally governed by the profiles of temperature and humidity in the atmosphere, and the contribution by clouds. This means that L^+ can be considered as an independent quantity, which is not directly effected by processes near the surface.

The outgoing longwave radiation from the surface, L^-, depends primarily on the surface temperature. It can be regarded as a dependent quantity, since the surface temperature is also related to the surface fluxes of heat and to the soil heat flux. A suitable measure for the independent parameters determining the net radiation is the isothermal net radiation, Q_i^*. This is the net (longwave) radiation that would occur at the surface, if the air in the lower atmosphere, between a reference level z_r and the surface would be isothermal (Monteith, 1981).

Due to radiative cooling at the surface, generally the air will be stably stratified. This implies that turbulence generated by surface friction, will be suppressed. For small wind speeds this results in weak turbulence and therefore low values for the fluxes of
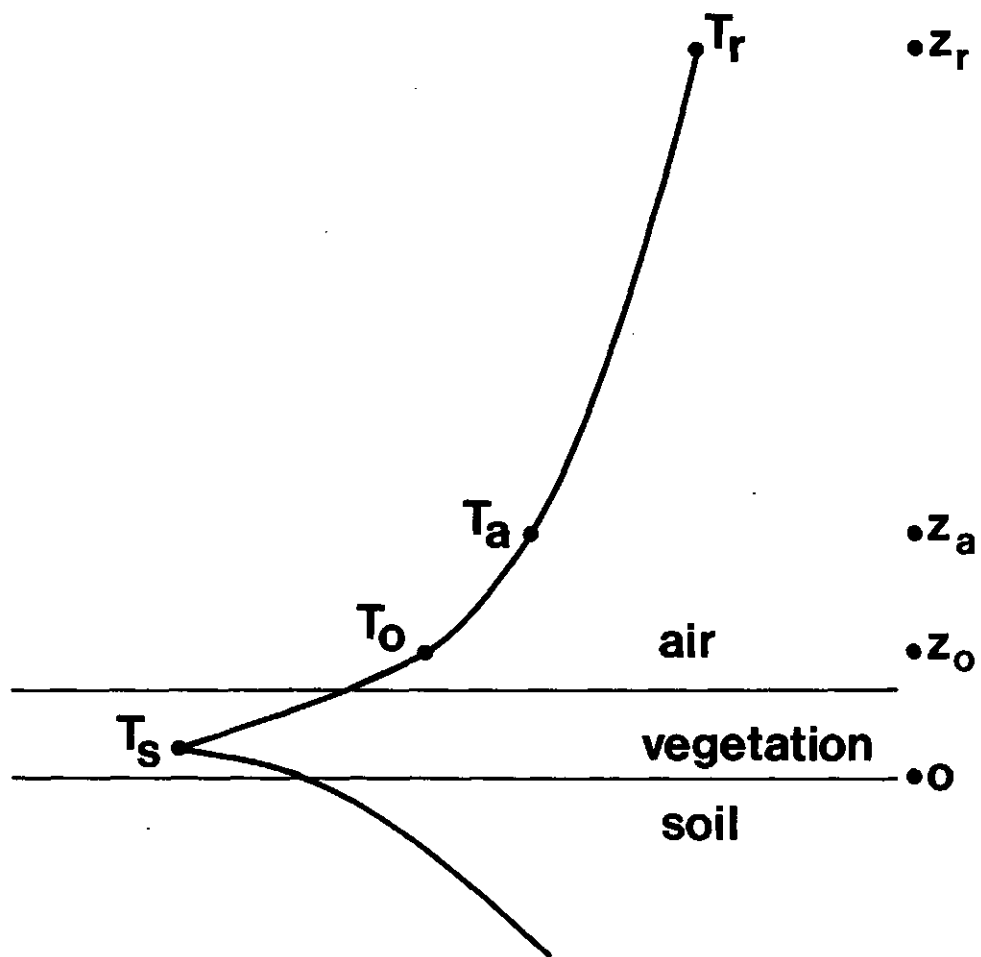
Fig. 1.
Schematic view of the temperature profile with indicated temperatures
as explained in the text. At the right hand side the heights above
the soil surface are indicated.

sensible and latent heat are expected. At the same time large gradients occur in the profiles of wind, temperature and humidity. For larger wind speeds the gradients are less and the fluxes are larger. These phenomena will be described with flux-profile relationships.

Due to the radiative cooling at night the surface temperature may fall below that of the contacting moist air. The ensuing condensation on the surface gives rise to an inverted vapour lapse rate so that turbulence leads to a downward flux of water vapour, known as dew fall (Oke, 1978). This phenomenon is confined to a limited range of wind speeds. For small wind speeds turbulence cannot be maintained and dew fall vanishes. On the other hand, for larger wind speeds the surface is heated by a downward heat flux, which tends to destroy the vapour inversion. Then the water vapour transfer can be upwards. In this respect the nocturnal situation differes from that during daytime, since then generally only evaporation occurs.

An important feature of the nocturnal energy balance is the fact that the soil heat flux G is not small compared to the other energy budget terms. Moreover, G is not fully understood. In particular, the contribution to G of water and water vapour transport in the soil is not completely known and rather difficult to model (Ten Berge, 1986). An other complication is that G depends on soil parameters (such as thermal conductivity and heat capacity), which show a large spatial variability. For these reasons we will describe the soil heat flux semi-empirically.

The condensation of water vapour from the soil at the vegetation of the surface is called <u>destillation</u> or <u>dew rise</u> (Monteith, 1963). At low wind speeds dew rise can be as effective as dew fall to wet the vegetation. We will account for dew rise in our approach in a simple empirical way. Unfortunately, no direct measurements of dew rise are available in our data set.

The quantities of the surface radiation and energy budget are re-lated to the temperature profile of the atmospheric surface layer and that within the soil. In our model these profiles are described as shown in Fig. 1. Firstly, we distinguish the surface radiation tempe-rature T_s, which is thought at a level within the vegetation layer.

Secondly, we define T_0 as the temperature at the level of the surface roughness length for momentum z_0. Next, T_a is the air temperature at screen height (z_a) and T_r is the air temperature at a reference height z_r. The latter height is chosen above the layer in which normally strong temperature gradients occur. Here we took $z_r = 50$ m.

In the next sub-sections we propose parameterizations and relations for all the quantities of the surface radiation and energy budget, in terms of the temperatures shown in Fig. 1 and other input data. With these proposals we can solve the surface energy balance in relation with the atmospheric temperature profile up to z_r (see section 5).

3.2 The net radiation

The incoming longwave radiation, L^+, can be written as

$$L^+ = \epsilon_r \sigma T_r^4, \tag{3}$$

where ϵ_r is the apparent emissivity of the atmosphere, σ is Stefan-Bolzmann's constant and T_r the air temperature at level z_r.

At clear skies L^+ is determined by the contribution of the gaseous atmosphere (mainly water vapour and carbon dioxide). A suitable parameterization of ϵ_r for clear skies is given by Swinbank (1963):

$$\epsilon_{ro} = c_1 T_r^2, \tag{3a}$$

where $c_1 = 9.35 \ 10^{-6} K^{-2}$ is an empirical constant. Often the screen height (1-2 m) temperature is used instead of T_r. As discussed by Swinbank (1964), however, T_r should be taken above the layer where strong temperature gradients occur. Van Ulden and Holtslag (1983, 1985) found that $z_r = 50$ m is a suitable choice.

In the presence of clouds L^+ increases. For mid-latitudes, Paltridge and Platt (1976) proposed:

$$\epsilon_r = \epsilon_{ro} + c_2 \ N/\sigma T_r^4, \tag{3b}$$

where N is total cloud cover, ϵ_{ro} is given by (3a) and c_2 = 60 W/m^2. For T_r = 280 K we obtain with Eqs. (3a) and (3b), ϵ_r = 0.73 at clear skies (N = 0) up to ϵ_r = 0.90 at total overcast (N = 1).

We compared estimates of L^+ given by Eqs. (3) - (3b) with L^+ obtained from observations. For the estimates we have used the temperature at 50 m height (interpolated between 40 m and 80 m temperature observations). Since, direct measurements of L^+ appear to be unreliable (Wessels, 1984), we took $Q^* + \sigma T_s^4$ as the "observed" value where Q^* and T_s are observed at the micro-meteorological field. We note that this will introduce additional inaccuracy in our comparison for L^+. Both for clear and cloudy skies (N ≤ 0.25 and N ≥ 0.75, respectively) no systematic errors were found, whereas the rms error was 15 W/m^2 and 18 W/m^2, respectively (the mean values appear to be 300 W/m^2 and 340 W/m^2, respectively).

If the temperature at screen height is used in Eqs. (3)-(3b), the rms error is only slightly larger at clear skies (σ = 16 W/m^2). However, L^+ is underestimated by ~10 W/m^2. These results confirm Swinbanks (1964) arguments for using a temperature above screen height.

Eqs. (3a)-(3b) do not contain the water vapour pressure. Indeed in our data set no significant variation of L^+ with water vapour pressure could be detected. It must be noted, however, that in the present data set the relative humidity always exceeded 60 percent (at 1.1 m). In that case the water vapour pressure is interrelated with the air temperature, because the saturated water vapour pressure is temperature dependent. For lower values of the relative humidity a moisture influence in ϵ_r might be relevant, see e.g. Brutsaert (1982).

The outgoing long wave radiation from the surface L^- is given by Stefan-Boltzmann's law as

$$L^- = \epsilon_s \sigma T_s^4, \qquad (4)$$

where ϵ_s is the emissivity of the surface and σ is Stefan-Boltzmann's constant. For grass a good approximation is ϵ_s = 1 (Brutsaert, 1982) and this value is adopted here.

Combination of Eqs. (2)-(4) provides an expression for the net radiation Q^*, which can be linearised.
This results in

$$Q^* = Q_i^* + 4\sigma T_r^3 (T_r - T_s),$$ (5)

where Q_i^* is defined by

$$Q_i^* = -\sigma T_r^4 (\varepsilon_s - \varepsilon_r).$$ (5a)

Q_i^* is the isothermal net longwave radiation (Monteith, 1981). During nighttime this is the net radiation that would occur if the lower atmospheric layer is isothermal (i.e. $T_r = T_s$).

The last term in Eq. (5) accounts for the temperature difference that normally occurs between z_r and the surface. As discussed by Van Ulden and Holtslag (1983, 1985) this term is important under stable conditions.

3.3 The temperature profile in the lower atmosphere

In the atmospheric surface layer a temperature difference $T_2 - T_1$ between two levels z_2 and z_1 is given by (Monin and Yaglom, 1971):

$$T_2 - T_1 = \frac{\theta_*}{k} \left\{ \ln(\frac{z_2}{z_1}) - \psi_H(\frac{z_2}{L}) + \psi_H(\frac{z_1}{L}) \right\} - \Gamma_d(z_2 - z_1),$$ (6)

where k is the Von Kármán constant, Γ_d is the dry adiabatic lapse rate and ψ_H is a function of z and the Obukhov length scale L, defined by (Obukhov, 1946)

$$L = \frac{u_*^2}{k \frac{g}{T} \theta_*}.$$ (7)

Here g is acceleration of gravity and T is absolute air temperature (at $z = z_a$ for instance). Furthermore, θ_* is the turbulent temperature scale, which follows from

$$H = -\rho C_p u_* \theta_*,$$ (8)

where ρC_p is the volumetric heat capacity of the air and u_* is the friction velocity.

The friction velocity u_* can be related to a wind speed U_z at level z by a similar expression as (6):

$$u_* = \frac{k \, U_z}{\ln(\frac{z}{z_o}) - \psi_M(\frac{z}{L}) + \psi_M(\frac{z_o}{L})} , \qquad (9)$$

where z_o and ψ_M are the surface roughness length and the stability function for momentum, respectively.

For the atmospheric surface layer the stability functions ψ_H and ψ_M are usually given by

$$\psi_H = \psi_M \qquad (10)$$

and

$$\psi_M = -5 \, z/L, \qquad (11)$$

which are adequate for $z/L \lesssim 0.5$ (e.g. Dyer, 1974). For larger values of z/L several empirical forms are proposed in literature. Carson and Richards (1978) reviewed the topic and concluded that (10) remains applicable and that the findings of Hicks (1976) are most suitable to describe ψ_M. The latter has been confirmed by Holtslag (1984a; Ch. V) for Cabauw wind profiles up to $z/L \approx 10$.

Carson and Richards (1978) also proposed analytical approximations to the findings of Hicks (1976) in three intervals of z/L. We have found that one expression is able to describe the entire range of z/L. The result is

$$-\psi_M = a\frac{z}{L} + b(\frac{z}{L} - \frac{c}{d}) \exp(-d\frac{z}{L}) + \frac{bc}{d}, \qquad (12)$$

where $a = 0.7$, $b = 0.75$, $c = 5$ and $d = 0.35$. Eq. (12) is similar to the one proposed by Van Ulden and Holtslag (1985) for $z/L \lesssim 10$. For larger values of z/L, Eq. (12) results in linear profiles for wind

and temperature if it is used in combination with Eq. (9) and
Eq. (6), respectively (see section 4).

With (6), (10) and (12) it is possible to describe the
temperature profile above the surface layer for strong stability. An
experimental verification with our data is given in section 6.

3.4 The surface fluxes of sensible and latent heat

The surface fluxes of sensible and latent heat can be evaluated
with resistance or transfer equations between the surface and a level
in the atmospheric surface layer. Combination of the latter formula-
tions with the energy budget of Eq. (1) leads to a "combination"
equation for λE, which can be written as (Slatyer and McIlroy, 1961;
Monteith, 1981)

$$\lambda E = \frac{s}{s+\gamma} (Q^*-G) + \frac{\rho c_p}{s+\gamma} (\delta q_a - \delta q_s) D_{sa} u_*. \qquad (13)$$

Here s is the slope of the saturation specific humidity curve
($s = \partial q_{sat}/\partial T$), γ is the psychrometer constant ($\gamma = C_p/\lambda$), and δq_a
and δq_s are defined by

$$\delta q_i = q_{sat}(T_i) - q_i, \qquad (14a)$$

where $q_{sat}(T_i)$ is the saturation specific humidity at temperature T_i
($i = s, a$). The specific humidity deficit of the air δq_a can be
written as

$$\delta q_a = (s + \gamma)(T_a - T_{wa}), \qquad (14b)$$

where T_{wa} is the wet bulb temperature of the air at z_a.

Furthermore, D_{sa} of Eq. (13) is a transfer coefficient for the
air between the surface and level z_a within the surface layer. Often
$D_{sa} u_*$ is written as $1/r_a$, where r_a is the aerodynamic resistance for
sensible and latent heat. We prefer the use of $D_{sa} u_*$ because then the
influence of u_* on λE is made explicitly.

The sensible heat flux density reads as

$$H = -\rho C_p \, D_{sa} \, u_*(T_a - T_s).$$
<div align="right">(15)</div>

It is assumed that D_{sa} is equal for latent and sensible heat transfer. We will evaluate D_{sa} with our data in the next sub-section.

Note that Eq. (13) in its form is quite similar to the usual Penman-Monteith equation (Monteith, 1981). The advantage of Eq. (13) is that some special cases are more easily recognised. For instance, in equilibrium conditions with a constant specific saturation deficit, e.g. $\delta q_a = \delta q_s$, we note that the second term of the RHS of Eq. (13) cancels. In such cases the Bowen ratio is given by $B_o = H/\lambda E = \gamma/s$. The latter expression is only a function of temperature and this equation can be used as a first estimate of B_o in practical situations (Priestley and Taylor, 1972; De Bruin and Holtslag, 1982).

In connection with nighttime dew fall above a land surface, Monteith (1963) has called the equilibrium value $\lambda E = \frac{s}{s+\gamma} (Q^* - G)$, the "potential" rate of dew formation. Monteith argues tat this value is the maximum fall from the atmosphere on the vegetation. For clear sky conditions and $G = 0$, the maximum value is about 0.07 mm water per hour, which is equivalent with $-\lambda E \approx 50$ W/m². For the Wangara experiments, Hicks (1983) confirms that this maximum fall is never exceeded. This can be explained by the fact that normally $G \neq 0$ and $\delta q_a > \delta q_s$. Here we note that for dew fall the surface will be close to saturation e.g. $\delta q_s = 0$.

For large values of $\delta q_a - \delta q_s$ or u_*, λE can be positive due to transpiration of the vegetation. In that case

$$\delta q_s = \frac{\gamma \lambda E}{\rho C_p} r_c,$$
<div align="right">(16)</div>

where r_c is the canopy resistance (Monteith, 1981). During nighttime r_c is expected to be large. After experimentation with different values we have adopted $r_c \approx 500$ s/m. The total evaporation from the surface is calculated as the sum of the transpiration from the vegetation and the contribution of the vapour flux from the soil (see below). Results are presented in section 5.

Fig. 2.
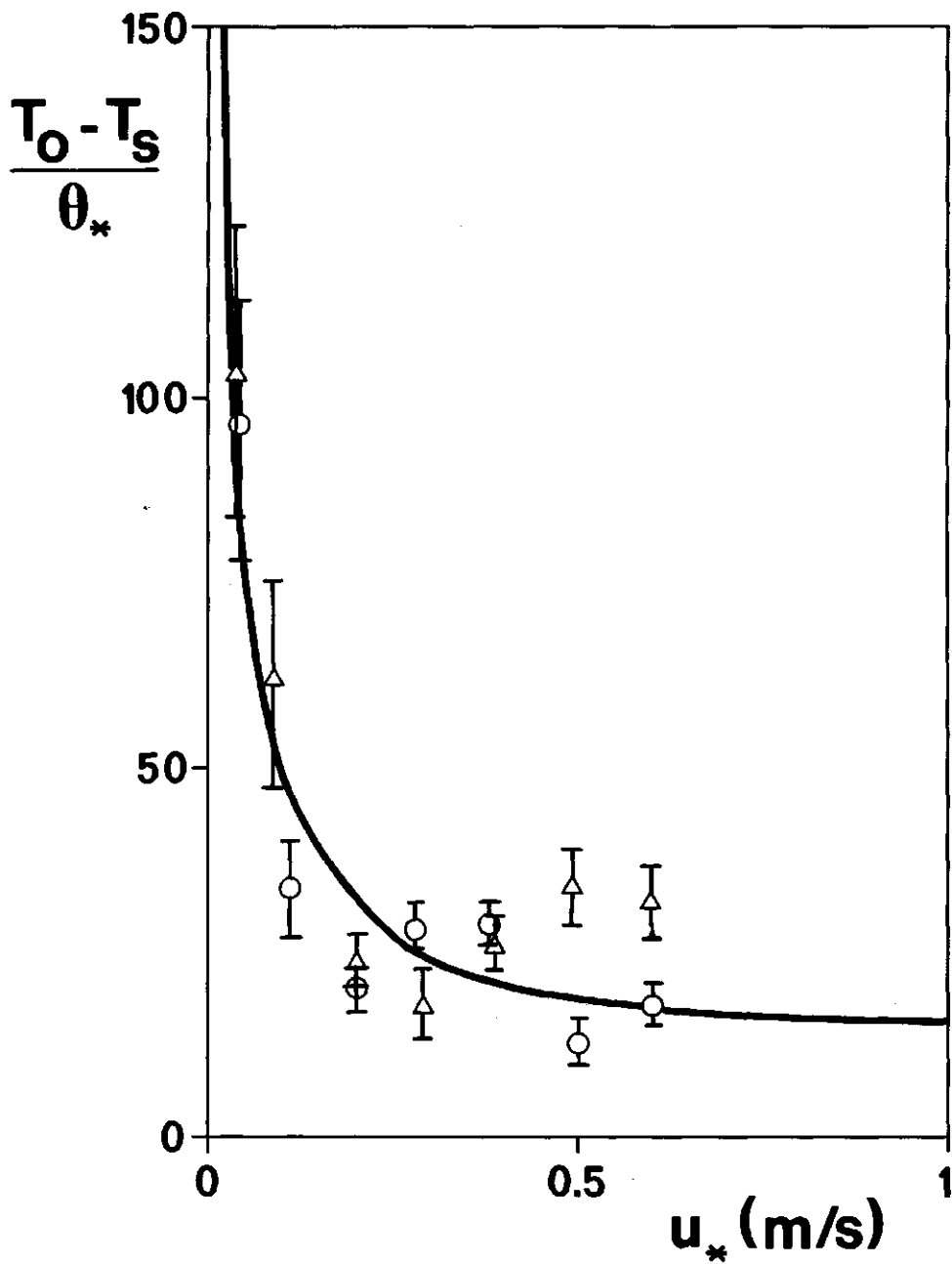
The normalised temperature difference $(T_o - T_s)/\theta_*$ near the surface as a function of friction velocity u_* for clear skies ($N \leq 0.25$). A distinction is given for cases with specific humidity deficit $\delta q_a < 1$ (dots) and $\delta q_a \geq 1$ (triangles). The average values for δq_a are 0.66 g/kg and 2.2 g/kg, respectively. The indicated line is given by Eq. (18).

3.5 The transfer coefficient D_{sa}

In the preceeding sub-section we have defined a transfer coefficient D_{sa} between the surface and a level z_a in the surface layer. From (8) and (15) it follows that $(T_a - T_s)/\theta_* = D_{sa}^{-1}$. Since $T_a - T_s = (T_a - T_o) + (T_o - T_s)$ we may write

$$\frac{1}{D_{sa}} = \frac{T_a - T_o}{\theta_*} + \frac{T_o - T_s}{\theta_*} , \qquad (17)$$

where T_a, T_o and T_s are given in Fig. 1. Eq. (17) shows that D_{sa}^{-1} refers to the transfer processes of two adjacent layers. The first term at the RHS of Eq. (17) is the normalised temperature difference across the lower part of the surface layer and is described by Eq. (6) between $z_2 = z_a$ and $z_1 = z_o$.

For the evaluation of the second term at the RHS of (17), we followed an empirical approach; T_o is derived by extrapolating Eq. (6) downwards to the level of the effective surface roughness length of momentum z_o. This is done by using observations of air temperature at 2 m and the fluxes derived with profile method 1 (section 2). T_s is measured directly with a infrared thermometer installed a few meters above the surface (Wessels, 1984). Analysing the available data set we found that

$$\frac{T_o - T_s}{\theta_*} = c_v + \frac{u_o}{u_*}, \qquad (18)$$

where c_v and u_o are empirical coefficients. In Fig. 2, Eq. (18) is indicated with $c_v = 10$ and $u_o = 4.2$ m/s. Probably c_v and u_o are dependent on the surface roughness length z_o and on transfer mechanisms within the canopy sublayer. Unfortunately, our data does not allow further examination.

From Fig. 2 it can be seen that Eq. (18) describes the observations reasonable well. In this figure the observations are represented by averages in classes of u_*. The indicated error bars are obtained with $\sigma/\sqrt{n}$, where σ is standard deviation and n is the number of observations within each class.

The sudden increase of $(T_o - T_s)/\theta_*$ for low u_* in Fig. 2, is striking. On the average $(T_o - T_s) \approx 6$ K for $u_* \approx 0.05$ m/s. So strong temperature differences appear within the canopy sub-layer at low wind speed. For $u_* > 0.3$ m/s our results show $(T_o - T_s) \approx 1$ a 2 K.

In literature often $(T_o - T_s')/\theta_* = B^{-1}$, is denoted (e.g. Garratt and Hicks, 1973). Here T_s' is the surface temperature which acts as the source or sink for sensible heat. Brutsaert (1982) concludes that typically $B^{-1} \approx 6$ for homogeneous grass covered surfaces. Our findings, however, show that $(T_o - T_s)/\theta_* \approx 20$ if $u_* \geq 0.3$ m/s, which is more than 3 times larger. A similar value has been used by Van Ulden and Holtslag (1983, 1985) for all values of u_*.

The difference between our findings and those in literature can probably be explained by the fact that we have used a larger scale roughness length for the derivation of u_* and that $T_s \neq T_s'$. The latter has been obtained also by Keijman and De Bruin (1979) for Cabauw observations during daytime. This subject certainly needs more investigation. For the time being we adopt Eq. (18) as a practical relation for the estimation of $T_o - T_s$.

3.6 The total soil heat flux

During nighttime the soil heat flux G_z is generally directed upwards and is primarily determined by conduction. It is described by

$$G_z = - k_s \frac{\partial T_z}{\partial z}, \tag{19}$$

where T_z is a soil temperature at depth z and k_s is the "apparent" thermal conductivity of the soil. This conductivity may differ from the usual conductivity due to vapour movement in the soil. Condensation of vapour at the soil surface or at the vegetation provides an additional energy term in the energy budget, which can be taken into account by increasing the heat flux of conductivity. The corresponding wetting of the vegetation is known as destillation or dew rise (Monteith, 1963).

Combination of (19) with an equation for conservation of heat in the soil, provides the well known diffusion equation. This equation

76

can be solved for a given initial temperature profile and a boundary condition, which results in a variation of G_z and T_z with z for given properties of the soil (e.g. Groen, 1947; Van Wijk and Derksen, 1963, Ten Berge, 1986). Such a solution of the diffusion equation, however, is rather complicated for practical applications, and most times the required input parameters are not available. For that reason we search for a simple empirical relation for G.

A simple estimate for G has been proposed by Van Ulden and Holtslag (1983, 1985)

$$G = -a_G \, (T_b - T_s),$$ \hfill (20)

where a_G = 5 W/m², T_b is a reference temperature not to deep in the soil and T_s is the surface radiation temperature. In general such a simple relation will give serious errors, because normally phase shifts occur between G and $T_b - T_s$ due to the diurnal cycle (e.g. Van Wijk and Derksen, 1963). However, in the case of a vegetated surface the heat flux passes through a layer with a low thermal conductivity and a low heat capacity in comparison with that of the soil material. These aspects will reduce the phase shift in general.

For the application of Eq. (20), T_b is needed. As a first guess Van Ulden and Holtslag (1985) took $T_b = T_r$, where T_r is the reference temperature at 50 m (see Fig. 1). In table 2 results are given from a comparison of G_H with $T_r - T_s$ for the present data set. It is seen that the estimate of G_H with Eq. (20) causes serious errors, which are probably caused by the approximation $T_b = T_r$. It should be noted that G_H reflects heat conduction in the soil only.

In table 2 also a comparison is given of G_H with net radiation Q^*, and sensible heat flux H. In the comparison of G_H with Q^* the parameter b in table 2 is found not to be significant on the 5% level. Over all, the observations suggest $G_H \sim 1/3 \, Q^*$, which confirms the findings of Nickerson and Smiley (1975) for nighttime cases. This estimate for G_H, however, is not consistent with the surface energy budget of Eq. (1) in very stable conditions. In such conditions we expect that the surface fluxes are small and therefore $G \approx Q^*$!

Table 2
Comparison of G_H with $T_r - T_s$ (T_r is taken on the 50 m height), Q^* and H for our data set. Values are given for the regression coefficients a, b and c in $G = aX + b$ and $G = cX$, where X is one of the independent variables. Further, σ_1 and σ_2 are the rms errors in the regressions, respectively; $\bar{x}$ is the average value, n is number of observations and r is the correlation coefficient. For each variable the left colomn shows the results for clear skies (N $\leq$ 0.25) with $\bar{G} = -19.6$ W/m^2 and the right colomn refers to cloudy skies (N $\geq$ 0.75) with $\bar{G} = -8.4$ W/m^2.

X	$T_r - T_s$ (K)		Q^*(W/m^2)		H(W/m^2)	
n	134	210	193	312	193	312
$\bar{x}$	4.9	1.4	-55.9	-22.0	-25.0	-22.3
r	- 0.14	0.27	0.22	0.48	- 0.47	- 0.40
a	- 0.58	1.62	0.20	0.26	- 0.25	- 0.23
b	-17.0	-10.2	- 8.4	- 2.8	-25.9	-13.6
σ_1	9.7	8.7	9.1	7.3	8.3	7.6
c	- 3.4	- 1.7	0.34	0.34	0.44	0.19
σ_2	12.3	11.5	9.2	7.5	16.8	10.6

In Fig. 3 a comparison is given between observations of G_H and H for the two classes of total cloud cover and two classes of specific humidity deficit in the air at 1.1 m height (δq_a). All the points represent averages for given values of H. Also the error bars for each average are indicated, as in Fig. 2. It is seen that a linear relation is a fairly good approximation for the two classes of N, while the influence of δq_a appears to be insignificant. In this way we arrived at

$$G_H = -a_G H + b_G Q_i^*. \qquad (21)$$

Here $a_G = 1/4$, $b_G = 1/3$, and Q_i^* is the isothermal net radiation of Eq. (5a). The rms error of this estimate is about 8 W/m^2.

According to Eq. (21), $|G_H|$ and $|H|$ are correlated negatively for given values of Q_i^*. This can be explained as follows. If for some reason T_s decreases as a response on an atmospheric forcing, $|G_H|$

78
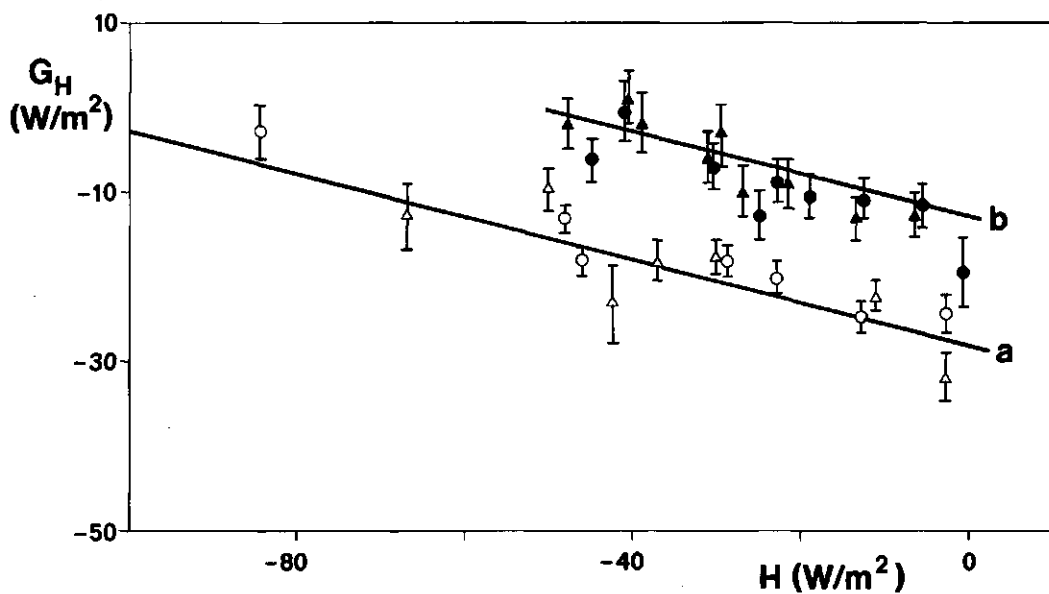
Fig. 3.

The soil heat flux due to conduction G_H as a function of sensible heat flux H for clear skies (a) and cloudy skies (b). A distinction is made in two classes of specific humidity deficit δq_a as in fig. 2. The indicated lines are given by Eq. (21), with $Q_i^* = -83$ W/m² for clear skies and $Q_i^* = -39$ W/m² for cloudy skies.

will increase due to a larger temperature difference. This is the case, because in the soil the temperature responses more slowly to atmospheric variations then T_s. On the other hand, a decrease of T_s relative to T_r means a more stable stratification in the atmospheric surface layer e.g. $|H|$ decreases. Similarly an increase of T_s will lead to a decrease of $|G_H|$ and an increase of $|H|$. In very stable conditions Eq. (21) provides $G_H = 1/3 \; Q_i^*$. This limit will be discussed into more detail in section 4.

As noted before, G_H of Eq. (21) is the soil heat flux due to conduction only. To account for the influence of the water vapour movement in the soil we write

$$G = G_H + G_v, \tag{22}$$

where G_v is the contribution to vertical heat transfer due to a water vapour flux. For soils with saturated air, Ten Berge (1986) shows that G_v can amount 10 to 25 per cent of G_H, while for very dry soils this percentage even can be 50 percent. A simple parameterization for G_v is, therefore,

$$G_v = c_G \; G_H. \tag{23}$$

Here we adopt $c_G = 0.2$. We realise that this parameterization is a very simple description of the complicated transfer processes in the soil; c_G can easily vary with a factor of two.

4. The critical wind speed

It is to be expected that when the wind speed drops below a certain value, U_{cr}, turbulence cannot be maintained any longer in the surface layer, which means that u_*, θ_* and L will vanish. Due to the difference in emissivities of the atmosphere and the surface, a temperature difference will remain between z_r and the surface. This "critical" temperature difference can be evaluated from the present model equations as follows.

For $U \le U_{cr}$ it follows $H = \lambda E = 0$. According to Eqs. (1), (21), (22) and (23) then $G = Q^*$ and $G = b_G(1+c_G) \; Q_i^*$. Combining this with Eqs. (5)-(5a) we arrive at

$$\Delta T_{cr} = (T_r - T_s)_{cr} = \frac{(1 - b_G')}{4} (\epsilon_s - \epsilon_r) \; T_r, \tag{24}$$

where $b_G' = b_G(1+c_G)$. This equation shows that the temperature difference is zero if $\epsilon_r = \epsilon_s$. Moreover, if $b_G' = 0$ (e.g. $G = Q^* = 0$), the temperature difference is only regulated by emissivity differences between the surface and the atmosphere. This might occur for a surface which is completely isolated from the soil layer beneath. We have found, however, $b_G' = 0.4$, typically. Combining this with

$\epsilon_r = 0.73$ for clear skies (section 3.2) we find $\Delta T_{cr} = 11.3$ K for $T_r = 280$ K. For cloudy skies with $\epsilon_r = 0.90$ we arrive at $\Delta T_{cr} = 4.2$ K. These are realistic values, which can occur across the lower atmospheric and canopy layers in very stable conditions.

Alternatively, $T_r - T_s$ is given by Eq. (6) and Eq. (18). In the limit to strong stability the temperature profile of Eq. (6) is linear and $\psi_H = \psi_M$ is approaching $\psi_H \rightarrow - a\, z/L$ (see Eq. (12)). Combination of this with (6) and (18) provides an equation for θ_*/u_*, which can be written as

$$(\frac{\theta_*}{u_*})_{cr} = \frac{u_o}{2\frac{g}{T}z_r a}\{-1 + [1 + \frac{4\frac{g}{T}a\,z_r\,\Delta\theta_{cr}}{u_o^2}]^{\frac{1}{2}}\}. \qquad (25)$$

Here $\Delta\theta_{cr} = \Delta T_{cr} + \Gamma_d z_r$, where ΔT_{cr} is given by Eq. (24). Eq. (25) shows that the critical value of θ_*/u_* is given by the surface vegetation coefficients and atmospheric parameters. We note that $(\theta_*/u_*)_{cr}$ varies with a square root dependence on the critical temperature difference.

From Eqs. (12) and (9) we also note that in strong stability, the wind profile tends to a linear shape. This implies a critical wind speed U_{cr} at level z given by

$$U_{cr} = a\,z\,\frac{g}{T}(\frac{\theta_*}{u_*})_{cr}. \qquad (26)$$

With the above equations we can calculate typical values for $(\theta_*/u_*)_{cr}$ and U_{cr}. For instance, if $T_r = 280$ K, $z_r = 50$ m and using the numerical values for the coefficients as proposed in section 3, we arrive at $(\theta_*/u_*)_{cr} \approx 1.8$ Ks/m at clear skies (N = 0) with $\Delta T_{cr} = 11.3$ K. For the 10 m level then Eq. (26) provides $U_{cr} \approx 0.45$ m/s. For total overcast (N = 1) we obtain $(\theta_*/u_*)_{cr} = 0.9$ Ks/m and $U_{cr} \approx 0.23$ m/s. These values for the critical wind speed are surprisingly low and are close to the threshold wind speed of cup anemometers.

The present results differ from that obtained earlier by Venkatram (1980), using a constant temperature scale θ_* and

$\psi_H = \psi_M = -5z/L$. The latter author arrives at a critical wind speed at 10 m of $U_{cr} \approx 2.5$ m/s. This value is much to large, because θ_* does not tend to zero for strong stability. Moreover, the used ψ_H and ψ_M functions are valid only for $z/L < 0.5 - 1$ (see section 3.3).

Carson and Richards (1978) discuss the influence of different ψ_M and ψ_H functions on a critical bulk Richardson number $Ri_{B_{cr}}$. For the profile functions of Hicks (1976) as used by us one obtains

$$Ri_{B_{cr}} \approx 1/a, \qquad (27)$$

where a is the coefficient of Eq. (12). For $a = 0.7$ it follows that $Ri_{B_{cr}} \approx 1.4$.

5. Results

For the calculation of the surface fluxes and the other terms of the proposed model equations we need to specify a single wind speed U_z (usually at 10 m height), the surface roughness length of momentum z_0, total cloud cover N, and dry and wet bulb temperatures T_a and T_{wa}, respectively. The latter two temperatures provide the specific humidity deficit in the air, δq_a (see Eqs. (14a) and (14b)).

The model equations can be solved for all terms in the energy budget of Eq. (1), by using Newton-Raphson's iteration method. The iteration is done with help of the Obukhov length L, of which an interval is specified. Within this interval, a value of L is sought which balances the terms of (1). Table 3 gives a summary of how the quantities in the scheme are calculated from the equations and the available inputs. The calculation of λE is done with Eq. (13), where initially $\delta q_s = 0$. However, if it appears that $\lambda E > 0$ we use a specified canopy resistance r_c to evaluate λE from Eqs. (13) and (16). This provides the transpiration of the vegetation. The total evaporation from the surface in these cases is obtained by taking the sum of λE of Eq. (13) and $|G_v|$ of Eq. (23). The latter can be regarded as the contribution of the soil, when the vapour inversion profile is destroyed (see section 3).

82

Table 3
Summary of the calculation procedure for the quantities of the
scheme with equation numbers and inputs. The computation is
started with a prescribed value of Obukhov length L.

Quantity	Equation numbers	Inputs
u_*	(9), (12)	U_z, z_0, L
θ_*	(7)	u_*, L, T_a
T_r	(6), (12)	T_a, L, θ_*, z_r
T_0	(6), (12)	T_a, L, θ_*, z_0
T_s	(18)	T_0, θ_*, u_*
Q_i^*	(5a), (3b)	T_r, N
Q^*	(5)	T_r, T_s, Q_i^*
H	(8)	u_*, θ_*
G_H	(21)	H, Q_i^*
G_V	(23)	G_H
G	(22)	G_H, G_V
D_{sa}	(17)	θ_*, T_a, T_s
λE	(13), (16)	Q^*, G, δq_a, u_*, D_{sa}

Using the above scheme we finally arrive at all the components of
Eq. (1). Iteration with a new value of L is continued, until all the
terms of (1) are in equilibrium. This might sometimes take more than
10 iteration steps to obtain an accuracy of 1 W/m^2 in Eq. (1).

In the next we will describe the model output in terms of Q_i^* (see
Eq. (5a)), δq_a and u_{*N}. The latter is obtained from Eq. (9) for
z/L = 0 and z = 10 m. These quantities can be considered as the
independent input parameters of the scheme. For the simulations we
used z_0 = 0.15 m, z_a = 1.1 m for the level where δq_a is specified and
T_r = 10°C for z_r = 50 m. Normally, however, T_r needs to be calculated
from T_a and the other inputs (see table 3).

In Fig. 4 the dependence of θ_* on u_{*N} is given for specified
values of δq_a and Q_i^* = -83 W/m^2. The latter value for Q_i^* corresponds
for our data set to N = 1/8 and T_r - 10°C, and is representative for

clear skies. In Fig. 4 three values for δq_a are indicated, ranging from a saturated atmosphere (Fig. 6a) to dry conditions (Fig. 6b) with $\delta q_a = 0.66$ g/kg and $\delta q_a = 2.2$ g/kg (Fig. 6c). The latter two values are representative for the sub-data sets of Figs. 2 and 3.

From Fig. 4 we note the linear dependence of θ_* on u_{*N} for $u_{*N} \leq 0.2$ m/s, irrespective of the value for δq_a. However, the peak values of the curves are dependent on δq_a. This is mainly caused by the variation of λE with δq_a and u_{*N}, as depicted in Fig. 5 for $Q_i^* = -83$ W/m². However, except for saturated conditions ($\delta q_a = 0$), λE is relatively small and θ_* is not influenced very strongly by δq_a.
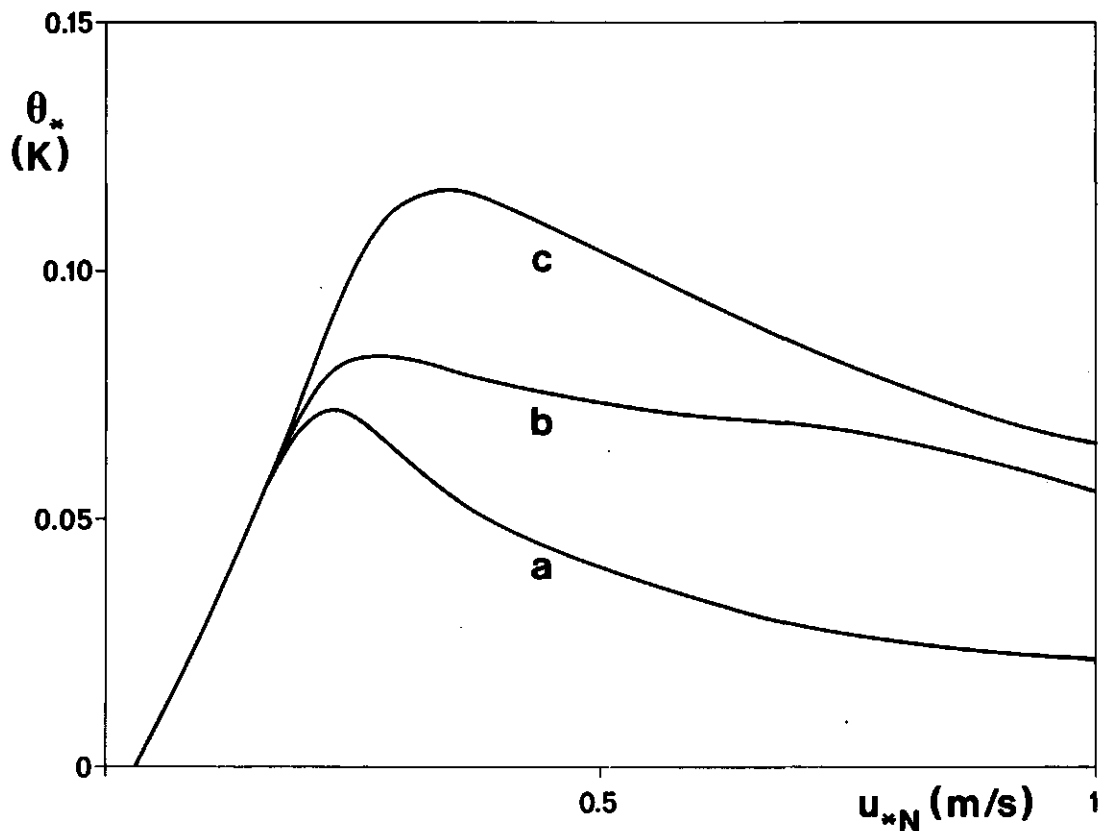
Fig. 4.
The dependence of θ_* on u_{*N} for $Q_i^* = -83$ W/m² as obtained from the model equations (e.g. N = 1/8, T_r = 10°C) for three values of specific humidity deficit e.g. a: δq_a = 0, b: δq_a = 0.66 g/kg and c: δq_a = 2.2 g/kg.

In Fig. 5 the typical behaviour of λE is shown for 4 values of δq_a. For increasing values of wind speed (e.g. u_{*N}), firstly λE decreases but later it increases to become positive. This behaviour can be explained with the aid of Eq. (13), which shows a balance between two relatively large opposite terms (if $\delta q_a > 0$ and $u_* > 0$). To obtain the curves of Fig. 5 we have used $r_c = 500$ s/m if $\lambda E > 0$. Subjectively, the latter value showed the best agreement with our data in clear sky conditions ($N \leq 0.25$). The curve of Fig. 5d represents the variation of λE with u_{*N} for $\delta q_a = 1.5$ g/kg. The latter value is typical for our data set at clear skies (see table 1).
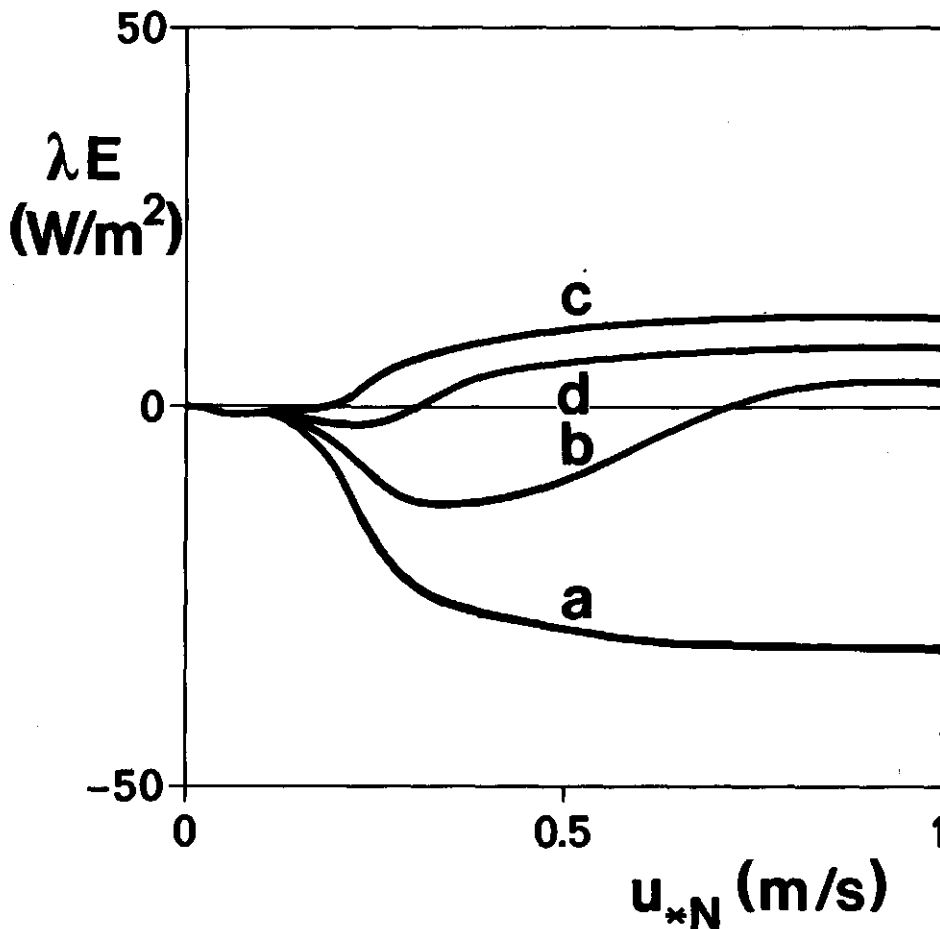
Fig. 5.

The dependence of λE on u_{*N} for $Q_i^* = -83$ W/m² as obtained from the model equations. A distinction is made for four values of specific humidity deficit e.g. a: $\delta q_a = 0$; b: $\delta q_a = 0.66$ g/kg; c: $\delta q_a = 2.2$ g/kg and d: $\delta q_a = 1.5$ g/kg.
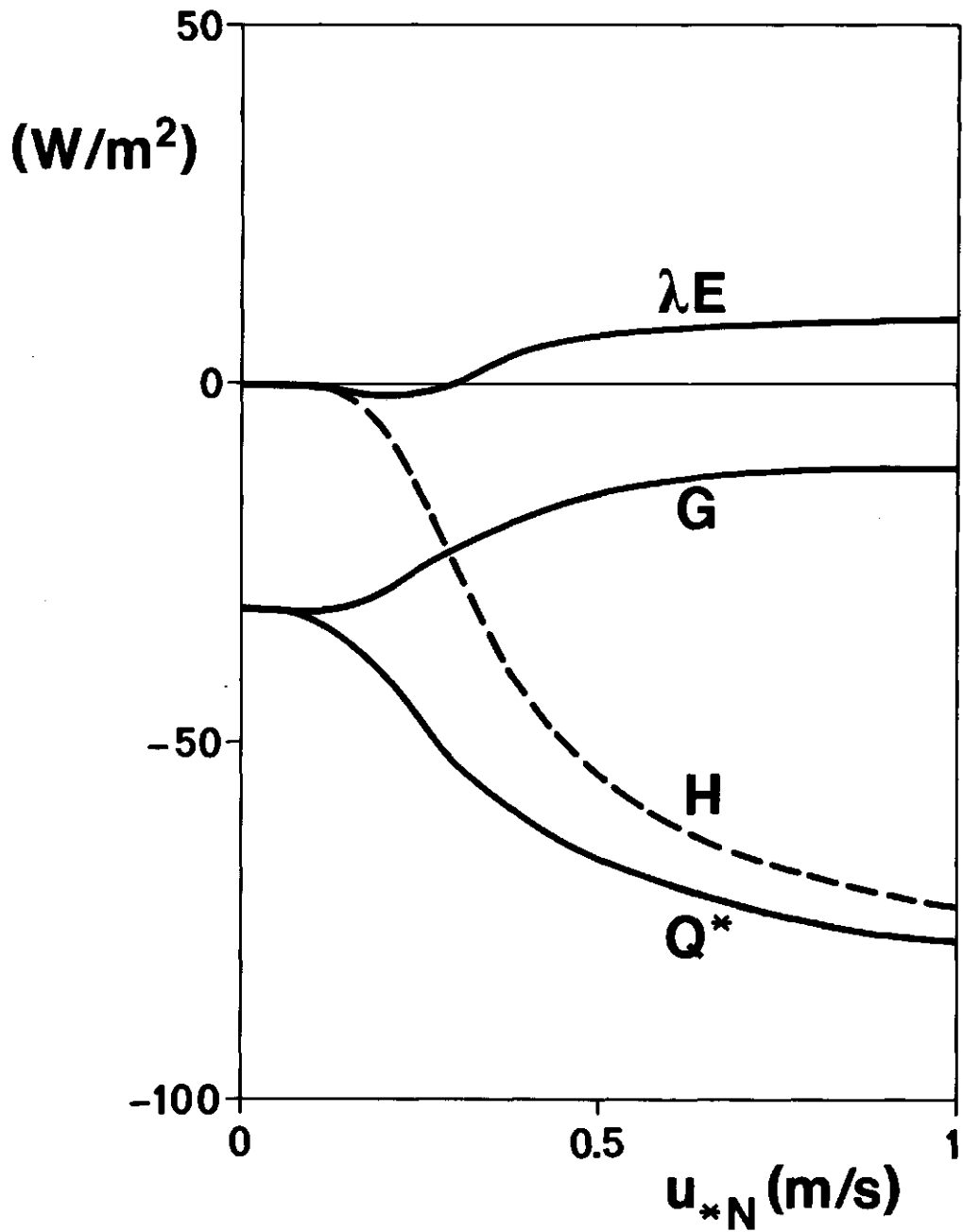
Fig. 6.
The variation of λE, G, H and Q^* with u_{*N} for $Q_1^* = -83$ W/m² (clear skies).
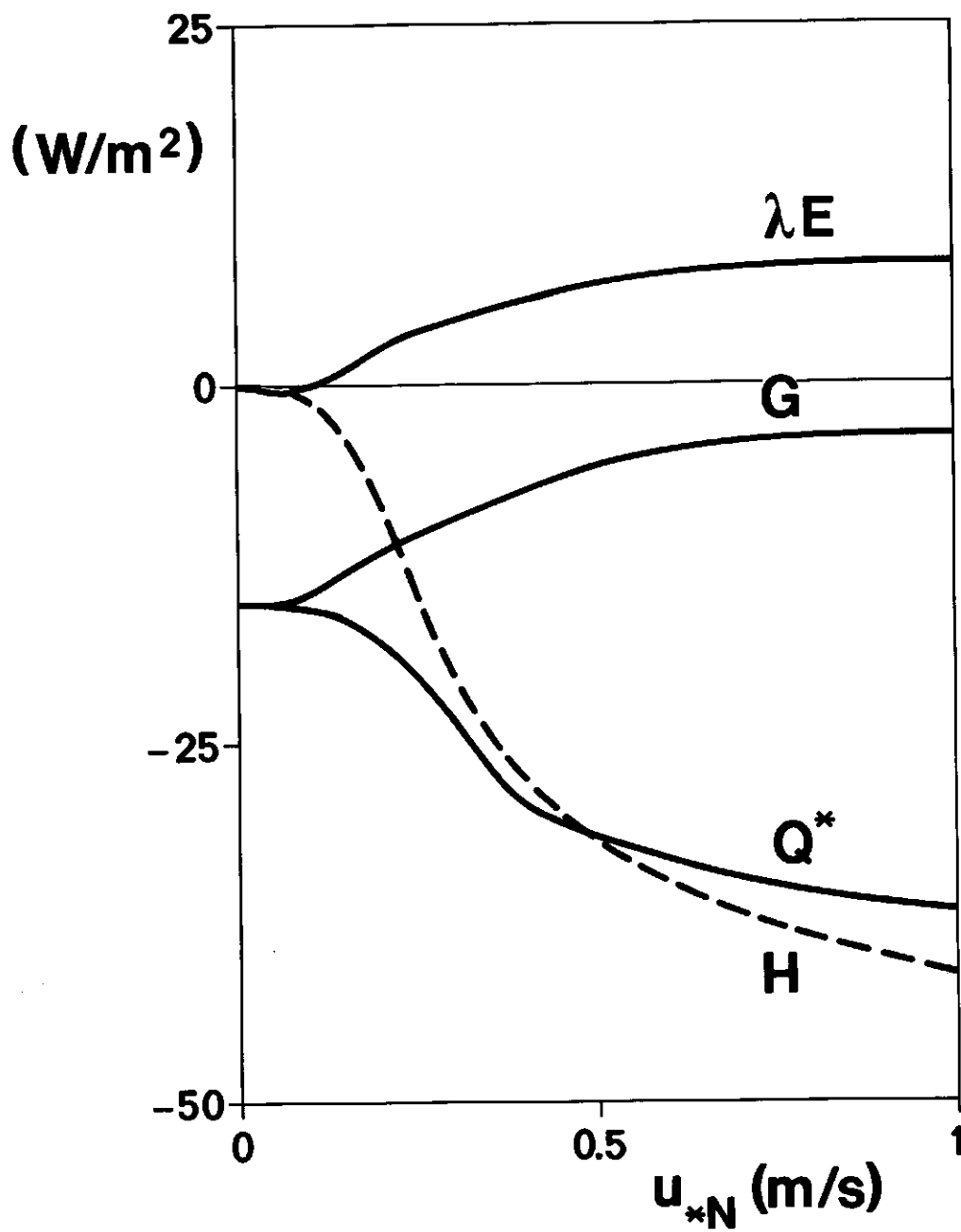
Fig. 7.
As Fig. 6 for $Q_i^* = -39$ W/m² (cloudy skies).

In Fig. 6 we have given the dependence of all the terms in Eq. (1) with u_{*N} for clear sky conditions (i.e. $Q_i^* = -83$ W/m^2) and $\delta q_a = 1.5$ g/kg. It is seen that the sensible heat flux H shows a large variation with u_{*N}. For large wind speeds the present model equations show that $Q^* \rightarrow Q_i^*$. This means that for large wind speeds H approaches Q_i^* if we neglect λE and G (see Fig. 3). The results for cloudy skies (N $\geq$ 0.75) with $Q_i^* = -39$ W/m^2, are illustrated in Fig. 7. It shows a similar behaviour as Fig. 6 for the terms in the surface energy budget. Note that now for large wind speeds $|H| > |Q^*|$ which can be explained by the larger relative influence of λE in the surface energy budget under these conditions.
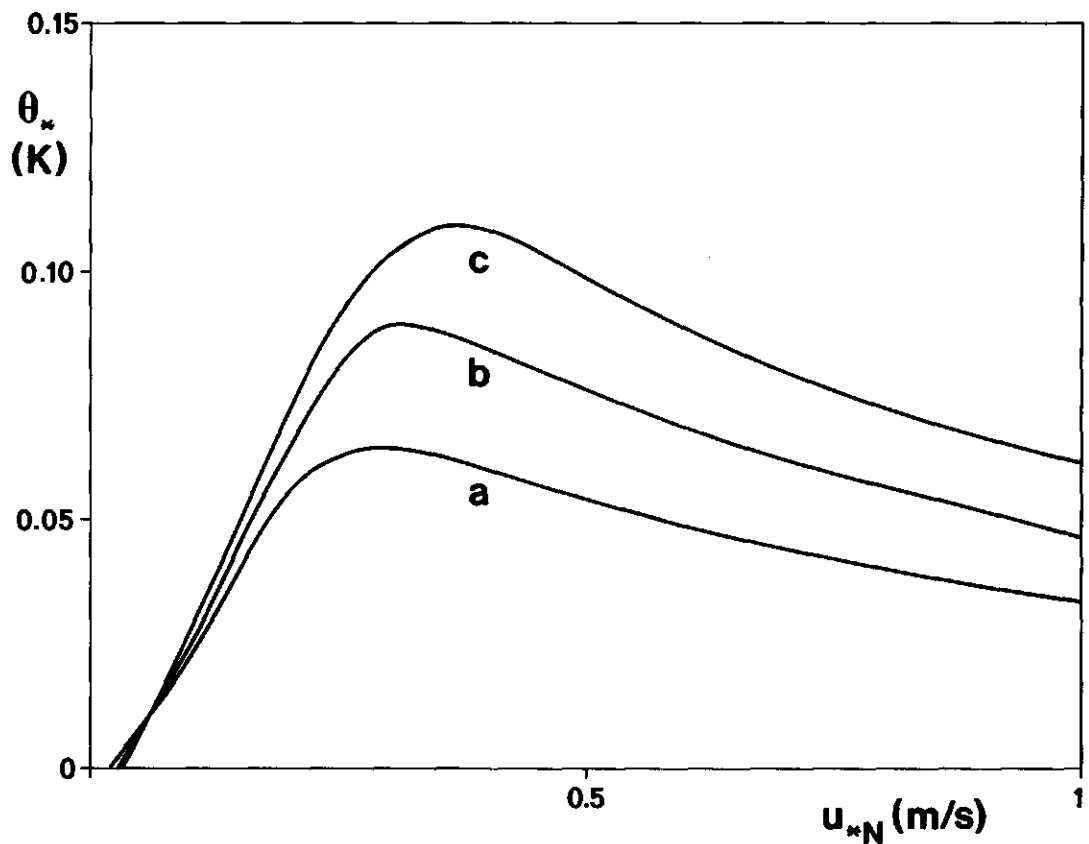
Fig. 8.

The dependence of θ_* on u_{*N} for $\delta q_a = 1.5$ g/kg as obtained from the model equations. A distinction is made for three values of cloud cover with $T_r = 10°C$ e.g. a: N = 7/8 ($Q_i^* = -39$ W/m^2), b: N = 4/8 ($Q_i^* = -61$ W/m^2), and c: N = 1/8 ($Q_i^* = -83$ W/m^2).

Table 4a
Comparison of model estimates with observations for clear skies
(N ≤ 0.25). Here n is number of observations, $\bar{x}$ is the average of
calculations, $\bar{y}$ is the average of observations; σ is rms error
and r is correlation coefficient. Units are K for θ_*, °C for T_s,
m/s for u_*, and W/m^2 for the other terms.

	u_*	θ_*	H	λE	G_H	Q^*	T_s
n	193	193	193	131	193	193	134
$\bar{x}$	0.22	0.086	−24.5	− 4.5	−21.0	−54.0	7.6
$\bar{y}$	0.21	0.095	−25.0	− 5.8	−19.6	−55.9	7.9
σ	0.03	0.028	9.0	5.6	8.9	12.9	1.8
r	0.98	0.43	0.85	0.86	0.33	0.33	0.92

Table 4b
As table 4a for cloudy skies (N ≥ 0.75).

|	u_*	θ_*	H	λE	G_H	Q^*	T_s
n	312	312	312	291	312	312	210
$\bar{x}$	0.37	0.045	−20.0	1.8	− 7.4	−27.4	7.8
$\bar{y}$	0.36	0.050	−22.3	8.3	− 8.4	−22.0	8.4
σ	0.02	0.021	9.3	12.0	7.5	16.1	1.7
r	0.99	0.35	0.78	0.70	0.44	0.25	0.93

In Fig. 8 the dependence of θ_* on u_{*N} for $\delta q_a = = 1.5$ g/kg is
shown. Distinction is made for three values of Q_i^*. From this figure
we note that the variation of θ_* with Q_i^* (i.e. N) dominates above the
variation with u_{*N}, as long as $u_{*N} \geq 0.2$ m/s. This result is
consistent with the findings of Venkatram (1980) and Holtslag and Van
Ulden (1982).

In Tables 4a and 4b a comparison is given for u_*, θ_*, H, λE, Q^*,
G_H and T_s obtained from observations and the model equations. A
distinction is made between clear skies (N ≤ 0.25) and cloudy skies
(N ≥ 0.75). In Tables 4a and 4b the derived values for u_*, θ_* and H
from profile method 1 are used for comparison with the values of the
scheme. Since in method 1 the same 10 m wind speed and roughness
length are used as in our model calculations, some bias will be

apparent. The same is true when we compare H (and λE) of the scheme
with the derived values of profile method 2. In that case the
specific humidity deficit is a common quantity. Such a comparison
leads to the same skill for H as for the comparison with profile
method 1 (see table 4a). In section 2 it is shown that a comparison
of the two profile methods with different input data leads to
σ - 11.6 W/m^2, which is slightly larger than the value of table 4a.

From tables 4a and 4b it can be seen that on average the agree-
ment is reasonable between observations and estimates, but that a
large difference may occur between individual observations and model
estimates. Possibly, the skill for λE under cloudy conditions can be
improved by taking a smaller value for r_c (larger λE if $\lambda E > 0$). This
approach is not followed here, because of the large uncertainty
in λE under these conditions.

The surface radiation temperature T_s is well reproduced by the
present model equations (σ - 1.8 K; $r = 0.92$). The skill of H, Q^* and
θ_* is comparable with the results of the model by Van Ulden and
Holtslag (1983), which is a more simple approach. This shows that the
final results for these quantities are not very sensitive to the
assumptions in the model equations.

6. Simulation of the temperature profile

As a part of the present scheme the temperature profile is des-
cribed with Eqs. (6), (10) and (12). In tables 5a and 5b a comparison
is given between the temperature observations and calculations at 5
heights for the two classes of total cloud cover. For the calcula-
tions we used the observed temperature at 2 m, the fluxes of the
present scheme and the above mentioned equations. So, only routine
weather data were used as input variables.

From Tables 5a and 5b it is seen that the agreement between
observations and calculations is surprisingly good. However, the
skill decreases with increasing height. An illustration of the
generally good agreement is shown in Fig. 9 for clear skies. At each
level error bars are indicated for the mean of the temperature
observations (e.g. $\sigma/\sqrt{n}$). The data are divided into three classes of

Table 5a
Comparison of model estimates with Cabauw temperature observations at
different heights (z) up to 80 m. All data for clear skies (N $\leq$ 0.25)
are used. Symbols are as in tables 4a and 4b; units are in °C.

z(m)	5	10	20	40	80
n	193	193	193	193	193
$\bar{x}$	12.1	12.4	12.8	13.3	13.7
$\bar{y}$	12.2	12.4	12.7	13.3	14.2
σ	0.24	0.42	0.59	0.81	1.50
r	0.99	0.99	0.99	0.98	0.94

Table 5b
As table 5a for cloudy skies (N $\geq$ 0.75).

z(m)	5	10	20	40	80
n	312	312	312	312	312
$\bar{x}$	10.9	10.9	11.0	10.9	10.8
$\bar{y}$	10.9	11.0	11.0	11.0	11.0
σ	0.10	0.17	0.25	0.42	0.79
r	0.99	0.99	0.99	0.99	0.99

stability, defined with Obukhov length L as 45 $\leq$ L < 90 (Fig. 9a),
20 $\leq$ L < 45 (Fig. 9b) and 5 $\leq$ L < 20 (Fig. 9c). Mean values for the
Obukhov length are 54 m, 29 m and 12 m respectively.

From the evidence shown in Table 5 and Fig. 9, we conclude that
the scheme with the chosen stability functions is suitable to des-
cribe the nocturnal temperature profile up to 80 m. This corresponds,
on average to z/L = 7 in Fig. 9c. At first sight, this is surprising,
because we used surface layer variables for the description of the
temperature profile. An explanation for this discrepancy is, that
above the surface layer the temperature profile is determined by the
local Obukhov length and the local fluxes (Nieuwstadt, 1984a), which
are often closely related to their surface values (Holtslag and
Nieuwstadt, 1986). Apparently these relationships are incorporated in
the stability function of Eq. (12). Similar findings for the wind
profile at Cabauw were obtained by Holtslag (1984a).
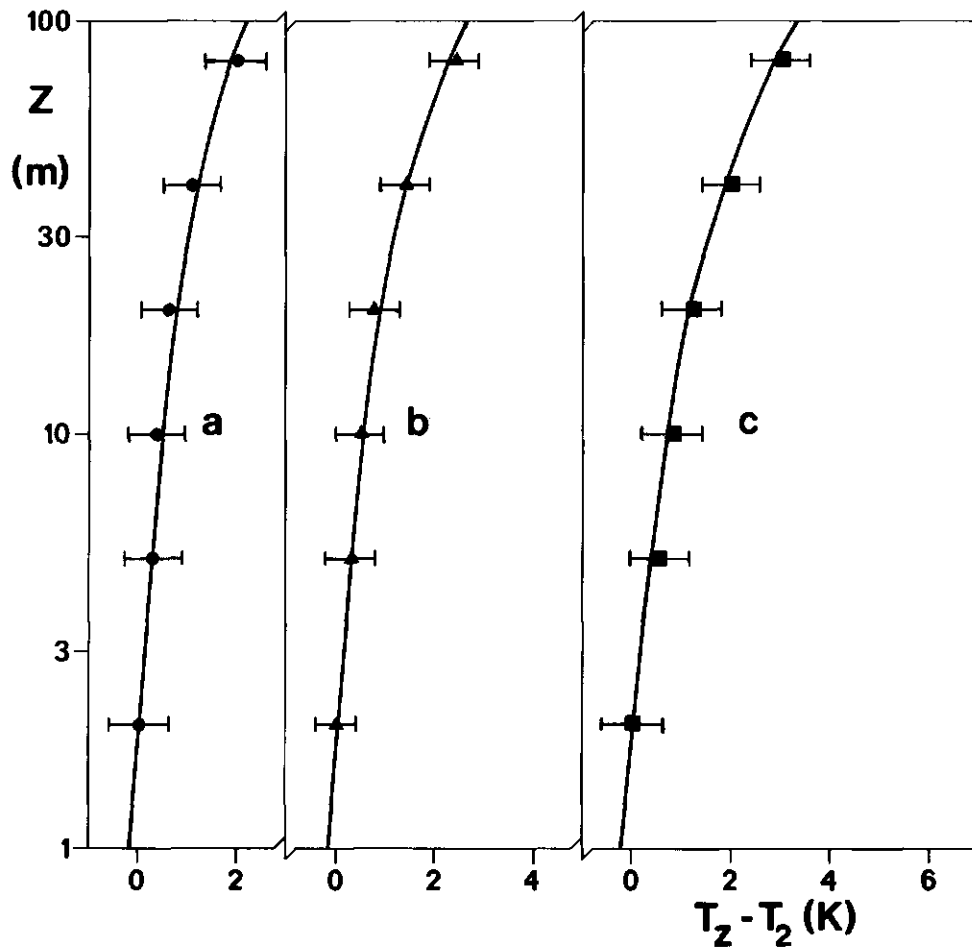
Fig. 9.

The temperature profile at Cabauw, averaged in three classes of
stability. Number of observations (n), and mean values for L and θ_*
are given by

a: n=50, L = 54 m, θ_* = 0.10 K;

b: n=79, L = 29 m, θ_* = 0.09 K;

c: n=29, L = 12 m, θ_* = 0.08 K.

The results are obtained with Eqs. (6), (10) and (12) and with the
use of the modelled surface fluxes. The indicated error bars
represent twice the standard deviation of the temperatures T_z (not
$T_z - T_2$) at each level.

For very strong stability conditions (e.g. $z/L > 5$ a 10) inter-
mittent turbulence will occur in the NABL (Holtslag and Nieuwstadt,
1986) and Eq. (12) is expected to be unreliable. In such cases also
the exchange coefficients for heat and momentum may be different e.g.
$\psi_H \neq \psi_M$ (Turner, 1976; Hicks, 1976). Also, divergence of radiation
appears to be significant above the turbulent layer (Estournel and
Guedalia, 1985).

These results imply that with our choice for $z_r \approx 50$ m, the
fluxes of our scheme are less reliable for $L < 5$ a 10 m. The latter
corresponds to very low values for u_* and θ_* ($u_* < 0.07$ m/s and
$\theta_* < 0.07$ K). On the other hand, however, we have found that when the
reference height z_r is chosen below a height of approximately 30 m,
serious errors are introduced in the simulation of the temperature
profile.

7.   Summary and discussion

In this chapter we have presented a semi-empirical scheme, which
relates the surface fluxes to routine weather variables during
nighttime over land. The routine weather variables are total cloud
cover, wind speed and wet and dry bulb temperature of the air. The
latter three variables are only needed at a single height in the
atmospheric surface layer (below 50 m). Observations above a grass-
covered surface in Cabauw, The Netherlands, are used to design some
of the parameterizations and to investigate findings from literature.
In the scheme parameters are included which must be adjusted to other
vegetation types.

In the scheme the incoming longwave radiation L^+ is parameterized
with Swinbank's (1963) formula and the cloud cover correction by
Paltridge and Platt (1976). The agreement with our observations is
good.

For the calculation of the outgoing longwave radiation L^- we use
Stefan-Boltzmann's law. Here the surface radiation temperature T_s is
related to the temperature T_0 at the height of the effective
roughness length of momentum z_0. We have found that typically

$T_o - T_s = 1$ a 2 K if $u_* > 0.3$ m/s, but for low wind speeds $T_o - T_s$ may increase up to 6 K! Based on our observations a parameterization is proposed for $(T_o - T_s)/\theta_*$ as a function of u_*. A discussion is given between the difference in our findings and those of literature (e.g. Garratt and Hicks, 1973; Brutsaert, 1982). Further verification with independent data, however, is recommended.

The parameterizations of the longwave radiation terms provide the net radiation. Subsequently, the soil heat flux G is parameterized, which is generally an important term in the nighttime energy balance. We have used our observations to evaluate several formulations for G (Nickerson and Smiley, 1975; Van Ulden and Holtslag, 1983, 1985). It appears that a new formulation for G in terms of sensible heat flux and isothermal net radiation is a better descriptor than the other formulations. In our approach we also take account of the influence of water vapour transport in the soil on the soil heat flux. Often the surface vegetation might be wetted from below by the vapour transport in the soil, which is known as destillation or dew rise (Monteith, 1963).

The remaining terms in the surface energy budget are the surface fluxes of sensible heat (H) and latent heat (λE). The latter quantity is described with an equation similar to the usual Penman-Monteith equation (e.g. Monteith, 1981). During nighttime this relation shows a balance of two opposite terms, normally resulting in small values of λE. For small wind speeds condensation occurs, while for large wind speed evaporation might occur. For the latter case a canopy resistance is used, which is large compared with normal daytime values (e.g. De Bruin and Holtslag, 1982).

At the hand of the model equations and parameterizations of the scheme we obtain all components of the surface radiation and energy balance. For very low wind speeds (10 m wind speed ≤ 0.5 m/s) no turbulence can be maintained in the surface layer. The latter is connected to a critical wind speed, a critical temperature difference and a critical bulk Richardson number of 1.4. Above the critical wind speed the present formulations show a reasonable agreement with our observations, on average. In this comparison cases with fog or rain were excluded. Because of the generally low values of the terms in

94

the energy balance, the uncertainty in the data is quite significant. The output of the scheme is illustrated as a function of the main forcing terms.

The surface fluxes of heat and momentum from the present scheme are used to simulate the Cabauw temperature profile up to 80 m in stable conditions. For this purpose we have adopted semi-empirical extensions of the log-linear profile (Hicks, 1976; Carson and Richards, 1977). An new analytical approximation to the latter findings is given. It appears that the Cabauw observations are well-described by the present methods up to $z/L - 7$, which is far above the surface layer (z is height, L is Obukhov length scale).

The present model equations can be regarded as extensions of the proposals by Van Ulden and Holtslag (1983, 1985). The advantage of the present scheme is that the surface temperature can be calculated. Moreover, in the present scheme the temperature profile is in better agreement with observations. Also, account is given for dew rise and the evaluation of the soil heat flux from observations.

Nevertheless, for the sensible heat flux and the net radiation our results are comparable with those of Van Ulden and Holtslag (1983, 1985). For simple estimates of H also the empirical approach by Venkatram (1980) and Holtslag and Van Ulden (1982) is consistent with the present approach. These approaches were used by Holtslag (1984a) for the estimation of stable wind profiles and by Nieuwstadt (1984b) for the calculation of the turbulent boundary layer depth.

Because of its reasonable agreement with observations and its physical basis we believe that the present scheme is relevant for several applications of boundary layer meteorology and related fields. For instance, the equations can be used for stability estimation of the air in pollution dispersion models. Also the present scheme can be used as a surface layer module for short term weather forecast models, for applications in agricultural meteorology (frost prediction), and in remote sensing studies (e.g. the interpretation of infrared imageries).

Chapter V

ESTIMATES OF DIABATIC WIND PROFILES FROM NEAR-SURFACE WEATHER
OBSERVATIONS[*]

Abstract

In this chapter we analyse diabatic wind profiles observed at the 213
m meteorological tower at Cabauw, The Netherlands. It is shown that
the wind speed profiles agree with the well-known similarity func-
tions of the atmospheric surface layer, when we subsitute an effec-
tive roughness length. For very unstable conditions the agreement is
good up to at least 200 m or $z/L = -7$ (z is height, L is Obukhov
length scale). For stable conditions the agreement is good up to
$z/L = 1$. For stronger stability a semi-empirical extension is given
of the log-linear profile, which gives acceptable estimates in a
major part of the turbulent boundary layer (up to - 100 m). Besides a
discussion is given on the turning of wind direction with height up
to 200 m. A scheme is used for the derivation of the Obukhov length
scale from single wind speed, total cloud cover and air temperature.
With the latter scheme and the similarity functions, wind speed pro-
files can be estimated from near-surface weather data only. The re-
sults for the wind speed depend on height and stability. Up to 80 m
the rms difference with observations is 1.1 ms^{-1} on average. At 200 m
it is smaller than 0.8 ms^{-1} for very unstable conditions up to
2.1 ms^{-1} for very stable conditions. The proposed methods simulate
the diurnal variation of the 80 m wind speed very well. Also the
simulated frequency distribution of the 80 m wind speed agrees well ·
with the observed one. It is concluded that the proposed methods are
applicable up to at least 100 m in generally level terrain.

1. Introduction

Knowledge of the mean wind profile is of importance for e.g. air pollution and wind energy studies. In practice, however, often only surface weather observations are available such as 10 m wind speed. In such cases there is a need for the description of the mean wind speed with height as some function of the available data. During adiabatic (neutral) conditions the variation of mean wind speed with height is well described by a logarithmic relationship. This relationship has been found to satisfy observations in the lower atmosphere up to 100 m or more (e.g. Lumley and Panofsky, 1964; Tennekes, 1982). In diabatic conditions, however, when the surface heat flux is significantly different from zero, stability corrections should be made to the logarithmic relationship. These stability corrections are important, for instance, for the correct simulation of the diurnal variation of wind speed. Also the frequency distribution of wind speed is affected by stability.

The stability corrections may result from the application of Monin-Obukhov similarity theory for the atmospheric surface layer (Monin and Yaglom, 1971). With the latter theory we can obtain flux-profile relationships for the surface layer. In the past two decades much research is done on these relationships in diabatic conditions above homogeneous terrain. A review of the relations is given by Dyer (1974) and Yaglom (1977). With the flux-profile relationships we can obtain the diabatic wind speed profile using a single wind speed observation, the surface roughness length and the Obukhov length scale (see section 2). Problems may arise, however, when the relations are applied for terrain with upwind inhomogenities. In such cases an effective roughness length is appropriate (Fiedler and Panofsky, 1972). This is demonstrated by Korrell et al. (1982) and Beljaars (1982). A discussion on surface layer similarity under non-uniform fetch conditions is given by Beljaars et al. (1983).

In this paper we analyse the use of the Monin-Obukhov similarity functions for practical applications in generally level terrain. For that reason, the observations of diabatic wind speed profiles up to 200 m at the Cabauw tower are analysed in the first part of the

paper. We investigate the skill of similarity functions proposed in literature, together with the *effective roughness length* concept. We also discuss the change of wind direction with height up to 200 m. For the analysis of the wind profiles we use the Obukhov length scale derived from profiles of wind and temperature near the surface (profile method).

For practical application of the similarity functions, however, routine estimates of the Obukhove length scale and the effective surface roughness length are needed. Routine procedures for the derivation of the Obukhov length scale from near-surface weather data are given by Holtslag and Van Ulden (1982, 1983). Moreover, Wieringa (1976, 1980) has provided a routine method for the derivation of the effective surface roughness length for generally level terrain.

In the second part of the paper we will demonstrate the skill of the above methods for the routine application of the Monin-Obukhov similarity functions. For that purpose observations of 10 m wind speed, air temperature and total cloud cover or insolation are needed. As such the methods can replace empirical power "laws", the use of which has no physical foundation and only little practical advantage (Wieringa, 1981). Moreover the methods can serve for a mesoscale analysis of the surface layer wind, with procedures discussed by Cats (1980).

2. Background

2.1 Monin-Obukhov similarity theory

The mean wind profile in the atmospheric surface layer can be described, according to Monin-Obukhov similarity theory. First the Obukhov length scale L is defined as (Monin and Yaglom, 1971; Tennekes, 1982)

$$L = - \frac{u_*^3}{k \frac{g}{T} \overline{w\theta}_0}. \tag{1}$$

Here u_* is the friction velocity, k the Von Karman constant, g/T the buoyancy parameter (g accelaration of gravity, T air temperature) and

$\overline{w\theta_0}$ is related to the sensible heat flux H by

$$H = \rho C_p \, \overline{w\theta_0}, \tag{2}$$

where ρ is the density of air and C_p is specific heat at constant pressure.

With Monin-Obukhov theory the non-dimensional wind gradient can be written as

$$\frac{kz}{u_*} \left(\frac{\partial U}{\partial z}\right) = \phi_m\left(\frac{z}{L}\right), \tag{3}$$

where ϕ_m is a function of z/L only. Here U is the mean wind speed at the height z. As summarized by Rijkoort (1968) several form of ϕ_m have been proposed in the literature. For unstable conditions (L<0), we will investigate

$$\phi_m = (1-16 \, z/L)^{-\frac{1}{4}}, \tag{4a}$$

as reviewed by Dyer (1974) and proposed by Hicks (1976) for $-2 \leq z/L \leq 0$. Also

$$\phi_m = (1 - 16 \, z/L)^{-1/3}, \tag{4b}$$

as given by Carl et al. (1973) for $-10 \leq z/L \leq -1$ is investigated. The latter formulation agrees well with the well known KEYPS form and approaches the free convection limit for $z/L \to \infty$ (Lumley and Panofsky, 1964).

For stable conditions (L>0) the result for ϕ_m is usually written as

$$\phi_m = 1 + \alpha \frac{z}{L}, \tag{4c}$$

where α is a coefficient. Dyer (1974) proposes $\alpha = 5$ for moderate stable conditions. This is confirmed by Webb (1970), SethuRaman and Brouwn (1976) and Hicks (1976). But the latter authors indicate that

ϕ_m is different for stronger stabilities. This subject is discussed in more detail in section 6.

In Eqs. (4a)-(4c) the corresponding value of the Von Karman constant is given by $k = 0.41$.

2.2 Integral wind profiles

The wind speed profile is obtained from the integration of (3) between the surface and a height z in the surface layer, which results in

$$U_z = \frac{u_*}{k} \left\{ \ln(\frac{z}{z_0}) - \psi_M(\frac{z}{L}) + \psi_M(\frac{z_0}{L}) \right\} \qquad (5)$$

where U_z is wind speed at height z, z_0 is the appropriate surface roughness length and ψ_M is defined by

$$\psi_M(\frac{z}{L}) = \int_0^{z/L} \frac{1 - \phi_m(\xi)}{\xi} \, d\xi. \qquad (6)$$

In this paper we assume that a wind speed U_1 is available at one level z_1 in the surface layer. In that case (5) can be rewritten as

$$U_2 = U_1 \frac{\ln(\frac{z_2}{z_0}) - \psi_M(\frac{z_2}{L}) + \psi_M(\frac{z_0}{L})}{\ln(\frac{z_1}{z_0}) - \psi_M(\frac{z_1}{L}) + \psi_M(\frac{z_0}{L})}. \qquad (7)$$

With the aid of (7) U_2 is obtained at z_2 for given U_1, z_0 and L.

Finally (6) is applied to Eqs. (4a)-(4c). Application to (4a) leads to (Paulson, 1970)

$$\psi_M = 2 \ln(\frac{1 + x}{2}) + \ln(\frac{1 + x^2}{2}) - 2 \tan^{-1}(x) + \frac{\pi}{2}, \qquad (8a)$$

where $x = \phi_m^{-1}$. When (6) is applied to (4b) we obtain

$$\psi_M = \frac{3}{2} \ln(x^2+x+1) - \sqrt{3} \tan^{-1}(\frac{2x + 1}{\sqrt{3}}) - \frac{3}{2} \ln 3 + \frac{\pi}{3}\sqrt{3}, \qquad (8b)$$

where again $x = \phi_m^{-1}$, but here ϕ_m is given by (4b). Application of (6) to (4c) gives

$$\psi_M = -\alpha\frac{z}{L}. \tag{8c}$$

In this paper we will use (8a) and (8b) in their quite complex form. A simple practical approximation of (8a) is given by Jensen et al. (1984):

$$\psi_M = (1-16z/L)^{\frac{1}{4}} - 1, \tag{8d}$$

which gives similar results as (8a) for $0 < - z/L < 30$.

2.3 The effective surface roughness length

In the integral profiles (5) and (7) the surface roughness length is apparent. This surface roughness length may differ from the local roughness length of the terrain due to inhomogenities of the surface in the upwind direction. The upwind inhomogenities may occur due to occasional obstructions in a relatively smooth field or due to large perturbations. In both cases an effective roughness length (Fiedler and Panofsky, 1972) was found appropriate for use in the flux-profile relationship (5). This is discussed by Beljaars (1982) for near-neutral profiles in Cabauw. Korrell et al. (1982) showed the usefulness of an effective roughness length for the description of wind data obtained at the Boulder tower (40°N, 105°W).

In the above the effective surface roughness length is defined as the roughness length which is representative for a larger area than just the roughness of the local terrain. The value of the effective roughness length can be obtained from a method discussed by Wieringa (1976, 1980, 1983). This method relates the surface roughness length to the normalized standard deviation of wind speed. Alternatively, the ratio of the averaged wind speed observed in a given period and the maximum gust recorded during the same period can be used. The latter method is suitable for routine appllications. When no gust records are available we can obtain a crude estimate of z_0 from table 7, in chapter III.

With the effective roughness length we can apply (5) and (7) in non-uniform fetch conditions (Beljaars et al., 1983). Below we will

investigate the results of this application for the diabatic wind
speed profiles in Cabauw.

3. Cabauw data base

In this study we use observations of wind made with a 213 m
meteorological mast between 1 march 1977 and 1 March 1978. The mast
is located at 51°58'N and 4°56'E near the village of Cabauw, in the
center of The Netherlands. A full description of the Cabauw
facilities can be found in Driedonks et al. (1978).

The surroundings at the mast are topographically flat within a
radius of 20 km or more and consist of meadows with occasional lines
of trees, river dikes and small villages (Figure 1). The upwind ef-
fective roughness lengths vary - dependent on direction and season -
from 0.05 m to 0.35 m. These roughness lengths have been determined
by the maximum gust method of Wieringa (1976).

Wind speed and direction are observed at 7 levels in the boundary
layer, notably 10, 20, 40, 80, 120, 160 and 200 m, but at the 10 m
level no direction is observed. The measurements of windspeed and
direction are done with cup anemometers and wind vanes. The cup
anemometers have a low starting speed (< 0.6 ms^{-1}). Overspeeding is
unlikely to cause errors exceeding 5%.

The wind instruments are mounted 0.5 m above a boom which extends
9.4 m beyond the mast. Originally it was believed that this construc-
tion restricts the interference of the mast with the wind measure-
ments within 1% (Gill et al., 1967). However, a preliminary analysis
shows that for some wind directions the error due to obstruction by
booms and tower is much larger (Wessels, 1983). Therefore, in this
paper two wind direction categories were selected for which the above
systematic error is less than -2%. The two categories are South-East
(direction between 60 and 200 degrees to the North) and North-West
(between 280 and 340 degrees).

Within the selected two wind direction categories we have
selected data for which no instrumental or observational errors were
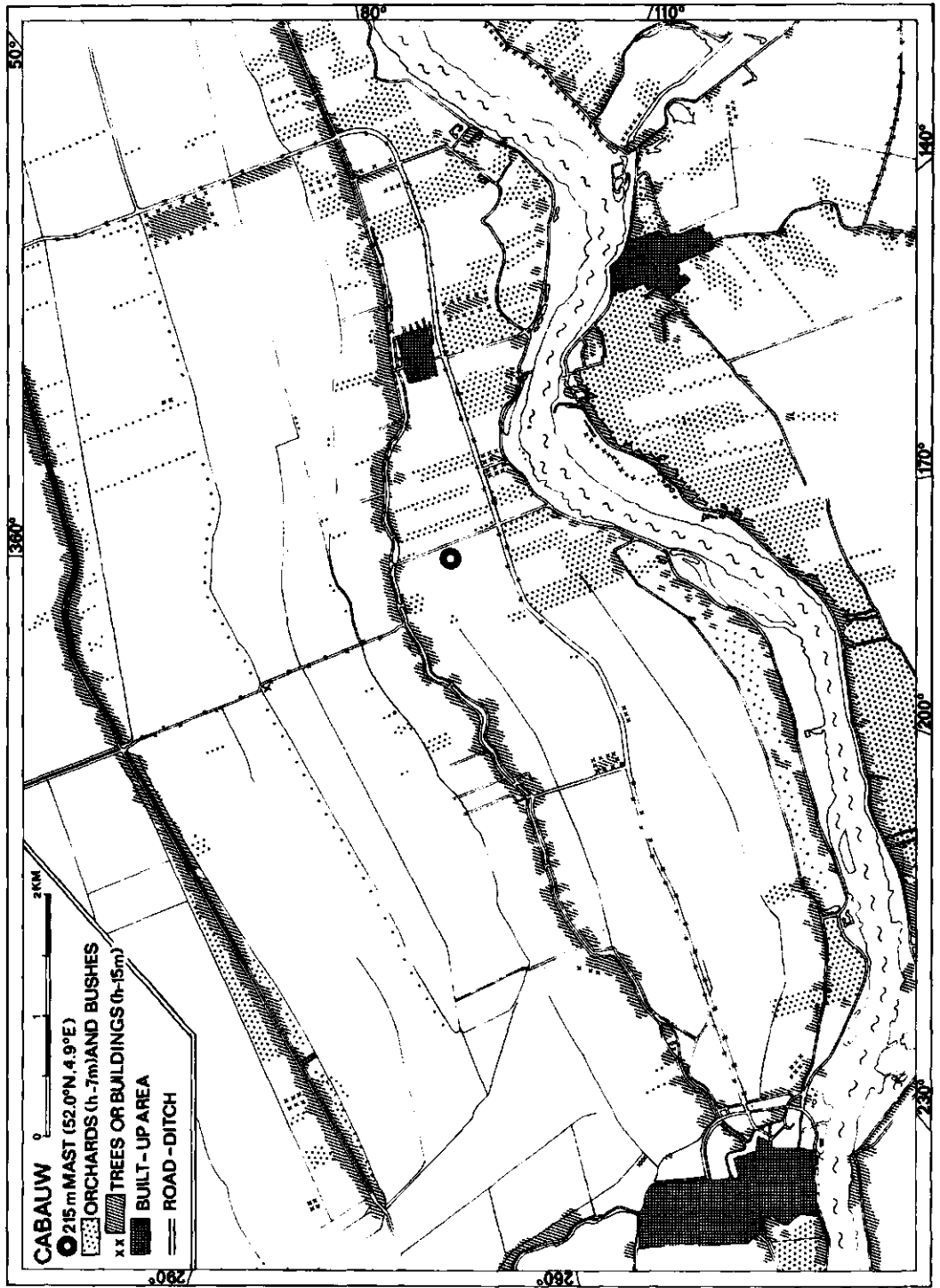reported and for which no rain, snow or fog appeared. We used

Fig. 1
Map of the Cabauw area (near the river Lek).

30 minute averages of each second half hour for which 10 m windspeed $U_{10} \geq 1$ ms^{-1}. The second half hour was used because in that half hour observations of total cloud cover were present at four nearby meteorological stations. The total cloud cover was taken as the average of the four values. Further the observed temperature in Cabauw at 2 m is used. The latter height agrees with the height of routine temperature observation. For the derivation of the Obukhov length with the profile method the observed temperature difference between 10 m and 0.6 m has been used (see section 4).

After the above data selection 1277 half hourly runs were retained for the South-East sector and 328 runs for the North-West sector. As will be shown below the selected runs represent a broad range of stability conditions. Because of the selection, however, the data set is not representative for the wind climate in Cabauw. This is caused in particular due to the deletion of directions from South-West, in which often high wind speeds are observed. In such cases, however, the stability correction is small, just as in cases with precipitation or mature fog. The value of the present analysis, therefore, is not affected by the above data selection.

4. Derivation of the Obukhov length scale

As discussed in section 2, the ratio z/L between the height z and the Obukhov length scale L determines the stability correction in the wind profiles. The parameter L can be obtained from delicate turbulence measurements, but such measurements are scarce in practice. In this section we discuss, therefore, two methods for the derivation of L from the available data. In fact both methods provide the surface fluxes of heat and momentum. Then L is easily obtained from (1).

The first method is the profile method in which the fluxes are obtained from the profiles of wind and temperature near the surface (McBean, 1979; Berkowicz and Prahm, 1982b; Holtslag and Van Ulden, 1983). From integration of (3) between the appropriate surface roughness length z_0 and a height in the surface layer z we obtain (Paulson, 1970)

$$u_* = k \ U_z [\ln(\frac{z}{z_o}) - \psi_M(z/L) + \psi_M(z_o/L)]^{-1}, \tag{9}$$

where ψ_M is given by (8a) for unstable conditions and (8c) for stable conditions. The equivalent for the temperature profile reads (Paulson, 1970)

$$\theta_* = k \ \Delta\theta[\ln(\frac{z_2}{z_1}) - \psi_H(\frac{z_2}{L}) + \psi_H(\frac{z_1}{L})]^{-1}, \tag{10}$$

where $\Delta\theta$ is a given temperature difference between two heights z_2 and z_1.

The function ψ_H is given by

$$\psi_H = 2 \ \ln(\frac{1 + y}{2}), \tag{11}$$

for unstable conditions (L < 0). Here $y = \phi_h^{-1}$, where ϕ_h is the counterpart of (3) for the temperature profile. As proposed by Dyer (1974) we take here $\phi_h = \phi_m^2$ for unstable conditions with ϕ_m given by (4a). In stable conditions we assume $\phi_h = \phi_m$ as supported by Webb (1970) and Hicks (1976) for values of z/L < 1. This results in $\psi_H = \psi_M$, where ψ_M is given by (8c) with α = 5. The temperature scale θ_* of (10) is related to the friction velocity u_* and the sensible heat flux H by

$$H = -\rho \ C_p \ u_* \theta_*. \tag{12}$$

From (9) and (10) u_* and θ_* can be obtained starting with a prescribed value of the Obukhov length scale L. We have used L = ∞ (e.g. $\psi_H = \psi_M$ = 0). Then first estimates of u_* and θ_* are computed. With these values L is computed using (1), (2) and (12). Subsequently, the new value of L is substituted in (9) and (10) to obtain improved estimates for u_* and θ_*. This cycle is repeated until successive values of L do not change more than 5%. It appears that usually not more than five iteration steps are needed to achieve the required accuracy for L. It must be noted that for stable conditions the above set of equations can also be solved analytically.

106

The above method for the derivation of L uses a single windspeed U_1, the effective surface roughness length z_0, air temperature T and a temperature difference $\Delta\theta$ near the surface. With this method estimates of L are obtained which agree with those from scarce turbulence measurements (Nieuwstadt, 1978; Beljaars, 1982). For that reason this method is used for the analysis of the Cabauw wind profiles in section 5. We have used 30 min. averages of the local observed 10 m wind speed and the observed temperature difference between $z_2 = 10$ m and $z_1 = 0.6$ m.

For routine applications, however, the above method is not suitable, because often the temperature difference $\Delta\theta$ is not available. In such cases we must parameterize the sensible heat flux (12). De Bruin and Holtslag (1982) and Holtslag and Van Ulden (1982, 1983) have given procedures for the derivation of the sensible heat flux from routine weather data only. Afterwards L is obtained from (1) and (9). In the appendix a summary of the parametrization of L is given. It appears that the estimates of L with the latter scheme are in good agreement with values of L obtained from the profile method. In sections 8 and 9 the usefulness of the routine method is demonstrated for the derivation of wind profiles.

With the above profile and routine method for the derivation of L, no reliable solutions exist for stable conditions in which the Richardson number Ri = $(z/L)/(1 + 5\,z/L)$ approaches the critical value of 0.20. This appear in very stable conditions, in which the transfer by turbulence is small. Moreover we have assumed $\phi_h = \phi_m$, but in extremely stable conditions Hicks (1976) obtained $\phi_h = 2\phi_m$. The latter means that the transfer mechanism for heat is smaller than for momentum. For that reason the application of the two methods is restricted to cases with $z/L \leq 1$. The value $z/L = 1$ results in Ri = 0.167, which is close to the critical value of 0.20. For $z/L \geq 1$ the fluxes are small and difficult to determine (e.g. Carson and Richards, 1978). A simple practical solution for L in these conditions is discussed in the Appendix. The consequence for the stable wind profile is treated in section 6.

5. Analysis of wind speed profiles

In this section we analyse the observed wind profiles at Cabauw in terms of the Monin-Obukhov theory described in section 2. To show the influence of stability on the wind profiles up to 200 m, we have distinguished 9 classes of stability. These classes range from very unstable ($\underline{a}$) to very stable ($\underline{i}$). The classes were defined with the use of the Obukhov length scale derived with the profile method (Table 1).

Table 1

Definition of our stability categories ($\underline{a}$-$\underline{i}$) with the aid of Obukhov length scale (L). Also the relation with Pasquill stability categories (B-F) is given for surface roughness length $z_0 = 0.2$ m, according to Golder (1972).

Our category		values of L(m)			Pasquill's category
$\underline{a}$	- 40	$\leq$ L $<$	-12		B
$\underline{b}$	- 200	$\leq$ L $<$	-40		C
$\underline{c}$	-1000	$\leq$ L $<$	-200		D
$\underline{d}$		$|L|$ $>$	1000		D
$\underline{e}$	200	$<$ L $\leq$	1000		D
$\underline{f}$	100	$<$ L $\leq$	200		E
$\underline{g}$	40	$<$ L $\leq$	100		E
$\underline{h}$	10	$<$ L $\leq$	40		F
$\underline{i}$	0	$\leq$ L $\leq$	10		(F)

The relation of these classes with the other categories of Table 1 is discussed below. For each class and height z, wind ratios were determined of $(\overline{U_z/U_{10}})$ and $(\overline{U}_z/\overline{U}_{10})$. The difference was found negligible as in Korrell et al. (1982). This means that $\overline{U}_z$ may be plotted as function of z to show the influence of stability in each class. Moreover in each class a central value of L can be given with $L_m = 1/(\overline{1/L})$.

Figure 2 shows the observed mean wind speed profiles for 4 classes of stability ranging from neutral to unstable conditions. In the figure we have used all available data of the South-East wind category between 1 May and 1 September (summer months) with effective roughness length $z_o \approx 0.2 \pm 0.02$ m. On each level error bars of $\pm \sigma/\sqrt{n}$ are denoted. Here σ is the standard deviation of the observed wind speeds in a given stability class; n is the number of observations in each class.

In Figure 2 we have also given the results of Eq. (7) with the two alternatives (8a) and (8b). In the calculation we have used the observed 10 m wind speed and the effective roughness length. It is seen that for our data the results of (8a) and (8b) do not differ significantly. Both equations show, on average, a rather good skill compared with the data. This is especially the case when we consider the fact that the wind profile for this wind direction category is influenced by a 10 m high orchard, which is present 300 m upwind (Wieringa, 1981; Beljaars, 1982). The findings of Figure 2, therefore, support the use of an effective roughness length together with stability information.

In the paper by Carl et al. (1973) the skill of the ϕ_m functions given by (4a) and (4b) is discussed. They conclude that (4b) shows a good agreement with their data up to z/-L $\approx$ 10, while (4a) fits better for small z/-L. The integral forms of (4a) and (4b), however, do not differ significantly (Fig. 2). In the unstable class a we obtain with our data that both integral functions (8a) and (8b) are applicable up to at least 200 m or z/-L $\approx$ 7, on average.

Figure 3 shows a comparison of (7) with observations for 2 stable classes of the South-East wind direction category during the four summer months. The agreement is good on average up to a level
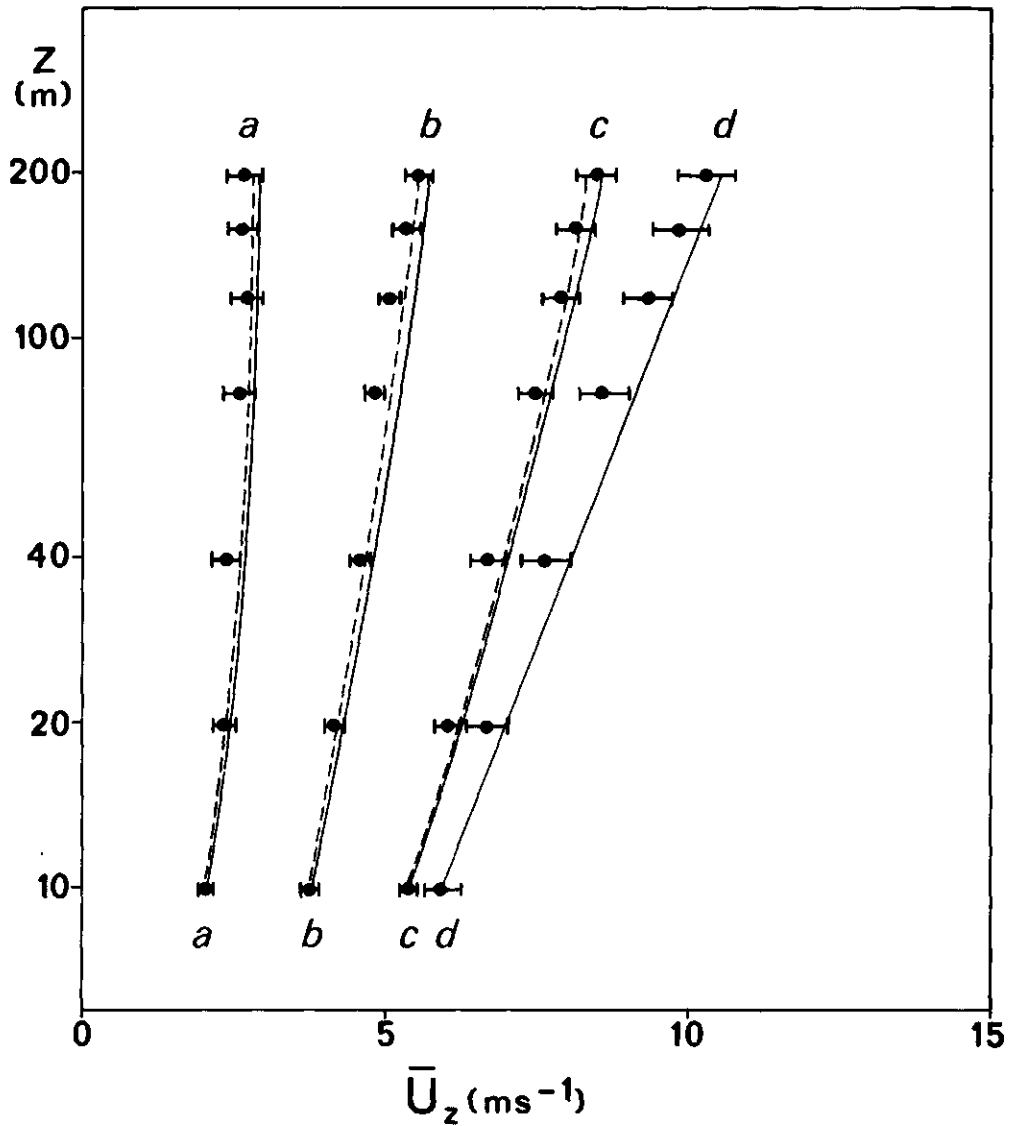
Fig. 2

The variation of mean wind speed $\bar{U}_z$ with height z for the 4 summer months in the South-East wind category. Results are given for 4 stability classes of Table 1: $\underline{a}$ (n = 17, L_m = -28 m), $\underline{b}$ (n = 66, L_m = -95 m), $\underline{c}$ (n = 42, L_m = -365 m), $\underline{d}$ (n = 30, L_m = 10^4 m). Here n is number of observations and L_m = $1/(\overline{1/L})$ where the overbar denotes the average. Dots with error bars refer in the figure to observations, while the indicated lines refer to Eq. (7) with (8a) (solid line) and (8b) (dashed line).
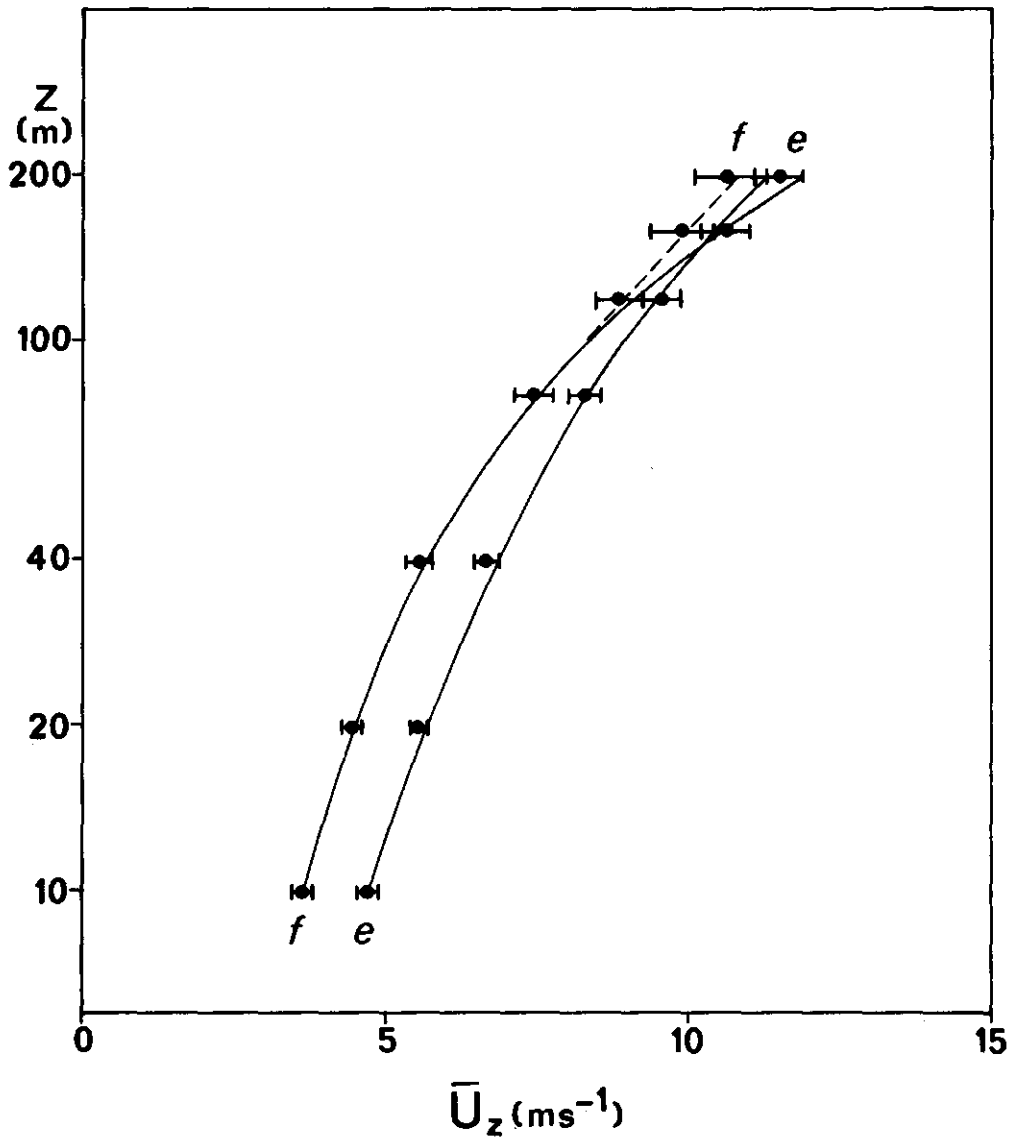
Fig. 3
As Figure 2 but for two stable classes: $\underline{e}$ (n = 43, L_m = 350), $\underline{f}$ (n = 28, L_m = 130 m). The solid line is Eq. (7) with (8c) and the dashed line is Eq. (14).
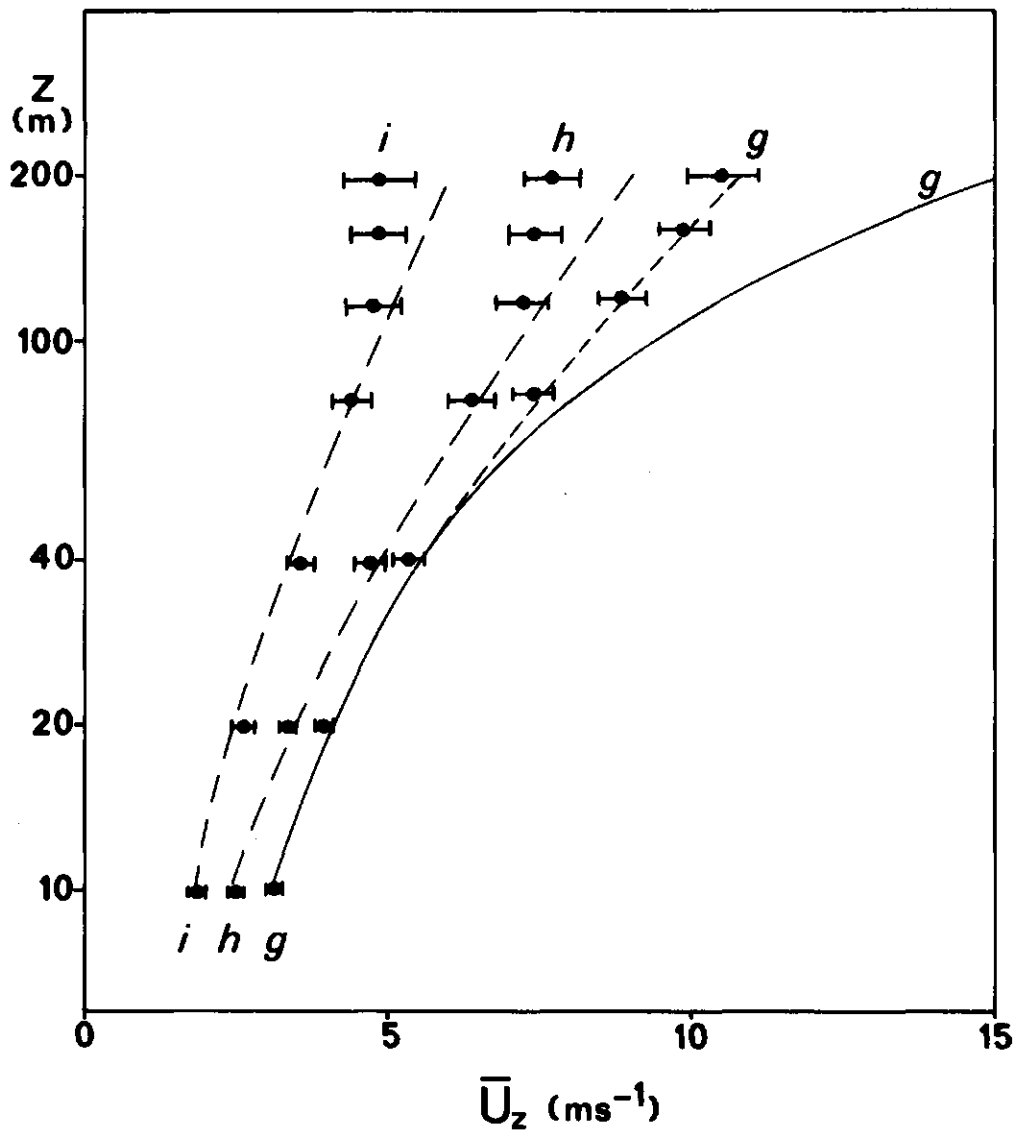
Fig. 4

As Figures 2 and 3 for the three most stable classes $\underline{g}$ (n = 30, L_m = 60 m), $\underline{h}$ (n = 15, L_m = 20 m) and $\underline{i}$ (n = 24, 0 < L_m ≤ 10 m). The solid line is Eq. 7 with (8c) and the dashed line is Eq. (14).

z $\approx$ L_m, but for heights z $\geq$ L_m large deviations may occur. For stronger stabilities, or larger heights this phenonmenon is evenmore apparent as shown in Figure 4. Therefore the log-linear function by (7) and (8c) with α = 5 appears to be suitable for the description of moderate stable conditions only. This is in agreement with the findings of other investigations above homogeneous terrain (Webb, 1970, Hicks, 1976; Sethuraman and Brown, 1976). In section 6 this subject is discussed in more detail.

In the Figures 2-4 we have used stability classes defined with the Obukhov length scale. In practice, so called stability categories are often used, which are determined from 10 m wind speed and amount of solar radiation. Golder (1972) has given a crude relation between stability categories, surface roughness length and the Obukhov length scale L. Table 1 shows the relation between our notation and the so-called Pasquill categories for surface length z_0 $\approx$ 0.2 m, based on Golder's results.

From table 1 it is seen that Pasquill's category D, for instance, covers $\underline{c}$, $\underline{d}$ and $\underline{e}$ of our notation. The latter categories correspond to three rather different wind profiles as shown in Figures 2 and 3. This result is also obtained when U_z/U_{10} is used as the independent variable in the figures instead of U_z (not shown here). Apparently significant stability variations can be found within a single stability category of Pasquill, especially at larger heights. This shows that in fact z/L is the proper stability parameter for wind profiles in the surface layer. This is one of the reasons why the use of power "laws" related to broad stability categories should be avoided in practice. A discussion on this subject is given by Wieringa (1981).

6. Extension of the stable wind speed profile to stronger
   stabilities

In section 5 we have seen that the log-linear relationship with α $\approx$ 5 provides good agreement, on average, with our data in stable conditions for z/L $\leq$ 1. In stronger stabilities the log-linear

profile with $\alpha = 5$ deviates from our data. The latter phenomenon is also observed in other investigations (Webb, 1970; Hicks, 1976, SethuRaman and Brown, 1976; Kondo et al., 1978).

In the paper by Hicks some surface layer wind profiles from the Wangara Experiment are discussed. It appears that the log-linear regime was substantiated but only up to, typically, $z/L \approx 0.5$. Beyond $z/L \approx 10$ a linear profile was found. This type of behaviour is also shown by the integral of (4c), where for large z/L the logarithmic term is of less importance (have a look at (5) with (8c)). However, according to Hicks (4c) is not suitable for the transition of the log-linear regime into the linear regime.

The findings of Hicks for the transition regime were approximated by Carson and Richards (1978) in an analytical form for ϕ_m, which reads

$$\phi_m = 8 - \frac{4.25}{(z/L)} + \frac{1}{(z/L)^2} . \tag{13}$$

This formulation describes the transition regime between $z/L \approx 0.5$ and $z/L \approx 10$ and is continuous with (4c) for $z/L = 0.5$. The integral form of (3) with ϕ_m given by (4c) for $z/L \leq 0.5$ and ϕ_m given by (13) for $z/L > 0.5$, can be written as

$$U_2 = U_1 \left[\frac{\ln(\frac{z_2}{z_o}) + 7 \ln (\frac{z_2}{L}) + \frac{4.25}{(z_2/L)} - \frac{0.5}{(z_2/L)^2} - 5(\frac{z_o}{L}) + 0.852}{\ln(\frac{z_1}{z_o}) + 5(\frac{z_1}{L}) - 5(\frac{z_o}{L})} \right]. \tag{14}$$

In (14) we have used (8c) and (9) for u_*. As discussed in section 4 this limits the use of (14) in principle to $z_1/L \leq 1$ or $L > 10$ m for $z_1 = 10$ m.

In Figures 3 and 4 the results of (14) are indicated together with the results of (7) with (8c) for the stable classes f and g. It is seen that for these classes the agreement improves markedly at larger heights. For the very stable class h the agreement is good for the whole wind profile up to 120 m e.g. $z/L \approx 6$. Note that the difference between (14) and (7) with (8c) is negligible for $0.5 \leq z/L_m \leq 1$.

114

In Figure 4 also the result of (14) is indicated for the most stable class $\underline{i}$ for which L < 10 m. In class $\underline{i}$ also cases are included for which the profile method of section 4 resulted in L = 0. The latter occurs for strong stability with Ri = 0.2. Therefore class $\underline{i}$ contains cases with little or no turbulence and application of (14) is in principle not permitted. Nevertheless when we use, empirically, L_m = 9 m in (14) we obtain a reasonable fit to the data of class $\underline{i}$ up to 100 m. As will be discussed in section 7, the cases of class $\underline{i}$ show a large change in wind direction with height.

From the comparison in the Figures 3 and 4 we conclude that (14) is a useful practical extension of the stable log-linear profile, as long as we are interested in the magnitude of U_z only. In fact (14) describes the wind profile in a major part of the turbulent boundary layer in generally level terrain. This can be illustrated with an estimate for the turbulent boundary layer height h, which reads (e.g. André, 1983, Nieuwstadt, 1984a)

$$h = 0.4(\frac{u_*}{f} L)^{\frac{1}{2}}. \tag{15}$$

Here f is the Coriolis parameter. With (15) we obtain for the average height h_m in classes $\underline{h}$ and $\underline{g}$ 120 and 160 m, respectively.

How can we explain that an extended surface layer description as (14), describes the wind speed profile in the major part of the stable boundary layer? In fact, as discussed in Chapter II, for the stable boundary layer local scaling and z-less scaling are appropriate. On basis of these scaling techniques we would expect that the local Obukhov length Λ is of importance rather than the surface Obukhov length L. However, we have seen that the values of Λ and L are closely related. This means that the surface Obukhov length has a high predictability for a major part of the turbulent boundary layer. In Eq. (14) this has been accounted for in an empirical way in agreement with observations at Wangara (Hicks, 1976) and the present observations at Cabauw. For practical use it is convenient to have one general equation for the stability function ψ_M for all values of z/L. Such an equation is given in Chapter IV.

Of course well above the boundary layer the wind speed should approach the "free" or geostrophic wind speed G. The latter, however, might be obscured by the presence of gravity waves or a low level jet. In such cases no simple estimate can be made anymore for the wind profile from surface data only. Perhaps an interpolation formula between the surface layer wind speed and the geostrophic wind speed is more suitable for these stable conditions (e.g. Van Ulden and Holtslag, 1980). This subject, however, needs more future research and is beyond the scope of the present study.

7. Analysis of the wind direction profile

The turning of wind with height is small within the surface layer ($z \leq 0.1$ h), because of the negligible influence of the Coriolis force. Above the surface layer normally a turning of wind with height is experienced, which will be influenced by stability. In this section we analyse the mean wind direction profile, observed along the Cabauw tower.

In table 2 we have given the mean difference D and the rms difference σ_D (corrected for the bias), between the wind direction at height z and the 20 m height. The data are divided in the 9 classes of stability from table 1. Also the average value L_m of the Obukhov length is given, together with an estimate for the turbulent boundary layer height h_m in stable conditions. Here h_m is calculated with Eq. (15). The values of L_m and h_m for class $\underline{i}$ are tentative values, obtained by fitting profile functions to the observed wind profiles up to 200m. We have not given h_m for the unstable classes because of the expected high variability of h within each class. In table 2 we have included all available data of the South-East and North-West direction categories.

From table 2 we note that the turning of wind is small below 200 m in near-neutral and unstable conditions. In stable conditions a mean turning up to 40 degrees is observed between 200 m and 40 m. For stable conditions we can order the data of table 2 by plotting $D = D_z - D_{20}$ as a function of z/h_m. The result is shown in Fig. 5. From this

Table 2

In this table we have given the mean difference D and the rms difference σ_D (corrected for the bias D) of the observed wind direction at height z and the 20 m height. A distinction is made in the 9 classes of stability, from table 1. For each class the mean Obukhov length $L_m = 1/(\overline{1/L})$ is given. Also for the stable classes, the mean ABL depth $h_m = \bar{h}$ is given, where h is computed with Eq. (15). Note that a positive value of D refers to a clockwise change in wind direction with increasing height. Data are given in degrees.

class	a	b	c	d	e	f	g	h	i	
$L_m(m)$	-30	-100	-370	10^4	350	130	60	20	(9)	
$h_m(m)$	-	-	-	-	330	220	160	120	(100)	
z(m)										
40	0	0	0	1	2	4	5	7	12	D
	2	2	2	2	2	4	3	4	5	σ_D
80	4	3	3	4	7	11	16	21	24	D
	8	6	5	6	7	9	10	12	12	σ_D
120	8	6	5	6	10	17	24	29	31	D
	13	12	7	8	8	11	14	14	14	σ_D
160	10	8	7	9	14	22	30	34	36	D
	17	16	11	12	10	16	18	17	17	σ_D
200	12	10	9	12	18	28	35	38	39	D
	17	18	14	12	11	17	21	18	20	σ_D

graph it is seen that the turning angle between the ground and h_m is about 35 degrees (denoted by D_h).

At the upper boundary of Fig.5 we have plotted D_z/D_h. An empirical fit to the data of Fig. 5 is given by Van Ulden and Holtslag (1985), as

$$\frac{D_z}{D_h} = d_1 \left\{1 - \exp(-d_2 z/h)\right\},\qquad (16)$$

where $d_1 = 1.58$, $d_2 = 1$ and $D_h = 35$ degrees.
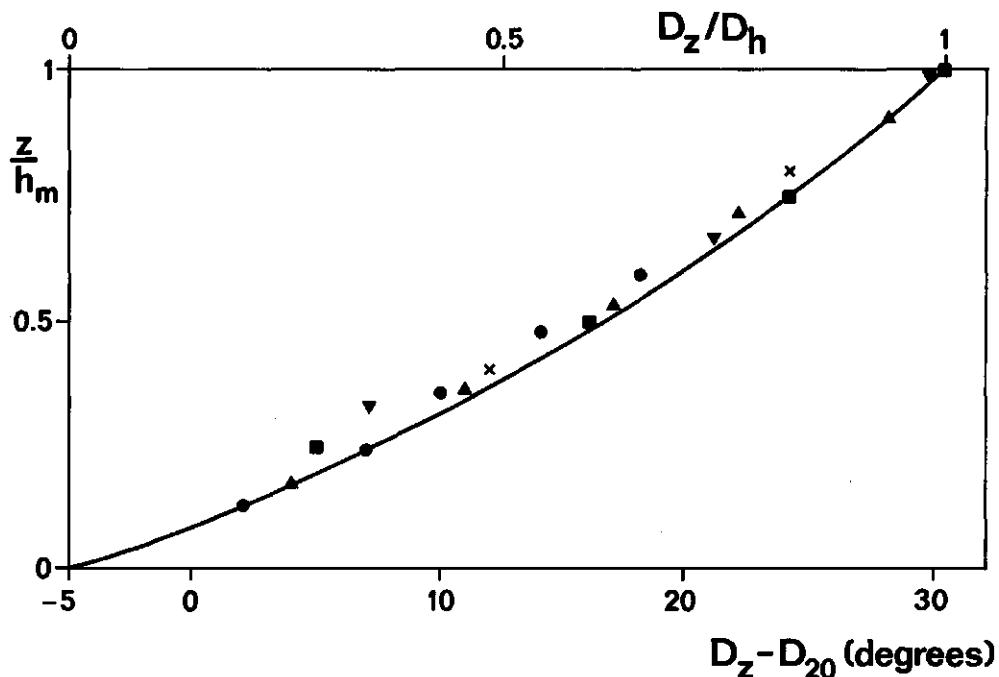
Fig. 5

The mean turning of wind direction D_z at height z with relative
height z/h_m in stable conditions. Dots represent class e, triangles
class f, squares class g, triangles "upside down" class h and crosses
class i.

Since (16) has been derived from observations between 20 and 200
m the use of (16) close to the surface should be avoided. The actual
variation of observed wind direction differences around D_z is quite
large, as given by σ_D in table 2. Nevertheless, the mean correction
of Eq. (16) is significant.

8. Results with near-surface weather observations

In this section we apply the findings of the preceeding sections
to the derivation of the wind speed profile from near-surface weather
data only. First the Obukhov length scale is estimated with the
routine method (see Appendix). After this (7) is used with ψ_M given

by (8a) for unstable conditions and ψ_M given by (8c) for stable conditions with $z \leq 0.5$ L. For $z > 0.5$ L in stable conditions we use (14). Further observed 10 m wind speed is used for U_1 in (7) or (14).

Table 3 contains averages of both observed ($\bar{y}$) and estimated ($\bar{x}_1$) wind speed for the 6 Cabauw levels. Also the RMS difference σ_1 between observations and estimates with the above scheme is given. We have used the whole data set as described in section 3. Again we distinguish classes of stability as given in table 1, from very unstable to very stable conditions. For comparison we have given the results of the logarithmic profile without any stability correction as well. These are denoted by $\bar{x}_2$ and σ_2. The logarithmic profile is obtained with (7) using L = ∞ or ψ_M = 0. This results in a constant ratio between U_z and U_{10} for given surface roughness length z_0.

From table 3 it is seen that the agreement between the estimates and observations vary with height and stability. For the near-neutral conditions of class $\underline{d}$ the stability correction is small and therefore $\sigma = \sigma_1 = \sigma_2$. For this class σ amounts to σ = 1 ms^{-1} at the 80 m level, which is ~11% of the observed average ($\bar{y}$). At 200 m σ = 2.2 ms^{-1}, which is 20% of $\bar{y}$. For the unstable conditions $\underline{b}$ and $\underline{c}$ about the same relative skill ($\sigma_1/\bar{y}$) is found. For class $\underline{a}$ σ_1 = 0.5 ms^{-1} at 80 m, which is ~20% of $\bar{y}$. When (8b) is used instead of (8a), we obtain comparable results with our calculations. This confirms our findings in Figure 2. Up to 40 m, the skill of the logarithmic profile might also be acceptable, but above this height σ_2 is typically 25% larger than σ_1 for unstable conditions. This is also true for the bias ($\bar{y}-\bar{x}$).

The stable conditions of class $\underline{e}$ and $\underline{f}$ have about the same relative skill as was found for class $\underline{d}$. For the very stable conditions of class $\underline{h}$ σ = 1.2 ms^{-1} at 80 m, which is ~18% of $\bar{y}$. At 200 m σ_1 = 2.1 ms^{-1} or ~25% of $\bar{y}$. Note that for the stable conditions σ_1 is less than, typically, 50% of σ_2. This means that the stability correction of the scheme improves the agreement with observations markedly.

Over all stabilities σ_1 = 0.6 ms^{-1} at 40 m (11% of $\bar{y}$), as can be seen from table 3. In Figure 6 we have illustrated the good agreement on this level. In the figure a distinction is made between stable

Table 3

Comparison of the averages of observations ($\bar{y}$) and estimates ($\bar{x}$) on 6 heights z(m) and the 9 stability classes of table 1. The estimate $\bar{x}_1$ refers to Eqs. (7) or (14) with stability correction of L with the routine method. The estimate $\bar{x}_2$ refers to Eq.(7) without stability correction e.g. the logarithmic profile (L = ∞ or ψ = 0). Of the two estimation methods also the rms differences with observations (σ_1 and σ_2, respectively) are given; n is the number of observations. Also the average of the 10 m wind speed is given for each class.

z	a	b	c	d	e	f	g	h	i	all	
10	2.1	3.9	5.4	6.3	5.2	3.9	3.3	2.6	1.9	4.0	$\bar{y}$
20	2.4	4.5	6.2	6.8	6.1	4.8	4.2	3.6	2.9	4.8	$\bar{y}$
	2.4	4.3	6.2	6.9	6.2	4.8	4.2	3.4	2.6	4.8	$\bar{x}_1$
	2.5	4.5	6.2	6.9	6.0	4.5	3.8	3.0	2.2	4.6	$\bar{x}_2$
	0.17	0.50	0.62	0.49	0.36	0.27	0.58	0.29	0.44	0.40	σ_1
	0.21	0.50	0.62	0.49	0.36	0.43	1.42	0.64	0.67	0.52	σ_2
40	2.4	4.8	6.9	7.7	7.2	6.1	5.6	5.0	4.2	5.9	$\bar{y}$
	2.6	4.8	6.9	7.9	7.3	6.0	5.4	4.7	3.5	5.7	$\bar{x}_1$
	2.8	5.1	7.7	7.9	6.8	5.1	4.3	3.4	2.6	5.2	$\bar{x}_2$
	0.25	0.52	0.70	0.64	0.54	0.49	0.58	0.67	0.94	0.63	σ_1
	0.46	0.63	0.74	0.64	0.69	1.10	1.42	1.74	1.76	1.16	σ_2
80	2.6	5.1	7.6	8.9	9.0	8.3	7.8	6.8	5.6	7.3	$\bar{y}$
	2.8	5.2	7.6	9.0	8.8	7.6	7.2	6.3	4.5	7.0	$\bar{x}_1$
	3.1	5.7	7.9	9.0	7.6	5.7	4.8	3.8	2.9	5.8	$\bar{x}_2$
	0.51	0.76	0.90	1.00	1.02	1.20	1.17	1.19	1.67	1.11	σ_1
	0.78	0.99	1.01	1.00	1.71	2.77	3.16	3.24	2.98	2.31	σ_2
120	2.7	5.4	8.1	9.7	10.6	9.4	9.3	7.8	6.1	8.4	$\bar{y}$
	2.9	5.4	8.0	9.7	9.9	8.9	8.5	7.4	5.2	7.8	$\bar{x}_1$
	3.4	6.1	8.5	9.7	8.1	6.7	5.1	4.1	3.3	6.2	$\bar{x}_2$
	0.63	1.01	1.07	1.46	1.61	1.84	1.60	1.54	1.88	1.52	σ_1
	0.94	1.22	1.26	1.46	2.87	4.21	4.40	4.09	3.48	3.19	σ_2
160	2.7	5.6	8.4	10.3	11.7	11.0	10.0	8.1	6.3	8.9	$\bar{y}$
	3.0	5.6	8.3	10.2	10.8	10.0	9.5	8.2	5.7	8.5	$\bar{x}_1$
	3.5	6.3	8.8	10.2	8.5	6.4	5.4	4.2	3.2	6.5	$\bar{x}_2$
	0.72	1.22	1.33	1.86	2.06	2.22	1.78	1.76	1.98	1.79	σ_1
	1.01	1.38	1.62	1.86	3.77	5.15	4.97	4.33	3.64	3.70	σ_2
200	2.7	5.8	8.8	10.9	12.7	11.6	10.4	8.3	6.5	9.4	$\bar{y}$
	3.1	5.7	8.5	10.7	16.7	10.9	10.4	8.8	6.1	9.1	$\bar{x}_1$
	3.6	6.5	9.1	10.7	8.7	6.6	5.5	4.4	3.3	6.7	$\bar{x}_2$
	0.84	1.49	1.64	2.21	2.51	2.41	2.04	2.05	2.11	2.06	σ_1
	1.05	1.55	1.86	2.21	4.60	5.69	5.29	4.45	3.77	4.09	σ_2
n	41	196	171	134	276	209	228	174	176	1605	n

120
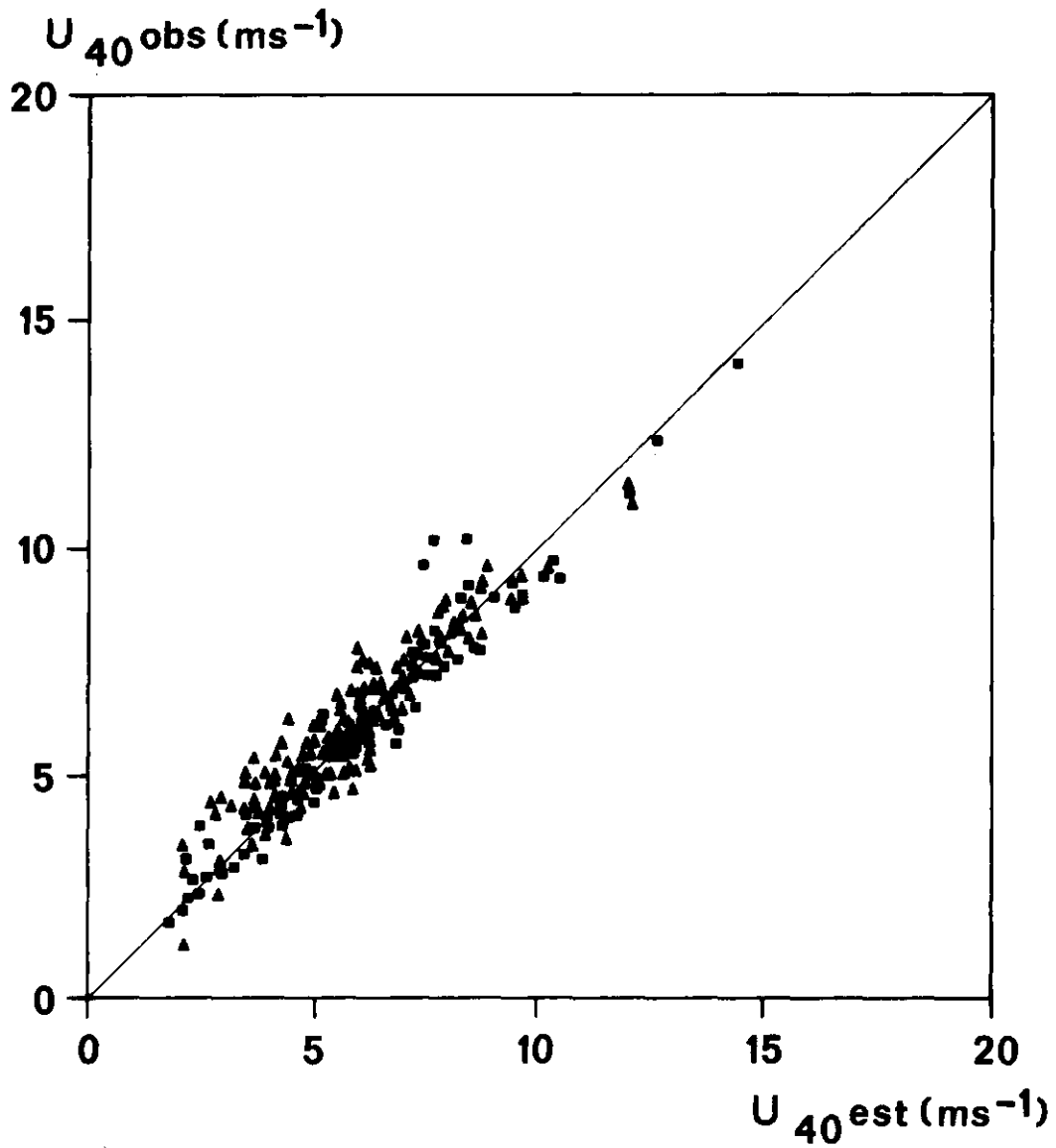
Fig. 6

Comparison of observed 40 m wind speed (U_{40} obs) and estimated wind speed (U_{40} est). Squares refer to unstable conditions (L < 0) and triangles to stable conditions (L > 0).
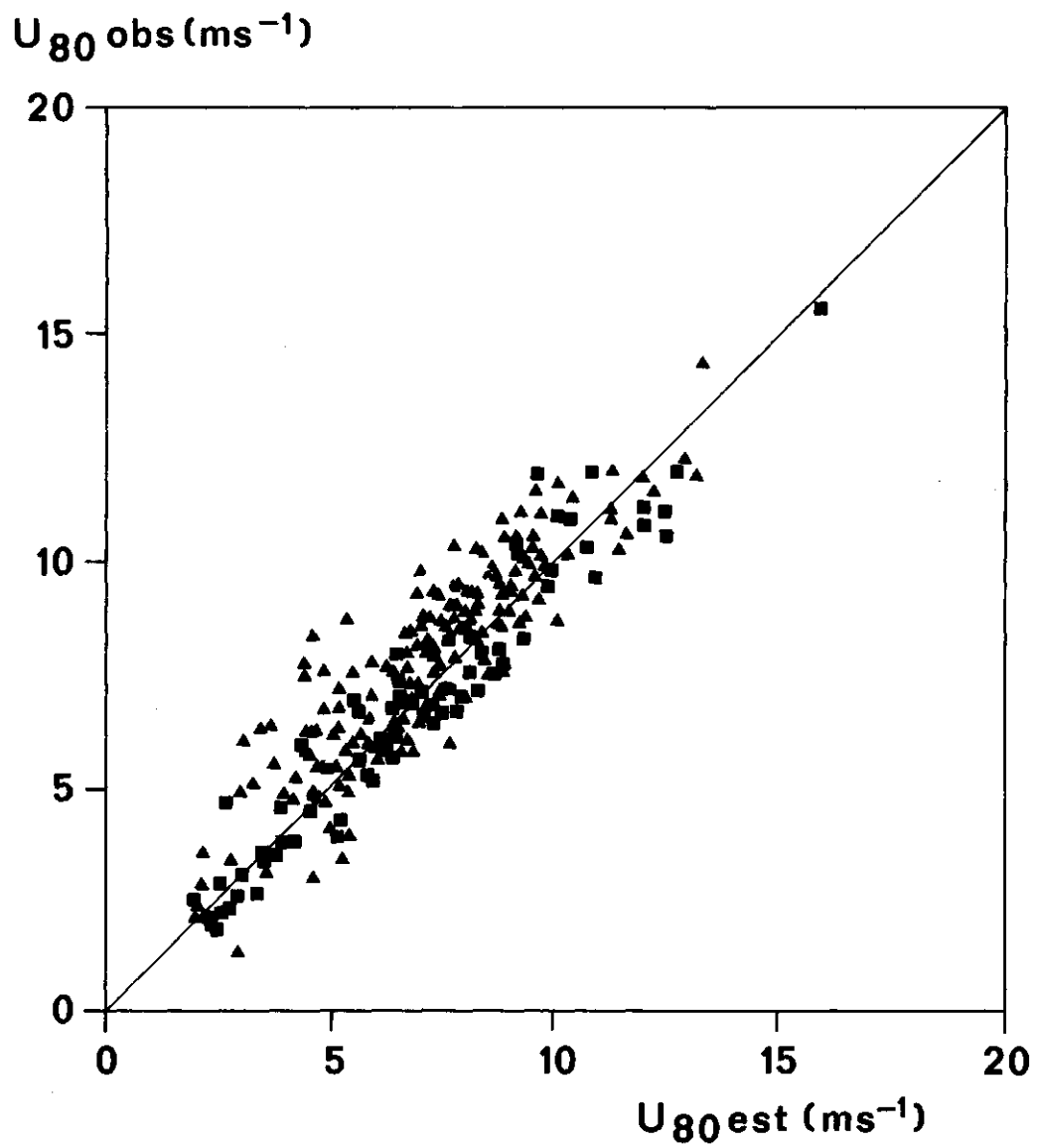
Fig. 7
As Figure 6 but for the 80 m wind speed.

conditions (triangles) and unstable conditions (squares) with a
random selection of the data in table 3. In Figure 7 the relatively
good agreement at the 80 m level is shown, for which $\sigma_1 = 1.1 \ ms^{-1}$
(15% of $\bar{y}$). Figure 8 shows the skill at the 200 m level for which
$\sigma_1 = 2.1 \ ms^{-1}$ (22% of $\bar{y}$). From Figure 8 it is clear that the error in
stable conditions can be large at the 200 m level. As can be seen
from table 3, however, the average bias is small. This is not true
for the logarithmic wind profile without stability correction.
Moreover, above 40 m σ_1 is less than 50% of σ_2 for the whole data
set. Therefore even for the calculation of a yearly average, sta-
bility corrections can not be neglected above say 40 m.

As discussed in section 3 we have excluded cases with low 10 m
wind speed $U_{10} < 1 \ ms^{-1}$ (calms). In such cases wind measurements
themselves become quite inaccurate. Therefore the present methods
give no reliable answer in the case of surface calms. For
$U_{10} \geq 1 \ ms^{-1}$ the scheme gives satisfactory results up to at least 100
m. Above this height the difference between estimates and observa-
tions may be large. The physical reasons for this are discussed in
the preceeding sections.

9. Some practical applications

In the foregoing sections we have seen that the proposed scheme
gives satisfactory agreement with data up to at least 100 m. In
practice, especially for wind energy purposes, also a good agreement
for the frequency distribution of wind speed is important. Such a
distribution is often approximated by a so-called Weibull dis-
tribution. The latter can be represented by (e.g. Sedefian, 1980;
Rijkoort, 1983)

$$f(U) = \frac{k}{a} \left(\frac{U}{a}\right)^{k-1} \exp\left[- \left(\frac{U}{a}\right)^k\right]. \tag{17}$$

Here a is a scale parameter and k is a shape parameter for the dis-
tribution f(U) of the wind speed U. The parameters a and k of f(U)
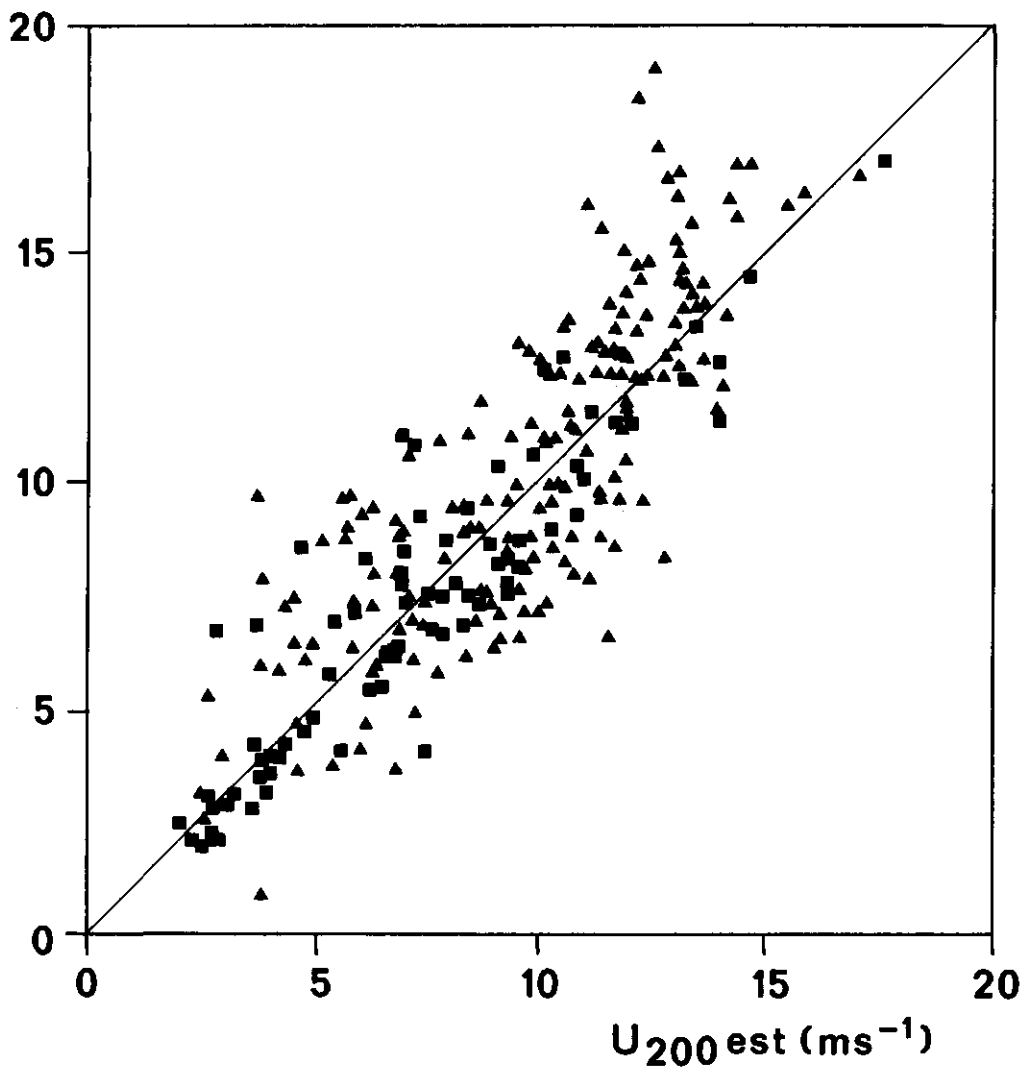can be obtained by fitting (17) to a given frequency distribution.

Fig. 8
As Figure 6 but for the 200 m wind speed.

Here this is done for wind speeds between 4 and 15 ms^{-1} (at the 80 m level).

Figure 9 shows the fitted Weibull distributions for the observed 80 m wind speed of our data set and the calculated 80 m wind speed with the proposed scheme. For comparison also the result of the logarithmic relationship is given (Eq. (7)) with $L = \infty$ or $\psi_M = 0$). Figure 9 shows clearly that the proposed scheme simulates the observed distibution very well. The result of the logarithmic profile, however, deviates markedly from the observed one. Therefore, neutral stability height extrapolation, as customary in wind energy calculations, disturbs the wind distribution severely (e.g. Sedefian, 1980). It must be noted that Figure 9 is not representative for the Cabauw wind climate. This is because of the data selection discussed in section 3. We may expect that the "real" distribution will have a higher frequency in the higher wind speeds. That distribution therefore, will be less peaked, which results in larger a and smaller k then given here.

Finally, Figure 10 shows the mean diurnal variation of the observed 10 m and 80 m wind speed. Also the results of the scheme at 80 m are given. We have used all available data of the South-East wind category for the four summer months (295 observations). It is seen that the diurnal variation of the 10 m and 80 m wind speed are reversed. This reversed diurnal cycle is simulated very well by the present scheme. When no stability corrections are made, however, the simulatated 80 m wind will have the same diurnal variation as the 10 m wind speed. Thus, provided the proper stability correction is made, the 10 m wind has a high predictive value for the 80 m wind.

In Figure 10 we have used the data of the summer months, only. In the latter months the diurnal variation of stability is much more pronounced than in the other months. Nevertheless, stability corrections should also be made in wintertime to obtain the correct behaviour of the wind at larger heights.
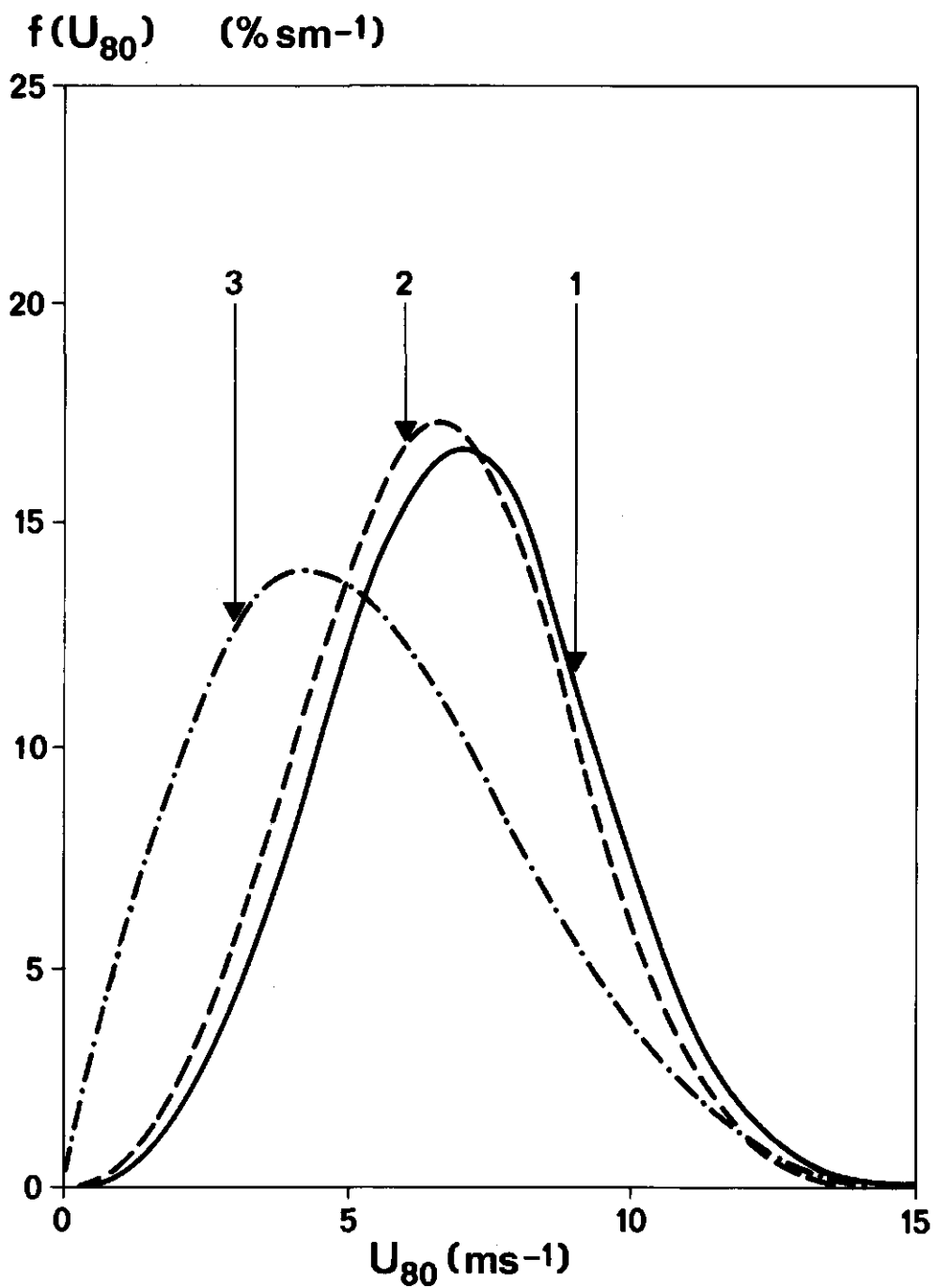
Fig. 9

Weibull frequency distributions $f(U_{80})$ for the 80 m wind speed:

1. Observed (a = 7.8 ms^{-1}, k = 3.4)

2. Proposed scheme (a = 7.4 ms^{-1}, k = 3.3)

3. Logarithmic relationship (a = 6.1 ms^{-1}, k = 2.0).

126

$\overline{U}_z (ms^{-1})$
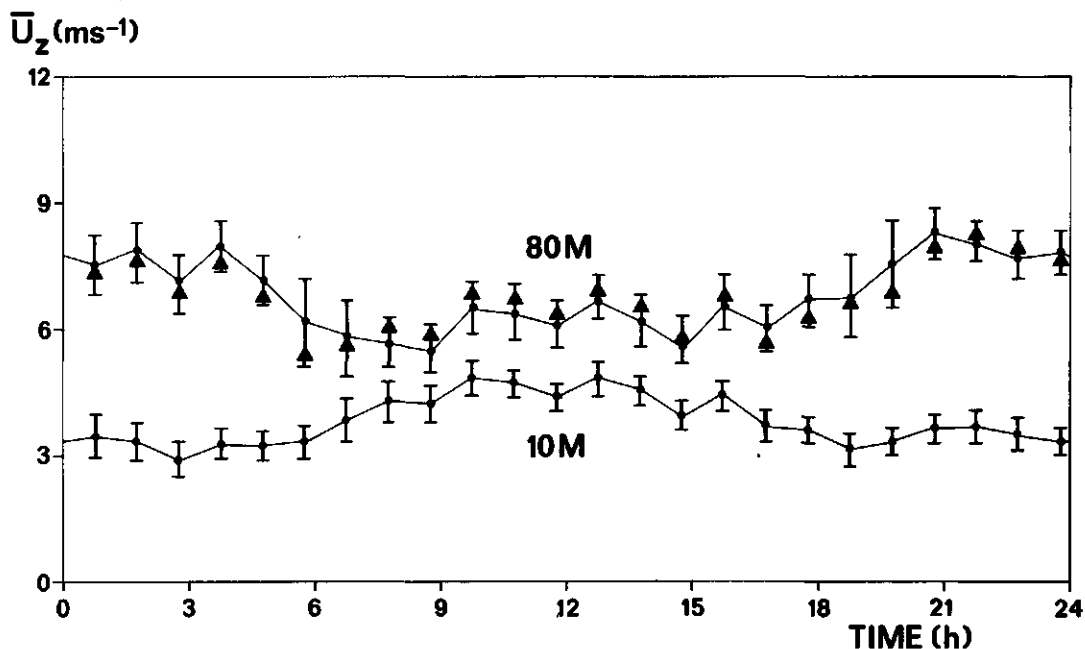
Fig. 10

The average diurnal variation of the observed 10 m and 80 m wind speed for the South-East wind direction category in the Summer months. Dots with error bars refer to the observations on each second half hour, while triangles reflect to the estimates of the proposed procedures at 80 m. The time is in hours of Greenwich Mean Time. Total number of observations n = 295.

10. Conclusions

In this paper we have analysed diabatic wind observations at the 213 m meteorological tower in Cabauw. The stability conditions vary from very unstable to very stable. It is shown that the wind profiles, on average, agree with the results of Monin-Obukhov similarity theory. This is the case when an effective roughness length is used, which represents inhomogenities of the surface in the upwind direction.

For very unstable conditions the agreement for the wind speed is good up to at least 200 m or z/L ≈ -7. For stable conditions the agreement is good up to z/L = 1. With a semi-empirical extension of the stable wind profile, acceptable agreement with observations is obtained for a substantial part of the stable boundary layer up

127

to ~ 100 m. The actual change of wind direction with height is discussed for all the stability conditions.

For routine application of the theory a scheme is used for the derivation of the Obukhov length scale from total cloud cover, 10 m wind speed (U_{10}) and air temperature at a height of 2 m. With the latter scheme and the similarity functions we obtain relatively good results for the wind speed up to at least 100 m. The rms difference σ between estimates and observations at 80 m is for all stabilities $\sigma \sim 1.1$ ms^{-1}, which is 15% of the observed average.

Above 100 m the estimate of the wind speed is still useful in unstable and moderately stable conditions. But in very stable conditions the agreement is less. For example at 200 m σ varies between 0.8 ms^{-1} for very unstable conditions up to 2.1 ms^{-1} for very stable conditions. Nevertheless, σ is reduced by typically 50% in comparison with the skill of the logarithmic wind profile, in which stability correction is neglected. In surface calms ($U_{10} < 1$ ms^{-1}) the present methods give no reliable answer.

As discussed the proposed procedures can serve as an alternative for the empirical power law with exponents related to stability categories. The procedures simulate the reversed diurnal variation of the 80 m wind speed very well. Also the simulated frequency distribution of the 80 m wind speed agrees well with the observed one. Therefore, the present methods are suitable for applied meteorological studies up to at least 100 m in generally level terrain. An application of the scheme for the description of the wind climate up to 80 m and its consequences for wind energy assessment studies, is given in Van Wijk et al. (1985).

Appendix

Derivation of the Obukhov length scale from near-surface weather data
with parameterized sensible heat flux and temperature scale.

For the application of Eqs. (7) and (14) the Obukhov length scale L,
defined by (1) is needed. Section 4 discusses two methods for the
derivation of L. Here a summary of the routine method is given, in
which the sensible heat flux or the temperature scale is para-
meterized. For unstable conditions we use the procedure developed by
Holtslag and Van Ulden (1983, Chapter III). First the incoming solar
radiation K^+ is calculated from total cloud cover N and solar
elevation ϕ:

$$K^+ = (1041 \sin\phi - 69)(1 - 0.75 N^{3.4}).\qquad\text{(A1)}$$

A simple procedure for the calculation of ϕ for given time and
location can be found in Holtslag and Van Ulden. Next net radiation
Q^* is calculated from K^+, N, the albedo r, air temperature T(K) and
surface heating coefficient c_3 by

$$Q^* = \frac{(1-r)K^+ + c_1 T^6 - \sigma T^4 + c_2 N}{1+c_3}.\qquad\text{(A2)}$$

We use r = 0.23, c_1 = 5.31 x 10^{-13} $Wm^{-2}K^{-6}$, σ = 5.67 x $10^{-8}Wm^{-2}K^{-4}$,
c_2 = 60 Wm^{-2} and c_3 = 0.12. Values of r and c_3 for other surface
conditions are discussed by Holtslag and Van Ulden.

Finally H is obtained from (De Bruin and Holtslag, 1982)

$$H = \frac{1-\alpha + \Upsilon/s}{1 + \Upsilon/s} (Q^* - G) - \beta,\qquad\text{(A3)}$$

where

$$G = c_G Q^*.\qquad\text{(A4)}$$

Here Υ/s is a universal thermodynamic function of air temperature
(see Holtslag and Van Ulden). In (A3)-(A4) we use α=1, β=20 m^{-2}, and

$c_G = 0.1$. The present values of the coefficients in (A1)-(A4) are shown to be suitable for typical climate and surface conditions in The Netherlands. For other sites, however, scarce measurements can be used to obtain adjusted values. In such cases the scheme can be applied to other conditions as well. A discussion on the variation of α, β, c_G and c_3 with surface conditions is given in Holtslag and Van Ulden (1983). Of course, when measurements of K^+, Q^* or G are available they can be incorporated in the scheme directly.

From (1), (2) and (9) L can be solved by iteration provided H is known by (A1)-(A4). We use the following procedure. The measured 10 m wind speed is used for U_z and for T the air temperature at screen height (2 m) is used. For z_0 the effective roughness length is taken. The computation starts with an estimate for u_* by way of (9) where we take initially $\psi_M = 0$ (L=∞). In this way with (1) and (2) an estimate for L is obtained. With this estimate (9) is used again to improve the estimate for u_* and so on. It appears that usually not more than five iterations are needed to achieve an accuracy of 5% in successive values of L.

For stable conditions (L > 0) with solar elevation $\phi < 0$ we parameterize L by using (Holtslag and Van Ulden, 1982)

$$\theta_* = 0.09 \ (1 - 0.5 \ N^2), \tag{A5}$$

where θ_* is the turbulent temperature scale (K) related to L by (1), (2) and (12). (A5) is a useful practical approximation to the rather complicated set of equations for the nighttime surface energy budget (see Chapter IV). Moreover θ_* of (A5) is in agreement with $\theta_* = 0.08$ K obtained by Venkatram (1980) for mainly clear sky conditions in the Prairie Grass, Kansas and Minnesota data.

With (1), (2), (8c), (9) and (12) we can obtain a quadratic equation in L, which solution can be written as

$$L = (L_n - L_0) + \{L_n(L_n - 2 \ L_0)\}^{\frac{1}{2}}. \tag{A6}$$

Here L_n and L_0 are length scales given by

130

$$L_o = \frac{\alpha \, z}{\ln(\frac{z}{z_o})} \, , \qquad\qquad\qquad (A7)$$

and

$$L_n = \frac{k \, U_z^2 \, T}{2g \, \theta_*\{(\ln(\frac{z}{z_o}))^2} \, , \qquad\qquad (A8)$$

where θ_* is given by (A5), $\alpha = 5$, $k = 0.41$, $g = 9.81 \text{ ms}^{-2}$, $z = 10$ m and T is air temperature (K). From (A5)-(A8) L can be calculated for given 10 m wind speed U_{10}, total cloud cover N and surface roughness length z_o. Real solutions exists, however, for $L_n \geq 2 \, L_o$ only. The lower limit for $L = L_o = 12.8$ m for $z_o = 0.2$ m.

It appears that the model gives real solutions for L, if $L \geq 12.8$ m. As discussed in section 4 and 6 lower values of L refer to the very stable class $\underline{i}$, in which there is little or no turbulence. A simple practical solution for $L < L_o$ is obtained by using

$$L = (L_o \frac{L_n}{2})^{\frac{1}{2}} , \qquad\qquad\qquad (A9)$$

which is continuous for $L = L_o$ and which results in $L = 0$ for $U_{10} = 0$. With (A9) and (14) we obtain a crude but simple extension of the wind profile in very stable conditions. As discussed in section 8 the agreement with observations is still useful for practical applications.

Finally, we discuss the estimates of L in transition periods with $L > 0$ and $\phi > 0$. In these periods the nighttime scheme is used as well, but here θ_* is calculated from

$$\theta_* = \theta_{*_s} \{1 - (\frac{\phi}{\phi_o})^2\} , \qquad\qquad (A11)$$

where θ_{*_s} is the value given by (A5). Here ϕ_o is the solar elevation for which $H = 0$. The latter can be obtained by putting $H = 0$ in (A3) and solving Q_* with the aid of (A4). With this value of Q_*, K^+ is calculated from (A2) and finally ϕ_o from (A1). It appears that, on average, $\phi_o = 13$ degrees for $N < 0.75$ increasing to $\phi_o = 23$ degrees for $N = 1$ (Holtslag and Van Ulden, 1983).

Chapter VI

APPLIED DISPERSION MODELLING BASED ON METEOROLOGICAL SCALING
PARAMETERS[*]

Abstract

A method for calculating the dispersion of plumes in the atmospheric
boundary layer is presented. The method is easy to use on a routine
basis. The input to the method are fundamental meteorological
parameters, which act as distinct scaling parameters for the tur-
bulence. The atmospheric boundary layer is divided into a number of
regimes. For each scaling regime we suggest models for the dispersion
in the vertical direction. The models directly give the crosswind-
integrated concentrations at the ground, χ_y, for non-buoyant releases
from a continuous point source. Generally the vertical concentration
profile is proposed to be other than Gaussian. The lateral concentra-
tion profile is always assumed to be Gaussian, and models for deter-
mining the lateral spread σ_y are proposed. The method is limited to
horizontally homogeneous conditions and travel distances less than 10
km. The method is evaluated against independent tracer experiments
over land. The overall agreement between measurements and predictions
is very good and better than that found with the traditional Gaussian
plume model.

133

1. Introduction

In practice most of the estimates of dispersion from continuous point sources are based on the Gaussian plume model. A basic assumption for the application of this model is that the plume is dispersed by homogeneous turbulence. However, due to the presence of the surface, turbulence is usually not homogeneous in the vertical direction. It is well established that for a ground level release a Gaussian concentration distribution is not found (Elliott, 1961; Gryning et al., 1983), and especially in very unstable conditions a Gaussian shape is not obtained for elevated releases (Deardorff and Willis, 1975; Briggs, 1985).

The input parameters to the Gaussian plume are often related to simple turbulence typing schemes or stability classes. A problem with these stability classes is that each covers a broad range of stability conditions, and that they are very site specific. Moreover, these classes are biased toward neutral stabililty when unstable or convective conditions actually exist (Weil, 1983). The influence of these factors on the calculated ground level concentrations is large (Kretzschmar and Mertens, 1984). To overcome some of the shortcomings of the stability classes, Hanna et al. (1977) recommended the use of turbulence measurements to estimate dispersion. Despite these recommendations, most people still use the traditional stability classes (Hanna et al., 1982).

In this chapter we divide the idealized boundary layer into a number of regimes, each characterized by distinct scaling parameters (Holtslag and Nieuwstadt, 1986, Ch. II). Based on these parameters we suggest operational dispersion models that contrast with the traditional Gaussian plume model in a number of regimes. The suggested models actually reflect the physical characteristics of the dispersion process within the various regimes of the boundary layer.

The suggested models directly give the crosswind-integrated concentrations at the surface, χ_y, for non-buoyant, non-depositing, surface and elevated releases from continuous point sources. The lateral concentration distribution is assumed to be Gaussian. The parameters of the models are briefly summarized and the models are evaluated with independent data from tracer experiments.

2. Characteristics of the Atmospheric Boundary Layer

The atmospheric boundary layer is generally regarded as that part of the atmosphere where the influence of surface friction, and surface heating or cooling is felt. The height of the atmospheric boundary layer during daytime, roughly coincides with the height to which pollutants are mixed (the so-called mixing height h). During nighttime stable conditions h is typically an order of magnitude smaller than the maximum daytime value over land. In this case, h is typically smaller than the height to which the surface radiation inversion extends. Above the sea, the diurnal variation of h is much smaller.

The turbulent structure of the boundary layer can be described with three length scales. These are the height above the surface z, the mixing height h, and the Obukhov length L. The height z limits the eddy size to the ground and h limits the vertical extent of the eddies. The Obukhov length L reflects the height at which the contribution to the turbulent kinetic energy from buoyancy forces and from the shear stress are comparable (Obukhov, 1946). The Obukhov length is defined by the surface fluxes of heat $H = \rho c_p \overline{w\theta}_0$ and momentum $u_*^2 = -\overline{uw}_0$ by

$$L = \frac{-u_*^3}{k \frac{g}{T} \overline{w\theta}_0} , \tag{1}$$

where k is the Von Kármán constant and g/T is the buoyancy parameter. For humid conditions, $\overline{w\theta}_0$ should be replaced by the virtual heat flux (Bush, 1973). The three length scales define two independent non-dimensional parameters. Here we choose z/h, the relative height, and h/L, which can be regarded as a stability parameter for the whole boundary layer.

Fig. 1, which is from Holtslag and Nieuwstadt (1986, Ch. II), shows several scaling regimes for the boundary layer. For unstable conditions (L<0) five distinct regimes are identified, in agreement with Panofsky (1978), Nicholls and Readings (1979) and Caughey

1.2
0.8

Entrainment layer

Mixed layer | Near neutral upper layer

$\dfrac{z}{h}$

N. neu. up. layer

z-less scaling layer

Intermittency layer

Local scaling layer

0.1

Free convection layer

Surface layer

Surface layer

0.01

−100 $\dfrac{h}{L}$ −10 UNSTABLE −1 0 1 NEUTRAL 5 STABLE $\dfrac{h}{L}$ 10
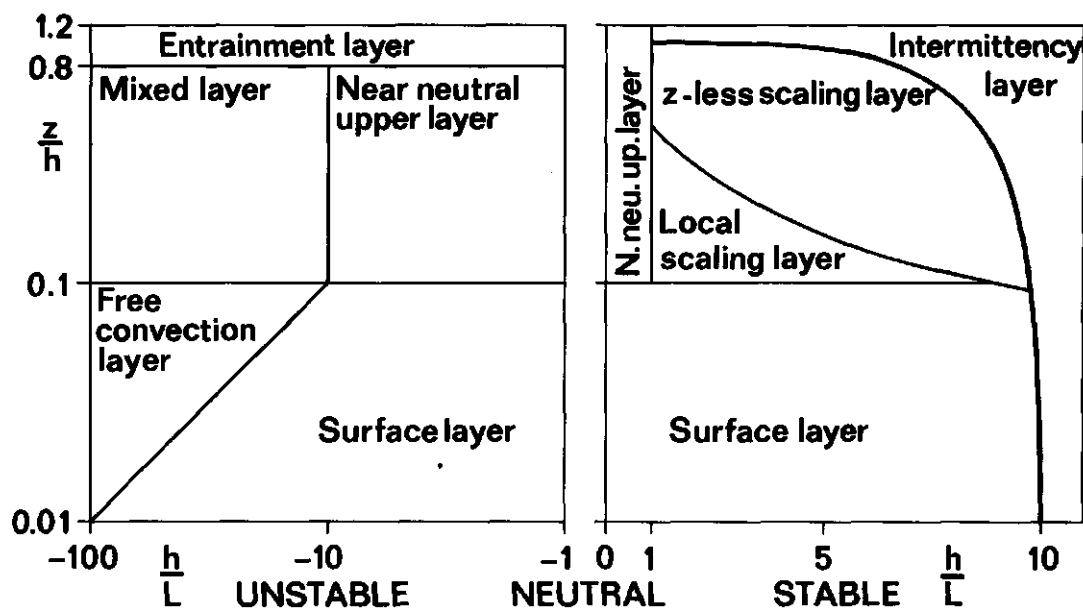
Fig. 1

The scaling regions of the atmospheric boundary layer, shown as function of the dimensionless height z/h, and the stability parameter h/L. A detailed discussion can be found in Holtslag and Nieuwstadt (1986). When used to determine dispersion regions, the dimensionless height is replaced by z_s/h where z_s is the source height. The boundaries between the regions are given in section 3.

(1982). The turbulent structures of the surface layer, the free convection layer, and the mixed layer are well understood under horizontally homogeneous and stationary conditions. Less is known for the near-neutral upper layer (Nicholls and Readings, 1979) and the entrainment layer (Deardorff et al., 1980; Driedonks and Tennekes, 1984).

The scaling regimes for the stable boundary layer (L > 0) are: the surface layer, the local scaling layer, the z-less scaling layer, the near-neutral upper layer, and the intermittency layer. The local scaling layer was recently introduced by Nieuwstadt (1984a, 1984b). Presently, no theory is available for the description of the inter-mittency layer.

136

The dividing lines between the regions of Fig. 1 are discussed by Holtslag and Nieuwstadt (1986, Ch. II). The turbulent structure of the stable boundary layer has been investigated less than the unstable counterpart, which means that the dividing lines between the stable regimes are more uncertain.

3. Vertical dispersion

In this section the structure of the turbulence and its implications for the vertical dispersion models are described. Models are proposed, which are based on the specific turbulent structure in the individual regimes of the atmospheric boundary layer. We do not treat dispersion models for the entrainment layer and the intermittency layer. The different dispersion regimes are defined in Fig. 1. To determine the dispersion regions we use z_s/h, where z_s is the source height.

3.1 The surface layer ($-z_s/L < 1$ and $z_s/h < 0.1$)

The wind shear and the radiational heating or cooling of the surface plays a dominant role for the structure of the turbulence in the surface layer. The effect of stability on the structure is described by Obukhov similarity theory. Nieuwstadt and Van Ulden (1978) have shown that the vertical dispersion from a ground-level source in the surface layer is adequately described by K-models. A number of investigations have shown that the diffusivity of matter, K, can be adequately approximated by the diffusivity of heat

$$K = k\ u_* \ z/\phi_h(z/L),\qquad (2)$$

where ϕ_h is the non-dimensional temperature gradient. The K-model is often solved numerically. Analytical solutions for the cross-wind-integrated concentration χ_y were obtained as early as in the 1930's with power laws inserted for the profiles of wind speed and eddy diffusivity. Part of the pioneering mathematical work is published by Köhler (1933). Van Ulden (1978) expresses the analytical solutions in the elegant way

$$\chi_y(z)/Q = (A/(\overline{z}.\overline{U}))\exp\left\{-(Bz/\overline{z})^s\right\}, \tag{3}$$

where Q is the source strength, A and B are functions of the shape
parameter s, $\overline{z}$ is the mean height of the plume and $\overline{U}$ is the mean
transport velocity of the plume. The definition of $\overline{z}$ and $\overline{U}$ can be
found in Gryning et al. (1983). Operational methods that can be used
to derive these quantities are given in the Appendix for ground level
and elevated sources. In Eq. (3) deposition is not taken into ac-
count.

The above method is applicable for $\overline{z}/z_s > 2$. Closer to the source
we recommend the use of the models proposed for the near-neutral
upper layer (Section 3.2). When the plume is so far downwind that
$\overline{z}$ is substantially larger than the height of the surface layer, the
dispersion is considered to be dominated by the layer above the sur-
face layer. For unstable conditions this is the mixed layer or the
near-neutral layer. We suggest this to be the case when $\overline{z}/h > 0.3$.
For elevated sources we recommend use of the models for these layers.

With Eq. (3) we obtain a Gaussian concentration profile when s=2.
It is characteristic that s is not generally 2 but varies as a
function of stability and downwind distance. Under neutral con-
ditions, s approaches 1 far downwind from the source. Under stable
conditions, s has an asymptotic limit of 3. The convective limit of s
is about 0.5, but the precise value is uncertain. The variation of s
has been experimentally verified for near-neutral conditions by
Gryning et al. (1983) and for stable conditions by Ogawa et al.
(1985).

3.2 Near neutral upper layer ($-10 < h/L < 1$ and $0.1 < z_s/h < 0.8-1$)

This layer often exists over the sea (Nicholls and Readings,
1979) and is present over land in overcast, windy conditions. The
characteristics of dispersion in the near-neutral upperlayer have not
been thoroughly investigated. Because our knowledge is so limited we
have retained the Gaussian plume model to calculate the crosswind
integrated concentration at ground-level, e.g.

138

$$\frac{\chi_y}{Q} = (\frac{2}{\pi})^{\frac{1}{2}} \frac{1}{U\sigma_z} (\exp [-\frac{1}{2} (\frac{z_s}{\sigma_z})^2]$$

$$+ \exp [-\frac{1}{2} (\frac{z_s}{\sigma_z})^2 (1 - \frac{2h}{z_s})^2] \qquad (4)$$

$$+ \exp [-\frac{1}{2} (\frac{z_s}{\sigma_z})^2 (1 + \frac{2h}{z_s})^2]).$$

The estimate of the vertical spread in the Gaussian plume model, σ_z, is based on Taylor's (1921) theory for plume dispersion in homogeneous turbulence. This theory relates σ_z to the standard deviation of the vertical wind fluctuations, σ_w. The relation can generally be written as

$$\sigma_z = \sigma_w t f_z(t/T_z), \qquad (5)$$

where t is travel time and T_z is the Lagrangian time scale. For practical use in the near-neutral upper layer we suggest an interpolation formula for f_z, which has the correct asymptotic limits for small and large travel times, e.g.

$$f_z = 1/(1 + (t/2T_z)^{\frac{1}{2}}), \qquad (6)$$

where T_z is given by

$$T_z = 300 \text{ s} \qquad \text{for } L < 0,$$
$$T_z = 30 \text{ s} \qquad \text{for } L > 0.$$

The suggestion for f_z and T_z for $L < 0$ is comparable to the formula proposed by Draxler (1976) for unstable conditions.

Whenever possible, measured values of σ_w should be used in Eq. (5). If direct measurements are not available, an estimate of σ_w for $z_s/h < 1$ can be obtained from

$$(\sigma_w/u_*)^2 = 1.5 \ [z_s/(-kL))]^{2/3} \exp(-2z_s/h)+(1.7-z_s/h) \quad \text{for } L<0,$$

$$\tag{7}$$

and Eq. (14) later in this paper for $L>0$. The equation for σ_w/u_* is based on an empirical model for shear-produced variance by Brost et al. (1982) and for buoyancy-produced variance by Baerentsen and Berkowicz (1984).

3.3 Mixed layer ($-h/L > 10$ and $0.1 < z_s/h < 0.8$)

The dispersion process in the mixed layer is dominated by the asymmetric structure of the turbulence. Throughout most of the layer downdrafts occupy a greater area than updrafts. Therefore, a particle released from an elevated non-buoyant source has a higher probability of travelling downward than upward. As a result, close to the source the line of maximum concentration descends until it reaches ground-level. Conversely, a particle released from a non-buoyant ground-level source is found to ascend in such a way that the line of maximum concentration rises. This is due to the strongly inhomogeneous structure of the turbulence near the surface (Van Dop et al., 1985). The plume behaviour discussed above has been observed in water tank experiments (Willis and Deardorff, 1978), in wind tunnel simulations (Porek and Cermak, 1984), in Monte Carlo numerical simulations (De Baas et al., 1986) and in field experiments (Briggs, 1983; 1985). In the mixed layer the relevant quantities are the heat flux $(g/T) \overline{w\theta}_0$ and the inversion height h. The characteristic velocity scale is (Deardorff, 1970; Tennekes, 1970)

$$w_* = (\frac{g}{T} \overline{w\theta}_0 h)^{1/3}. \tag{8}$$

The dispersion process in the mixed layer can be parameterized with w_* and h. The downwind dimensionless distance is then $X = (w_*/h)(x/U)$ where x/U is the travel time. The dimensionless crosswind-integrated concentration at ground-level is $C_y = \chi_y hU/Q$, where Q is the source strength. The dimensionless source height is $Z_s = z_s/h$, with z_s being the height of the source. Briggs (1985) pro-

vided an empirical parameterization among X, Z_s and C_y at ground-level

$$C_y = \frac{0.9 \, X^{9/2} \, Z_s^{-11/2}}{[Z_s^{-4} + 0.4 \, X^{9/2} \, Z_s^{-9/2}]^{4/3}}$$

$$+ \frac{1}{1 + 3 \, X^{-3/2} \, Z_s^{1/2} + 50 \, X^{-9/2}}. \tag{9}$$

Fig. 2 illustrates the behaviour of Eq. (9) for a number of Z_s values. It is characteristic that an X-range exists where the ground level concentration increases with source height. The sub-unity values of C_y near $X=2$ are associated with an elevated concentration maximum. It can also be seen that, irrespective of the release height, the plume will be well mixed between the ground and the mixing height beyond $X=5$. According to Briggs (1985), Eq. (9) is valid for non-buoyant plumes provided $0.04 \leq Z_s \leq 1$, and can thus be applied in a large part of the free convection layer as well. The model validation in section 5 reveals that a better fit is obtained when the curve of Eq. (9) is shifted towards higher values of X. Therefore, for practical use we suggest to replace X by $1.7 \, X$ in Eq. (9).

3.4 The free convection layer $(-z_s/L > 1 \text{ and } z_s/h < 0.1)$

This layer is a matching region of both surface layer and mixed layer scaling. To describe the dispersion from near surface releases, Nieuwstadt (1980) suggested

$$C_y = 0.9 \, X^{-3/2}, \tag{10}$$

which for convenience is expressed in mixed layer scaling parameters. It can easily be shown that Eq. (10) implies that C_y is independent of h and u_*, and consequently is applicable for the free convection layer. Comparison with results of the Prairie grass experiments shows that Eq. (10) is valid for $0.03 < X < 0.23$ (Nieuwstadt, 1980).
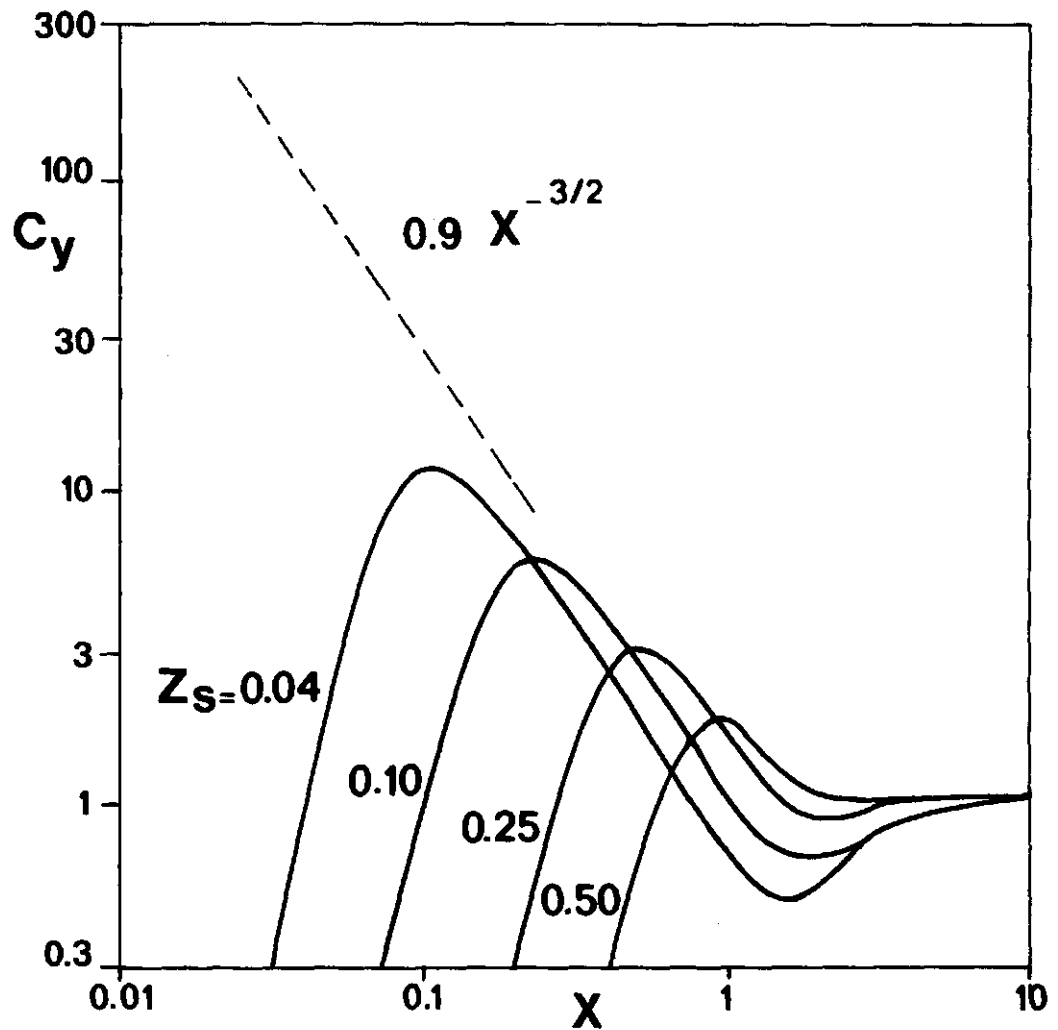
Fig. 2

The dimensionless ground level concentration C_y as function of dimensionless downwind distance X for the mixed layer as given by Eq. (9). This equation is illustrated for a number of dimensionless source heights Z_s (solid lines). The dashed line shows C_y as function of X for a ground level source in the free convection layer, as described by Eq. (10).

No expression similar to Eq. (10) exists for elevated sources in the free convection layer. However, Briggs (1985) suggests that Eq. (9) adequately describes the dispersion process in the free convection layer provided $Z_s > 0.04$. Fig. 2 shows the connection between Eq. (9) for mixed layer dispersion and Eq. (10) for dispersion in the free convection layer. Note that quantitative agreement between Eq. (9) when applied for low sources in the free convection layer and Eq. (10) for ground level sources is obtained by shifting the curve of Eq. (9) by a factor of ~1.7 towards higher values of X.

Holtslag (1984b) compared the free convection predictions using Eq. (10) with surface layer predictions of Eq. (3) (with s=1.5). The comparison was done on the Prairie grass data. At x = 50 m it was seen that the surface layer model performed better than the free convection layer model, confirming that at x = 50 m the plume was still within the surface layer. At x = 200 m and x = 800 m the predictions of the two models were found to be similar. This suggests that both scaling principles can be used at these distances. The borders between the scaling regions as depicted in Fig. 1, therefore, only give the order of magnitude for the separation of the scaling regions.

3.5 Local and z-less scaling layers

    (h/L > 1 and z_s/h > 0.1 and (h-z_s)/ Λ < 10)

The turbulence and dispersion in these stable layers have not been so well investigated as in the stable surface layer. Due to the stable stratification the turbulence is suppressed, resulting in a structure completely different from the convective counterpart. Above the stable surface layer, the turbulence scales with the local values of the momentum and heat fluxes (Nieuwstadt, 1984a). Based on the local fluxes, Nieuwstadt formed a local Obukhov length

$$\Lambda = \frac{-\tau^{3/2}}{k \frac{g}{T} \overline{w\theta}} ,$$

(11)

where τ and $\overline{w\theta}$ are the local fluxes of shear and heat. For horizontally homogeneous and steady state conditions Nieuwstadt (1984a) proposed

$$\Lambda/L = (1-z/h)^{5/4}. \tag{12}$$

Here the height of the turbulent layer h is given by

$$h = 0.4 \left(\frac{u_* L}{f}\right)^{1/2}, \tag{13}$$

as originally suggested by Zilitinkevich (1972). Pasquill and Smith (1983) report values in the range 0.2 - 0.7 of the constant in Eq. (13), which strongly stresses that measurements of h are preferred. When the turbulent eddies no longer feel the presence of the ground, z is no longer a characteristic scaling parameter for the turbulence and z-less scaling is appropriate (Wyngaard, 1973). Holtslag and Nieuwstadt (1986, Ch. II) suggest that z-less scaling is applicable for $z/\Lambda > 1$ and $(h-z)/\Lambda < 10$.

Our knowledge of the characteristics of the vertical dispersion in the local scaling and the z-less scaling layers is very scarce. Therefore we retain the use of the Gaussian plume model. The vertical spread parameter, σ_z, should be calculated in the same way as for the stable near neutral upper layer, Eq. (6), with $T_z = 30s$. This suggestion is shown by Irwin et al. (1985) to be nearly equivalent with the f_z function for stable conditions proposed by Venkatram et al. (1984). Direct measurements of σ_w are preferred and strongly recommended. If no measurements are available, however, σ_w can be estimated by

$$(\sigma_w/u_*)^2 = 1.7 (1-z_s/h)^{3/2}, \tag{14}$$

as proposed by Nieuwstadt (1984a) for horizontally homogeneous and stationary conditions.

4. Lateral dispersion

In the previous section the length scales of the turbulence and their implications for the vertical dispersion process were described. Because no restrictions exist in the lateral direction there are no obvious length scales and a similar approach is therefore not possible. The lateral dispersion can be viewed as the combined effect of turbulence of the air and shear in the wind direction. Only the first of these processes will be treated here. The shear effect is not believed to be important within the first 5-10 km from the source, except under very stable conditions (Pasquill and Smith, 1983).

Experiments show that the lateral profile of a plume resembles a Gaussian distribution. (Sivertsen, 1978; Gryning et al., 1978; Nieuwstadt and Van Duuren, 1979). Therefore, knowing the cross-wind-integrated concentration at the surface, $\chi_y(x,z = 0)$ we can calculate the concentration at the surface at any point using

$$\chi(x,y,o) = \frac{\chi_y(x,o)}{(2\pi)^{\frac{1}{2}}\sigma_y} \exp\left(- \frac{y^2}{2\sigma_y^2}\right), \tag{15}$$

where y is the crosswind distance and σ_y is the crosswind spread of the plume. Gryning and Lyck (1984) demonstrate that the best estimate for σ_y is obtained by using a simplified version of Taylor's (1921) formula for plume dispersion. The formula relates σ_y to the standard deviation of the lateral wind fluctuations

$$\sigma_y = \sigma_v \ t \ f_y(t/T_y), \tag{16}$$

where f_y is a function of the dimensionless travel time t/T_y and T_y is the Lagrangian time scale for the lateral dispersion.

A comparison of several empirical forms of f_y with field data suggests that the function proposed by Draxler (1976) is best overall (Irwin, 1983; Gryning and Lyck, 1984). Draxler's f_y-function can be written

$$f_y = 1/(1 + (t/2T_y)^{1/2}),\qquad\qquad\qquad (17)$$

and is appropriate for an averaging time of the order of $\frac{1}{2}$ to 1 hour. In accordance with Draxler (1976) we recommend that the Lagrangian time scale be taken as $T_y = 600s$ for elevated sources ($z_s/h > 0.1$) and $T_y = 200s$ for ground level sources irrespective of the atmospheric stability. However, $T_y = 600s$ should be used also for a ground level source when $\overline{z}/h > 0.1$. Irwin (1983) obtained good results for both elevated and ground level sources with $T_y = 600s$. Measured values of σ_v at source height are preferred in Eq. (16). The measured values should represent an averaging time that corresponds to the averaging time of the concentration values.

However, if measurements of σ_v are not available, it can be estimated for unstable conditions from

$$(\sigma_v/u_*)^2 = 0.35\,(-\frac{h}{kL})^{2/3} + (2 - z_s/h).\qquad\qquad (18a)$$

This equation is based on an empirical model for shear-produced variance by Brost et al. (1982) and for buoyancy-produced variance by Caughey (1982). For stable conditions we propose

$$(\sigma_v/u_*)^2 = 2(1 - z_s/h),\qquad\qquad\qquad (18b)$$

which is continuous with (18a) at the surface in neutral conditions ($h/L = 0$). The corresponding averaging time for Eq. (18) is roughly ~30 min. The expression for σ_v under stable conditions does not include the effect of gravity waves which for averaging times >10 min. can be very significant. This again stresses the importance to measure σ_v.

5. Validation

The individual models that we have proposed for calculating the
atmospheric dispersion in the various regimes of the atmospheric
boundary layer have been evaluated in the literature with observa-
tions from quite different sources. For low sources the Prairie Grass
Data often have been used (Nieuwstadt and Van Ulden, 1978; Van Ulden,
1978; Horst, 1979; Gryning et al. 1983; Holtslag, 1984b).

For elevated sources a wide variety of data sets exist which
cover several source heights, a variety of surface roughness con-
ditions, and a broad range of atmospheric stability conditions
(Irwin, 1983; Nieuwstadt and Van Duuren, 1978; Briggs, 1985). The
method of this paper has also been evaluated using independent data
from Copenhagen in Denmark, from Norway, and from the Hanford
diffusion grid in Washington.

Gryning and Lyck (1984) describe atmospheric dispersion experi-
ments that were carried out in the northern part of Copenhagen under
neutral and unstable conditions. The tracer sulphurhexafluoride was
released without buoyancy from a tower at a height of 115 m, and
collected at ground-level positions in up to three crosswind arcs of
tracer sampling units. The sampling units were positioned 2-6 km from
the point of release. Tracer releases typically started 1 hour before
the start of tracer sampling and stopped at the end of the sampling
period. The averaging time for tracer sampling was 1 hour. The site
was mainly residential with a roughness length of ~0.6 m. The meteo-
rological measurements taken during the tracer experiments included
continuous recording of the three-dimensional wind velocity fluctua-
tions at the height of release, radiosoundings, and time averaged
profile measurements of wind and temperature at the 200 m tower where
the tracer release took place. From these measurements, values of
σ_v, σ_w, the mean wind speed at the release heights, and the mixing
height were determined; the Obukhov lengths were calculated from the
profile measurements (Gryning, 1981).

Doran and Horst (1985) describe the sulphurhexafluoride tracer
experiments that were carried out at the Hanford diffusion grid in
Washington. The grid is located in a semi-arid region on generally

flat terrain. The vegetation consists primarily of desert grasses and
1 to 2 m high sagebrush. The roughness length of the area was 3 cm
with a displacement height of 1.4 m. The tracer was released at 2 m's
height and sampled in arcs 100, 200, 800 1600 and 3200 m from the
source. The friction velocity and the Monin-Obukhov length were
determined by a sonic anemometer and resistance thermometer in four
of the experiments, and determined from log-linear fit to observed
wind and temperature profiles in the remaining two experiments.

Sivertsen and Bøhler (1985) describe tracer experiments that were
carried out in Lillestrøm, a town situated in the southern part of
Norway, under stable atmospheric conditions. Only one of the experi-
ments were suited for this type of analysis. The remaining experi-
ments were carried out under meteorological conditions characterized
by Richardson numbers larger than 0.2, which makes determination of
the Obukhov length obscure. The release height of the tracer in this
experiment was 10 m. Sulphurhexafluoride was used as tracer. The
tracer was sampled near ground-level in arcs 0.7 and 1.5 km from the
source with a 15 min. averaging time. The site was a residential area
with a roughness length of 0.5 m. Meteorological measurements were
taken on a 36 m mast. Measurements of wind speed and σ_v were made at
the release height (10 m). Also, time averaged profiles of wind and
temperature were recorded at the mast. During the experiment a
minisonde was launched.

Table 1 shows a summary of the meteorological conditions during
the experiments by Gryning and Lyck (1984), Doran and Horst (1985),
and by Sivertsen and Bøhler (1985). The relevant scaling regimes for
each experiment are indicated. For the experiments in unstable con-
ditions, all of the scaling regimes are covered. For stable condi-
tions, most of the experiments occurred in the surface layer, and
only one experiment took place in the local scaling layer.

In Table 2 predicted and corresponding measured crosswind-in-
tegrated concentrations, for the various experiments are shown. The
comparison is illustrated for atmospheric unstable conditions in
Fig. 3, and for stable conditions in Fig.4.

The two experiments in the mixed layer scaling regime qualita-
tively support the general theory of the behaviour of plumes in the

148

Table 1

Summary of the meteorological conditions during the experiments that were used for the evaluation of the proposed method for dispersion calculations.

Experiment						Meteorological conditions						
No.	Date	Ref.	z_s (m)	h (m)	L (m)	σ_v (ms^{-1})	σ_w (ms^{-1})	u_* (ms^{-1})	u_s (ms^{-1})	z_s/h	h/L	Stability regime
1	20 Sep 78	GL	115	1980	-46	0.98	0.83	0.37	3.4	0.058	-43	FCL
2	26 Sep 78	GL	115	1920	-384	1.39	1.07	0.74	10.6	0.060	- 5	SL
3	19 Oct 78	GL	115	1120	-108	0.85	0.68	0.39	5.0	0.103	-10	ML
4	3 Nov 78	GL	115	390	-173	0.47	0.47	0.39	4.6	0.295	-2.3	NNUL
5	9 Nov 78	GL	115	820	-577	0.77	0.71	0.46	6.7	0.140	-1.4	NNUL
6	30 Apr 78	GL	115	1300	-569	2.26	1.33	1.07	13.2	0.088	-2.3	SL
7	27 Jun 78	GL	115	1850	-136	1.61	0.87	0.65	7.6	0.062	-14	SL
8	6 Jul 78	GL	115	810	-72	1.35	0.72	0.70	9.4	0.142	-11	ML
9	19 Jul 78	GL	115	2090	-382	1.71	0.98	0.77	10.5	0.055	-5.5	SL
10	5 Jan 84	SB	10	90*	60	0.17	-	0.09	0.9	0.11	1.5	LS
11	18 May 83	DH	2	325*	166	-	-	0.40	-	0.0019	2.0	SL
12	26 May 83	DH	2	135*	44	-	-	0.26	-	0.0044	3.1	SL
13	5 Jun 83	DH	2	182*	77	-	-	0.27	-	0.0033	2.4	SL
14	12 Jun 83	DH	2	104*	34	-	-	0.20	-	0.0058	3.1	SL
15	24 Jun 83	DH	2	157*	59	-	-	0.26	-	0.0038	2.7	SL
16	27 Jun 83	DH	2	185*	71	-	-	0.30	-	0.0033	2.6	SL

SB: Sivertsen and Bøhler (1985), GL: Gryning and Lyck (1984). DH: Doran and Horst (1985)

LS: Local scaling layer; ZL: z-less scaling layer; SL: surface layer;

FCL: Free convection layer; ML: mixed layer; NNUL: near neutral upper layer.

* indicates that h is estimated from Eq.(13).

mixed layer (Holtslag et al., 1986, Gryning, 1981), but the measured concentrations are larger than the predicted. As discussed by Briggs (1985) and Sivertsen et al. (1985) a better fit is obtained when the curve of Eq. (9) is shifted towards higher values of X. Therefore, in the comparison of this paper X was multiplied by a factor of 1.7 before using Eq. (9).

For atmospheric unstable conditions the mean fractional error (see list of Symbols and Notation) between measured and predicted cross-wind-integrated concentrations is near -2%. The standard deviation of the fractional errors, which describes the ability of the method to predict the variation in the measured χ_y-values, is 21%. In some of the experiments from Copenhagen, the measured crosswind-integrated concentrations were higher than could be predicted by a Gaussian model. This inconsistency is not present in the model proposed here.

In order to compare the skill of the Gaussian model with the method suggested in this paper, all the tracer experiments in the Copenhagen data set were simulated with the Gaussian model that is proposed for the near-neutral upper layer. When measured values

Table 2

Observed and estimated crosswind-integrated concentrations χ_y/Q and lateral spread parameter, σ_y, for the dispersion experiments of Table 1; "-" indicates that σ_y is not contained in the data set.

Scaling regime	Experiment number	Distance from source (km)	χ_y/Q Observed (10^{-4} sm^{-2})	χ_y/Q Estimated (10^{-4} sm^{-2})	σ_y Observed (m)	σ_y Estimated (m)
Local and z-less scaling layers	10	0.70	440	420	-	
		1.40	150	300	-	
Surface layer	2	2.10	5.38	5.47	239	196
		4.20	2.95	2.85	438	350
	6	2.00	3.96	4.12	-	
		4.20	2.22	2.21	-	
		5.90	1.83	1.78	-	
	7	2.00	6.70	5.84	290	289
		4.10	3.25	2.47	595	520
		5.30	2.23	1.69	786	637
	9	2.10	4.58	5.24	236	243
		4.20	3.11	2.91	460	434
		6.00	2.59	2.47	623	578
	11	0.20	117	261	-	
		0.80	37	78	-	
		1.60	21	43	-	
		3.20	13	25	-	
	12	0.20	367	446	-	
		0.80	129	155	-	
		1.60	91	92	-	
		3.20	72	56	-	
	13	0.20	181	412	-	
		0.80	59	132	-	
		1.60	33	76	-	
		3.20	18	45	-	
	14	0.20	486	628	-	
		0.80	201	215	-	
		1.60	131	128	-	
		3.20	91	78	-	
	15	0.20	424	441	-	
		0.80	105	144	-	
		1.60	86	85	-	
		3.20	66	51	-	
	16	0.20	611	375	-	
		0.80	134	120	-	
		1.60	61	70	-	
		3.20	31	42	-	
Free convection layer	1	1.90	6.48	6.79	254	326
		3.70	2.31	2.55	444	546
Mixed layer	3	1.90	8.20	10.46	184	207
		3.70	6.22	5.68	283	352
		5.40	4.30	3.29	404	471
	8	1.90	4.16	6.03	190	193
		3.60	2.02	3.24	402	330
		5.30	1.52	1.86	580	452
Near neutral upper layer	4	4.00	11.66	7.73	301	221
	5	2.10	6.72	6.20	185	160
		4.20	5.84	4.72	279	280
		6.10	4.97	3.80	376	375

150

Fig. 3

Estimated versus observed crosswind-integrated concentrations for the
experiments that were carried out during unstable conditions. The
symbols refer to the surface layer (open circles); the surface layer
when $\bar{z}/h > 0.3$ (solid circles); the near neutral upper layer
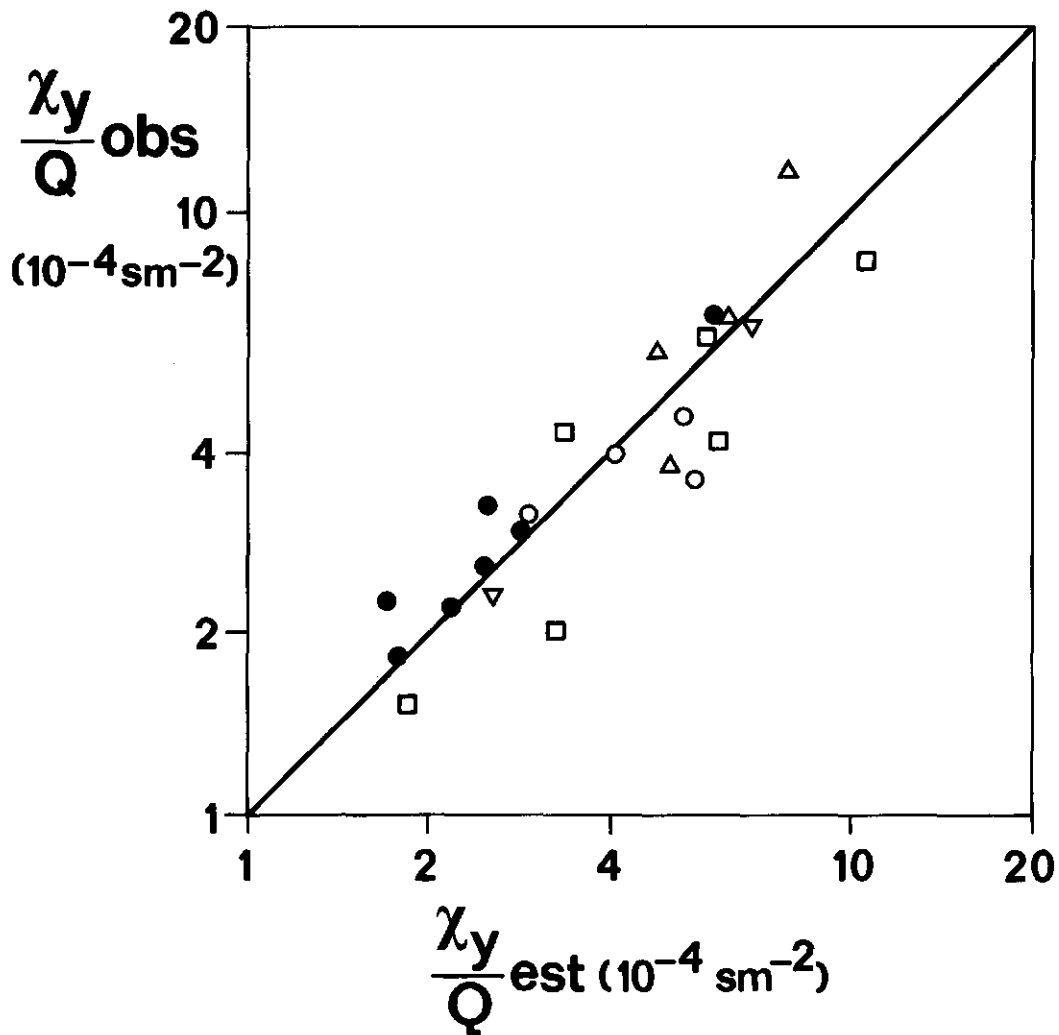(triangles); the mixed layer (squares); the free convection layer
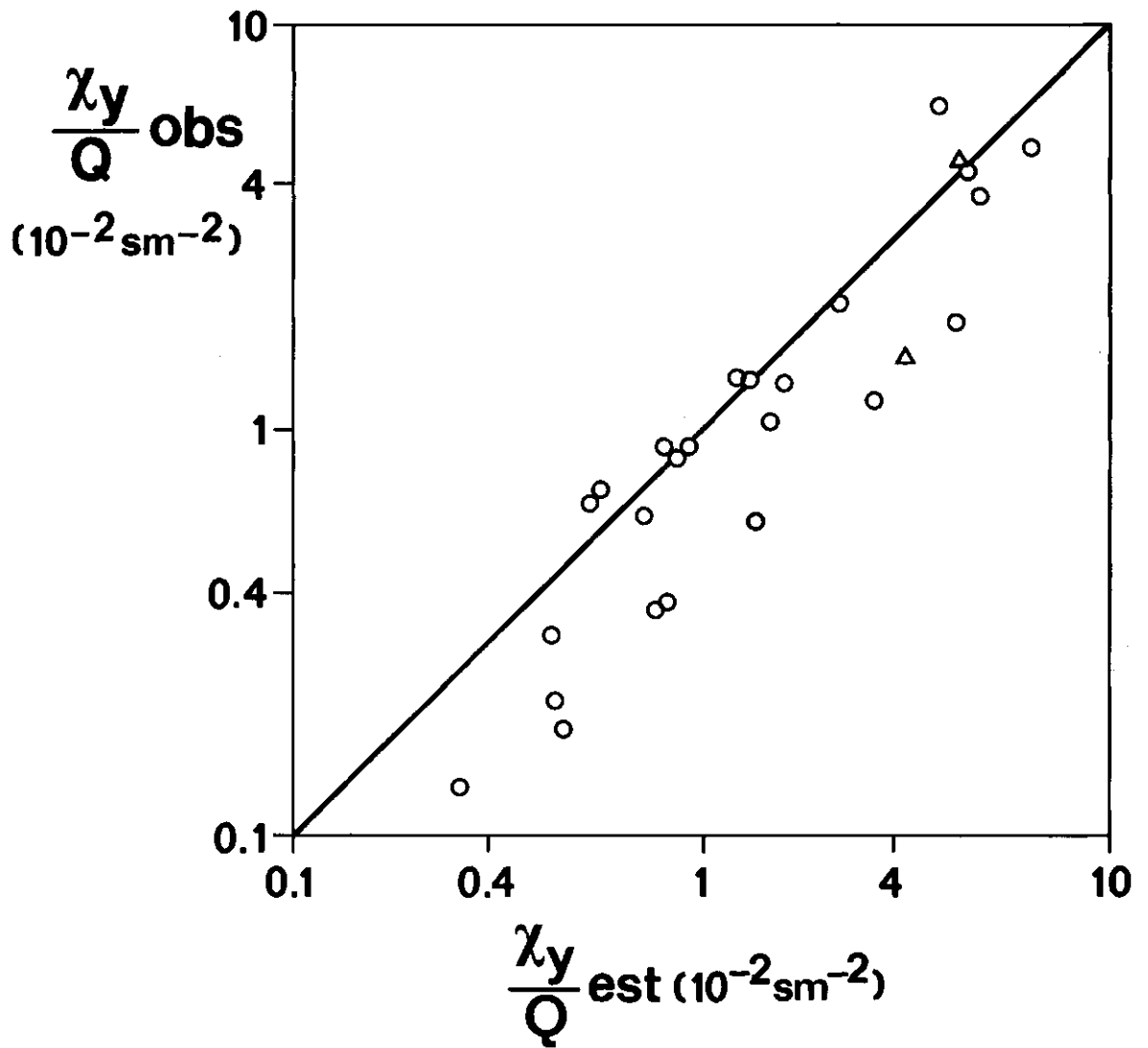(triangles upside down).

Fig. 4

Estimated versus observed crosswind-integrated concentrations for the experiments that were carried out during stable conditions. The symbols refer to the surface layer (circles); and to the local scaling layer (triangles).

of σ_w were used as input to the Gaussian model, the mean fractional error between measured and predicted crosswind-integrated concentrations is 6%, and the standard deviation of the fractional error is 34%. When the input to the Gaussian model was based on the recommendations in Turner (1970), which constitutes a kind of industry standard for dispersion calculations, the comparison with the Copenhagen data resulted in a mean fractional error of -4% and a standard deviation of 48%. Thus the method proposed by us compares better with the Copenhagen data than both of the methods based on the Gaussian model, that were tested above.

Gryning and Lyck (1984) report a comparison between measured and predicted crosswind integrated concentrations from the Copenhagen experiments. Several methods to derive the spread parameters in the Gaussian model were tested. These include methods based on a stability classification of the atmosphere stability and methods based on measured wind variances. The method proposed in this paper is better than any of the methods that were tested by Gryning and Lyck (1984) with regard to the mean as well as the standard deviation of the fractional error.

For atmospheric stable conditions, the method of this paper works well on most of the experiments. However, in experiments 11 and 13, the predicted crosswind-integrated concentrations are a factor of two larger than the measured ones. This illustrates the difficulties that are encountered when dealing with dispersion in stable flows. In the comparison we omitted the data from the 100 m arc in the Hanford diffusion grid because the influence of the sagebrush on this distance is expected to be described poorly with a displacement length.

Table 2 gives observed and predicted values of the lateral spread, σ_y, based on data from the Copenhagen experiments. The mean fractional error is -4% and the standard deviation of the fractional error is 16%. Fig. 5 illustrates the comparison. The ability of the method to predict σ_y under stable conditions was not tested because information on σ_y is not contained in this data set.
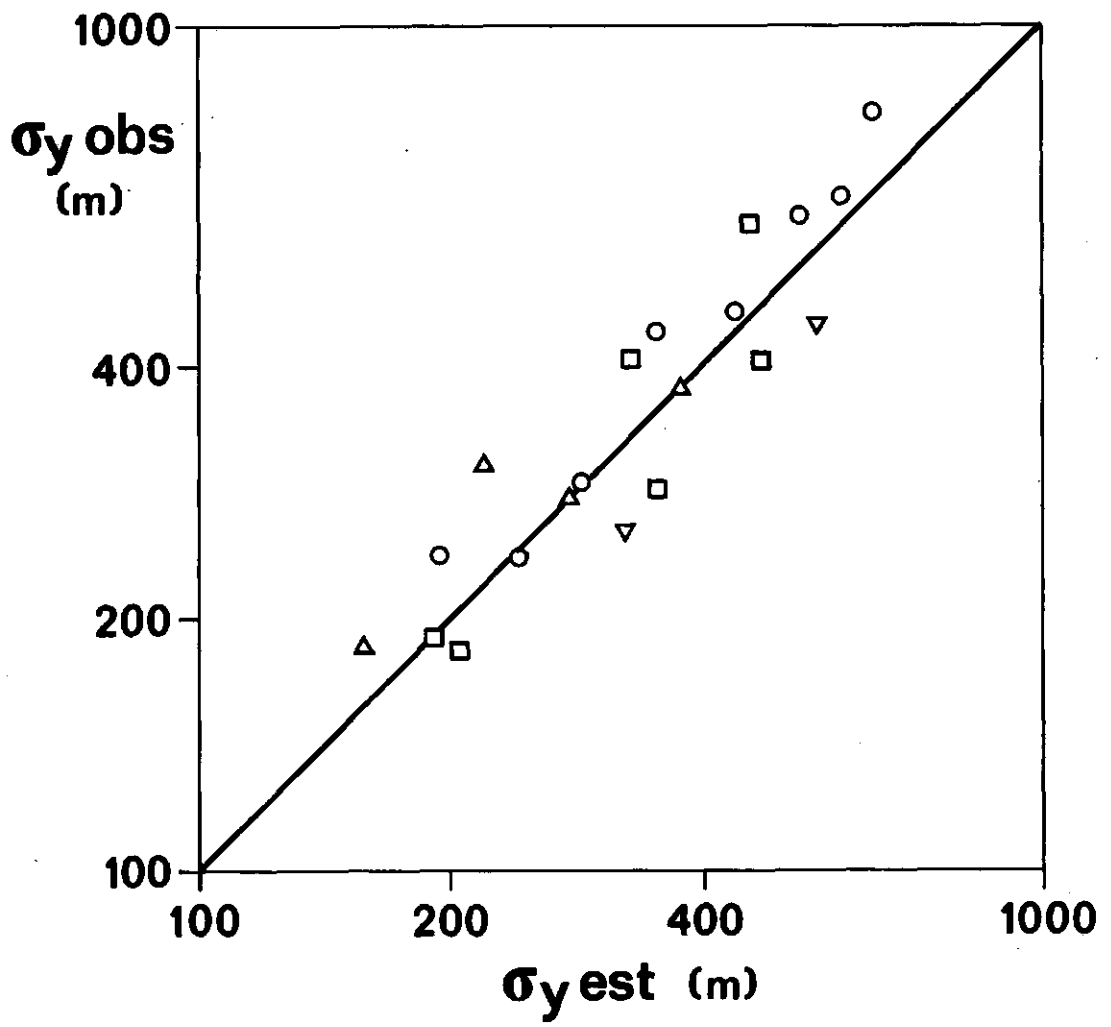
Fig. 5

Estimated versus observed values of σ_y for the experiments that were carried out during unstable conditions. The symbols refer to the surface layer (circles); the near-neutral upper layer (triangles); the mixed layer (squares) and the free convection layer (triangles upside down).

6. Discussion

In this chapter we have reviewed the scaling arguments for the dispersion of non-buoyant, non-depositing plumes in the turbulent boundary layer. Based on these arguments we related the dispersion of plumes to the turbulent state of the boundary layer. We described the dispersion process in the various scaling regimes of the boundary layer in terms of the dimensionless quantities h/L and z_s/h. The method is limited to horizontally homogeneous conditions and travel distances less than 10 km.

In general the vertical dispersion was found to be other than Gaussian. Therefore, we recommend the use of techniques that directly characterize the crosswind integrated concentration at the surface χ_y, whenever possible. For the lateral dispersion a Gaussian distribution is assumed, and the input parameters are suggested. Knowing χ_y, the ground level concentrations can be calculated.

We have compared the suggested models for χ_y with independent data from Copenhagen (Gryning and Lyck, 1984), the Hanford diffusion grid (Doran and Horst, 1985), and Norway (Sivertsen and Bøhler, 1985). It was shown that the overall agreement between estimates and measurements was very good. Under unstable atmospheric conditions the agreement was better than that obtained with the Gaussian plume model. Under these conditions the mean fractional error between measured and predicted crosswind-integrated concentrations was -2%. The standard deviation of the fractional errors, which describes the ability of the method to predict the variation in the measured χ_y-values, was 21%.

For convective conditions a quantitatively better agreement with the data is obtained when the curve of Eq. (9) is shifted towards higher values of non-dimensionalized distance X. As can be seen from Fig. 2 such a procedure gives a better agreement with the free convection prediction for surface sources as well (see Eq.(10)).

The evaluation of the models of this paper was performed with data from tracer experiments, where measurements of the meteorological input parameters were available. Irwin et al. (1985) discuss in-

strument requirements for this purpose. The derivation of the meteo-
rological parameters that are needed for air pollution models from
routine measurements, is reviewed by Van Ulden and Holtslag (1985)
and Irwin et al. (1985). Wilczak and Phillips (1984) show that the
meteorological parameters can be estimated with an accuracy of 10 to
30% during daytime.

We have not suggested dispersion models for the entrainment and
the intermittency layers because the dispersion in these layers is
poorly understood and has not been well investigated. Neither have we
suggested models to treat the effect of plume buoyancy, whose effect
is known to be pronounced. However, the field of plume rise is pre-
sently undergoing rapid development (e.g. Briggs, 1985) and is under
re-evaluation. Therefore, we have found it reasonable not to suggest
any applied model for treating the buoyancy effect, because such
models inevitably will turn out to be premature. A special complica-
tion in the use of the suggested methods arises at the border between
the regimes because crossing of the border results in a jump in the
calculated concentration.

Improvements in the models proposed here may be introduced by
continuous description of the vertical dispersion between the various
scaling regions of the boundary layer. Moreover, methods to estimate
the effect of buoyancy in the various scaling regimes may be included
when available.

Acknowledgements

for drawing our attention to the reference Köhler (1933). We want to thank the U.S. Environmental Protection Agency, the Royal Netherlands Meteorological Institute, the Norwegian Institute for Air Research and the Risø National Laboratory for making these meetings possible. We would also like to acknowledge our colleagues for useful discussions and suggestions.

Appendix
A practical surface layer dispersion model

In section 3.1 we introduced Eq. (3) for the calculation of χ_y/Q from the mean height of the plume $\bar{z}$, the shape parameter s, the mean transport velocity of the plume $\bar{U}$ and the functions A and B. Here we will summarize equations for the calculation of these quantities.

The mean height of the plume $\bar{z}$ depends on travel distance x, roughness length z_0 and Obukhov length L. Their relation can be approximated by (Van Ulden, 1978)

$$x+x_0 = (\bar{z}/k^2)[\ln(c\bar{z}/z_0) - \psi(c\bar{z}/L)][1-p\,a_1\,\bar{z}/(4L)]^{-\frac{1}{2}} \quad \text{for } L<0$$

$$\tag{A1a}$$

$$x+x_0 = (\bar{z}/k^2)[\{\ln(c\bar{z}/z_0)+2b_2 p\bar{z}/(3L)\}$$

$$. \{1+b_1 p\bar{z}/(2L)\}+(b_1/4-b_2/6)p\bar{z}/L] \qquad \text{for } L>0,$$

$$\tag{A1b}$$

where k is the von Kármán constant and x_0 is an integration constant that accounts for the height of the source (see below). The coefficients p and c in (A1) depend on s. For practical applications we propose p = 1.55 and c = 0.6. The remaining constants and the ψ-functions are related to the actual choice of the ϕ_m- and ϕ_h-functions, see Table A1. Gryning et al. (1983) and Holtslag (1984b) used the ϕ_m- and ϕ_h-functions suggested by Dyer (1974) with $a_1 = a_2 = 16$, $b_1 = b_2 = 5$ and $k = 0.41$.

Table A1

General expressions of the ϕ_h and ϕ_m functions that define the coefficients a_1, a_2, b_1 and b_2. The corresponding ψ-functions are given. The ψ-function for unstable conditions is an approximation suggested by Jensen et al. (1984).

For L < 0	For L > 0
$\phi_h(z/L) = (1 - a_1 z/L)^{-\frac{1}{2}}$	$\phi_h(z/L) = 1 + b_1 z/L$
$\phi_m(z/L) = (1 - a_2 z/L)^{-\frac{1}{4}}$	$\phi_m(z/L) = 1 + b_2 z/L$
$\psi(z/L) = \phi_m^{-1} - 1$	$\psi(z/L) = b_2 z/L$

The shape parameter s can be approximated by (Gryning et al., 1983)

$$s = \frac{1-a_1 c\bar{z}/(2L)}{1-a_1 c\bar{z}/L} + \frac{(1-a_2 c\bar{z}/L)^{-\frac{1}{4}}}{\ln(c\bar{z}/z_0)-\psi(c\bar{z}/L)} \qquad \text{for } L < 0, \qquad \text{(A2a)}$$

and

$$s = \frac{1+2b_1 c\bar{z}/L}{1+b_1 c\bar{z}/L} + \frac{1+b_2 c\bar{z}/L}{\ln(c\bar{z}/z_0)+b_2 c\bar{z}/L} \qquad \text{for } L > 0. \qquad \text{(A2b)}$$

It is seen that s is a function of $\bar{z}$, z_0 and L.

The mean transport velocity of the plume $\bar{U}$ is given by (Van Ulden, 1978)

$$\bar{U} = (u_*/k) \left\{ \ln(c\bar{z}/z_0) - \psi(c\bar{z}/L) \right\} \qquad \text{for } L < 0, \qquad \text{(A3a)}$$

$$\bar{U} = (u_*/k) \left\{ \ln(c\bar{z}/z_0) + b_2 \bar{z}/L \right\} \qquad \text{for } L > 0. \qquad \text{(A3b)}$$

158

The functions A and B are given by (Pasquill and Smith, 1983)

$$A = s \, \Gamma(2/s)/[\Gamma(1/s)]^2, \tag{A4}$$

$$B = \Gamma(2/s)/\Gamma(1/s), \tag{A5}$$

where Γ is the gamma function.

If the gamma function is not readily available on the computer, a useful approximation is

$$\Gamma(x) = 1 + \sum_{n=1}^{8} b_n (x-1)^n, \qquad 1 \leq x \leq 2, \tag{A6}$$

where

$$b_1 = -0.577191652 \qquad b_2 = 0.988205891$$
$$b_3 = -0.897056937 \qquad b_4 = 0.918206857$$
$$b_5 = -0.756704078 \qquad b_6 = 0.482199394$$
$$b_7 = -0.193527818 \qquad b_8 = 0.035868343.$$

From (A1) - (A5) and (3) the concentration profile can be determined. The input parameters for the model are z_0, L and u_*. The roughness length z_0 should be representative of the surrounding area, as discussed by Davenport (1960) and Wieringa (1980).

In practice, the computation with the above equations starts with Eq. (A1). First x_0 is computed by putting $\bar{z}$ equal to the source height z_s and x=0. For a ground level source x_0=0. Then we iteratively can determine $\bar{z}$ from (A1) for any downwind distance x. With $\bar{z}$ we solve for s and $\bar{U}$ using (A2) and (A3). Finally, A and B are calculated with (A4) and (A5). Finally (3) is evaluated for a given height z in the surface layer.

SYMBOLS AND NOTATION

The following symbols and notation are used throughout this report. Some symbols which are of local importance only, are defined when they are introduced. In general, small letters a to d with different subscripts are used for constants.

c_p	specific heat at constant pressure	$(Jkg^{-1}K^{-1})$
c_y	dimensionless crosswind-integrated concentration at ground level	(-)
D_{sa}	transfer coefficient between the surface and the air at level z_a	(-)
$D_{z,h}$	wind direction at indicated height	(degrees)
E	evaporation rate	$(kgm^{-2}s^{-1})$
$f_{y,z}$	diffusion functions of dimensionless travel time in y and z directions	(-)
g	accelaration of gravity	(ms^{-2})
G	surface soil heat flux density (subscripts H and V are used to distinguish heat conduction and water vapour movement)	(Wm^{-2})
h	mean height of the turbulent boundary layer	(m)
H	surface sensible heat flux density	(Wm^{-2})
k	Von Kármán constant	(-)
K^+	incoming solar radiation at the surface	(Wm^{-2})
L	Obukhov length scale	(m)
L^+	incoming longwave radiation from the atmosphere	(Wm^{-2})
L^-	outgoing longwave radiation at the surface	(Wm^{-2})
N	total cloud cover	(-)
P	pressure	(Nm^{-2})
q_{sat}	saturation specific humidity	(g/kg)
Q	source strength for pollutants	(kg/s)
Q^*	net radiation at the surface	(Wm^{-2})

Q_i^*	isothermal net radiation	(Wm^{-2})
r_a	aerodynamic resistance	(sm^{-1})
r_c	canopy resistance	(sm^{-1})
r	albedo of the surface	$(-)$
Ri	gradient Richardson number	$(-)$
Ri_f	flux Richardson number	$(-)$
Ri_B	Bulk Richardson number	$(-)$
s	slope of saturation specific humidity curve $(s = \partial q_{sat}/\partial T)$	(K^{-1})
s	shape parameter of surface layer dispersion model	$(-)$
t	(travel)time	(s)
T	(air)temperature	$(\text{K or } °\text{C})$
T_i	temperature at indicated heights $(i = a, o, r, s, z)$	$(°\text{C})$
T_{wi}	wet bulb temperature at indicated heights	$(°\text{C})$
$T_{y,z}$	diffusion time scale for y or z direction	(s)
u_*	friction velocity	(ms^{-1})
u_{*N}	neutral estimate of u_*	(ms^{-1})
U_z	wind speed at height z	(ms^{-1})
w_*	convective velocity scale based on h	(ms^{-1})
w_f	free convection velocity scale based on z	(ms^{-1})
$\overline{w\theta}$	kinematic heat flux	(Kms^{-1})
$\overline{w\theta}_o$	kinematic heat flux at the surface	(Kms^{-1})
x	distance in the direction of mean wind	(m)
X	dimensionless distance	$(-)$
y	lateral distance	(m)
z	height above the surface	(m)
z_o	(effective) roughness length for momentum	(m)

z_s	source height for emission of pollutants	(m)
Z_s	dimensionless source height	(-)
α	(modified) Priestley-Taylor parameter	(-)
β	coefficient in modified Priestley-Taylor formula	(-)
γ	psychrometric "constant" ($\gamma = C_p/\lambda$)	(K^{-1})
Γ_d	dry adiabatic lapse rate	(Km^{-1})
δq_i	specific saturation deficit at an indicated level (i = s,a)	(g/kg)
ε_i	apparent emissivity of the surface (i = s) or of the atmosphere (i = a, r)	(-)
θ	potential temperature	(K or °C)
θ_*	turbulent temperature scale	(K)
λ	heat of vapourization	(Jkg^{-1})
λE	surface latent heat flux density	(Wm^{-2})
Λ	local Obukhov length scale	(m)
ρ	density of the air	(kgm^{-3})
σ	Stefan-Boltzmann constant	($Wm^{-2}K^{-4}$)
$\sigma_{u,v,w}$	standard deviation of velocity fluctuations in x, y, z directions, respectively	(ms^{-1})
$\sigma_{y,z}$	diffusion parameters of the Gaussian plume model in the y and z directions, respectively	(m)
τ	local kinematic momentum flux	(m^2s^{-2})
τ_o	surface kinematic momentum flux (e.g. $\tau_o = u_*^2$)	(m^2s^{-2})
ϕ	solar elevation	(-)
$\phi_{m,h}$	dimensionless wind or temperature gradient	(-)
χ	concentration of contaminants	(kgm^{-3})
χ_y	crosswind-integrated concentration	(kgm^{-2})
$\psi_{M,H}$	stability functions for momentum and heat in the wind and temperature profiles	(-)

In the chapters we use some statistics as defined below.

x   model estimate of a quantity

y   observation of a quantity

$\bar{x}$ average value of all x-values

$\bar{y}$ average value of all y-values

n   number of (x,y) pairs

r   correlation coefficient

σ   root mean square error, defined as

$$\sigma = \left\{ \frac{1}{n} \Sigma (x-y)^2 \right\}^{\frac{1}{2}}$$

In chapter VI also use is made of the fractional error e, defined by

$$e = 2 \frac{(x-y)}{x+y} \, ,$$

for which the mean and standard deviation can be calculated.

164

REFERENCES

André, J.C., 1983, On the variability of the nocturnal boundary-layer
  depth. J. Atmos. Sci., 40, 2309-2311.
Arnfield, A.J., 1979, Evaluation of empirical expressions for the
  estimation of hourly and daily totals of atmospheric longwave
  emissions under all sky conditions. Quart. J. Roy. Met. Soc.,
  105, 1041-1052.
Baerentsen, J.H. and R. Berkowicz, 1984, Monte Carlo simulation of
  plume dispersion in the convective boundary layer. Atmospheric
  Environment, 18, 701-712.
Barad, M.L., Ed., 1958, Project Prairie grass, a field program in
  diffusion. Geophys. Res. Rap. no. 59, Vol. I and II. Geophysics
  Research Directorate, Bedford.
Beljaars, A.C.M., 1982, The derivation of fluxes from profiles in
  perturbed areas. Boundary-Layer Meteorol. 24, 35-55.
Beljaars, A.C.M., P. Schotanus and F.T.M. Nieuwstadt, 1983, Surface
  layer similarity under nonuniform fetch conditions. J.Climate
  Appl. Meteor. 22, 1800-1810.
Berkowicz, R. and L.P. Prahm, 1982a, Sensible heat flux estimated
  from routine meteorological data by the resistance method.
  J. Appl. Meteor., 21, 1845-1864.
Berkowicz, R. and L.P. Prahm, 1982b, Evaluation of the profile method
  for estimation of surface fluxes of momentum and heat.
  Atmospheric Environment 16, 2809-2819.
Briggs, G.A., 1983, Diffusion modeling with convective scaling and
  effects of surface inhomogeneities. AMS Speciality Conference on
  Air Quality Modeling of the Urban Boundary Layer, 29 November -
  2 December 1983, Baltimore, U.S.A.
Briggs, G.A., 1985, Analytical Parameterizations of Diffusion: The
  convective boundary layer. J. Climate Appl. Meteor., 24,
  1167-1186.
Brost, R.A., J.C. Wyngaard and D. Lenschow, 1982, Marine strato-
  cumulus layers. Part II: Turbulence budgets. J. Atmos. Sci., 39,
  818-836.
Brutsaert, W.H., 1982, Evaporation into the atmosphere. D. Reidel
  Publising Company, Dordrecht, Holland.
Burridge, D.M. and A.J. Gadd, 1977, The Meteorological Office
  Operational 10-level Numerical Weather Prediction Model.
  Scientific Paper 34, Meteor. Office London, 39 pp.
Busch, N.E., 1973, On the mechanics of atmospheric turbulence, in:
  Workshop on Micrometeorology, D.A. Haugen, ed., Amer. Meteor.
  Soc., Boston, 1-65.
Businger, J.A., 1973, Turbulent transfer in the atmospheric surface
  layer. Workshop on Micro-meteorology, Am. Meteorol. Soc., Boston,
  Mass., 67-100.
Cats, G.J., 1980, Analysis of surface wind and its gradient in a
  mesoscale wind observations network. Monthly Weather Rev., 108,
  1100-1107.
Carson, D.J. and P.J.R. Richards, 1978, Modelling surface turbulent
  fluxes in stable conditions. Boundary-Layer Meteorol. 14, 67-81.
Carl, D.M., T.C. Tarbell and H.A. Panofsky, 1973, Profiles of Wind
  and Temperature from towers over homogeneous terrain. J. Atmos.
  Sci., 30, 788-794.

Caughey, S.J., J.C. Wyngaard and J.C. Kaimal, 1979, Turbulence in the evolving stable boundary layer. J. Atmos. Sci., 6, 1041-1052.

Caughey, S.J., 1982, Observed characteristics of the atmospheric boundary layer, in: Atmospheric Turbulence and Air Pollution Modeling, F.T.M. Nieuwstadt and H. van Dop, (eds.), D. Reidel Publishing Company, Dordrecht, 107-158.

Collier, L.R. and J.G. Lockwood, 1974, The estimation of solar radiation under cloudless skies with atmospheric dust. Quart. J. Roy. Met. Soc., 101, 390-392.

Crease, B.A., S.J. Caughey and D.T. Tribble, 1977, Information on the thermal structure of the atmospheric boundary layer from acoustic sounding. Met. Mag., 106, 42-52.

Davenport, A.G., 1960, Rationale for determining design wind velocities, J. Struct. Div. Am. Soc. Civ. Eng., 86, 39-68.

Davies, J.A. and T.C. Uboegbulam, 1979, Parameterizations of surface incoming radiation in tropical cloudy conditions. Atmosphere-Ocean, 17, 14-23.

Deardorff, J.W., 1970, Convective velocity and temperature scales for the unstable planetary boundary layer and for Rayleigh convection. J. Atmos. Sci., 27, 1211-1213.

Deardorff, J.W., 1974, Three-dimensional numerical study of the height and mean structure of a heated planetary boundary-layer. Boundary-Layer Meteorol., 7, 81-106.

Deardorff, J.W. and G.E. Willis, 1975, A parameterization of diffusion in the mixed layer. J. Appl. Meteor., 17, 825-831.

Deardorff, J.W., G.E. Willis and B.H. Stockton, 1980, Laboratory studies of the entrainment zone of a convectively mixed layer. J. Fluid Mech., 100, 41-46.

De Baas, A.F. and A.G.M. Driedonks, 1985, Internal gravity waves in a stably stratified boundary layer, Boundary-Layer Meteorol. 31, 303-323.

De Baas, A.F., H. van Dop and F.T.M. Nieuwstadt, 1986, An application of the Langevin equation for inhomogeneous conditions to dispersion in a convective boundary layer. Quart. J. Roy. Met. Soc., 112, 165-180.

De Bruin, H.A.R., 1982, The energy balance of the earth's surface: a practical approach. Scientific Report 82-1, Royal Netherlands Meteorological Institute, De Bilt.

De Bruin, H.A.R. and A.A.M. Holtslag, 1982, A simple parameterization of the surface fluxes of sensible and latent heat during daytime compared with the Penman-Monteith concept. J. Appl. Meteor., 21, 1610-1621.

De Bruin, H.A.R., 1983, A model for the Priestley-Taylor parameter α. J. Clim. Appl. Meteor., 22, 572-578.

Deheer-Amissah, A., U. Högström and A.S. Smedman-Högström, 1981, Calculation of sensible and latent heat fluxes and surface resistance from profile data. Boundary Layer Meteorol. 20, 35-49.

Doran, J.C. and T.W. Horst, 1985, An evaluation of Gaussian plume-depletion models with dual-tracer field measurements. Atmospheric Environment, 19, 939-951.

Draxler, R.R., 1976, Determination of atmospheric diffusion parameters. Atmospheric Environment, 10, 99-105.

Driedonks, A.G.M., 1981, Dynamics of the well-mixed atmospheric boundary layer. Scientific Report 81-2, Royal Netherlands Meteorological Institute, De Bilt.

Driedonks, A.G.M., H. van Dop and W.H. Kohsiek, 1978, Meteorological observations of the 213 m mast at Cabauw in The Netherlands. Proceedings of the fourth Symposium on Meteorological Observations and Instrumentation, Amer. Meteor. Soc., Boston, Mass., 41-46.

Driedonks, A.G.M. and H. Tennekes, 1984, Entrainment effects in the well-mixed atmospheric boundary layer. Boundary-Layer Meteorol., 30, 75-105.

Driedonks, A.G.M., J. Reiff and A.A.M. Holtslag, 1985, Mesoscale results of an air mass transformation model. Contributions to Atmospheric Physics, 58, 361-379.

Dyer, A.J., 1974, A review of flux-profile relationships, Boundary-Layer Meteorol. 7, 363-372.

Elliott, W.P., 1961, The vertical diffusion of gas from a continuous source. Int. J. Air Water Pollut., 4, 33-46.

Estournel, C. and D. Guedalia, 1985, Influence of geostrophic wind on atmospheric nocturnal cooling. J. Atmos. Sci., 42, 2695-2698.

Fiedler, F. and H.A. Panofsky, 1972, The geostrophic drag coefficient and the effective roughness length. Quart. J. Roy. Met. Soc., 98, 213-220.

Garratt, J. R. and B.B. Hicks, 1973, Momentum, heat and water vapour transfer to and from natural and artificial surfaces. Quart. J. Roy. Met. Soc., 99, 680-687.

Gay, L.W., 1971, The regression of net radiation upon solar radiation. Arch. Met. Geoph. Biokl., Ser. B, 19, 1-14.

Gill, G.C., L.E. Olson, J. Sela and M. Suda, 1967, Accuracy of wind measurements on towers or stacks. Bull. Am. Meteor. Soc.,48, 665-674.

Golder, D., 1972, Relations among stability parameters in the surface layer. Boundary-Layer Meteorol. 3, 47-58.

Groen, P., 1947, Note on the theory of nocturnal radiational cooling of the earth's surface. J. Meteorol., 4, 63-66.

Gryning, S.E., 1981, Elevated source SF_6-tracer dispersion experiments in the Copenhagen area. Risø National Laboratory, Report No. R-446, Roskilde, Denmark.

Gryning, S.E., E. Lyck and K. Hedegaard, 1978, Short-range diffusion experiments in unstable conditions over inhomogeneous terrain. Tellus, 30, 392-403.

Gryning, S.E., A.P. van Ulden and S. Larsen, 1983, Dispersion from a continuous ground-lever source investigated by a K model. Quart. J. Roy. Met. Soc., 109, 355-364.

Gryning, S.E. and E. Lyck, 1984, Atmospheric dispersion from elevated sources in an urban area: Comparison between tracer experiments and model calculations. J. Clim. Appl. Meteor., 23, 651-660.

Gryning, S.E., A.A.M. Holtslag, J.S. Irwin and B. Sivertsen, 1987, Applied dispersion modelling based on meteorological scaling parameters. Atmospheric Environment, 21, 79-89 (see Chapter VI).

Hanna, S., G.A. Briggs, J. Deardorff, B.A. Egan, F.A. Gifford and F. Pasquill, 1977, AMS workshop on stability classification schemes and sigma curves - summary of recommendations. Bull. Am. Met. Soc., 58, 1305-1309.

Hanna, S., G.A. Briggs and R.P. Hosker, 1982, Handbook on atmospheric diffusion. U.S.A. Depart. of Energy TIC-11223, 102 pp.

Hicks, B.B., 1976, Wind profile relationships from the "Wangara" experiment. Quart. J. Roy. Met. Soc., 102, 535-551.

Hicks, B.B., 1981, An examination of turbulence statistics in the
    surface boundary layer. Boundary Layer Meteor., 21, 389-402
Hicks, B.B., 1983, A study of dewfall in an acid region: an analysis
    of Wangara data. Quart. J. R. Met. Soc., 109, 900-904.
Holtslag, A.A.M., 1984a, Estimates of diabatic wind speed profiles
    from near surface weather observations. Boundary-Layer Meteorol.,
    29, 225-250 (see Chapter V).
Holtslag, A.A.M., 1984b, Estimates of vertical diffusion from sources
    near the ground in strongly unstable conditions, in: Air
    Pollution Modeling and its Application III, C. de Wispelaere,
    ed., Plenum Press, New York, 619-630.
Holtslag, A.A.M. and A.P. van Ulden, 1982, Simple estimates of
    nighttime surface fluxes from routine weather data. Scientific
    Report 82-4, Royal Netherlands Meteorological Institute, De Bilt.
Holtslag, A.A.M. and A.P. van Ulden, 1983, A simple scheme for
    daytime estimates of the surface fluxes from routine weather
    data. J. Climate Appl. Meteor., 22, 517-529 (see Chapter III).
Holtslag, A.A.M, S.E. Gryning, J.S. Irwin and B. Sivertsen, 1986,
    Parameterization of the Atmospheric Boundary Layer for air
    pollution dispersion models, in: Air Pollution Modeling and its
    Application V, C. de Wispelaere, ed., Plenum Press, New York,
    147-175.
Holtslag, A.A.M. and F.T.M. Nieuwstadt, 1986, Scaling the atmospheric
    boundary layer. Boundary-Layer Meteorol., 36, 201-209. (see
    Chapter II).
Holtslag, A.A.M. and H.A.R. de Bruin, 1987, Applied modelling of the
    nighttime surface energy balance over land (Submitted to
    J. Climate Appl. Meteor., see Chapter IV).
Horst, T.W., 1979, Lagrangian similarity modelling of vertical
    diffusion from a ground-lever source. J. Appl. Meteor., 18,
    733-740.
Højstrup, J., 1982, Velocity spectra in the unstable planetary
    boundary layer. J. Atmos. Sci., 39, 2239-2248.
Irwin, J.S., 1983, Estimating plume dispersion - A comparison of
    several sigma schemes. J. Climate Appl. Meteor., 22, 92-114.
Irwin, J.S., S.E. Gryning, A.A.M. Holtslag and B. Sivertsen, 1985,
    Atmospheric dispersion modeling based on boundary layer
    parameterization. EPA report 600/3-85/056. U.S. Environmental
    Protection Agency.
Jensen, N.O., E.L. Petersen and I. Troen, 1984, Extrapolation of mean
    wind statistics with special regard to wind energy applications.
    W.M.O. World Climate Programme Report No. WCP-86.
Kaimal, J.C., J.W. Wyngaard, D.A. Haugen, O.R. Coté, Y. Izumi, S.J.
    Caughey and C.J. Readings, 1976, Turbulence structure in the
    convective boundary layer. J. Atmos. Sci., 33, 2152-2169.
Kasten, F. and G. Czeplak, 1980, Solar and terrestrial radiation
    dependent on the amount and type of cloud. Solar Energy, 24,
    177-189.
Keijman, J.Q. and H.A.R. de Bruin, 1979, A comparison of measured and
    calculated temperatures of a grass covered surface. Eos
    transactions, 60, No. 32, 583.
Kondo, J., O. Kanechika and N. Yasuda, 1978, Heat and momentum
    transfers under strong stability in the atmospheric surface
    layer. J. Atmos. Sci., 35, 1012-1021.

Korell, A., H.A. Panofsky and R.J. Rossi, 1982, Wind profiles at the
    Boulder tower. Boundary-Layer Meteorol., 22, 295-312.
Köhler, H., 1933, Meteorologische Turbulenzuntersuchungen. Kungl.
    Svenska Vetenskapsakad. Handl. 13, No. 1, 54 pp.
Kretzschmar, J.G. and I. Mertens, 1984, Influence of the turbulence
    typing scheme upon the cumulative frequency distributions of the
    calculated relative concentrations for different averaging times.
    Atmospheric Environment, 18, 2377-2393.
Large, W.G. and S. Pond, 1982, Sensible and latent heat flux
    measurements over the ocean. J. Physical Oceanography, 12,
    464-482.
Lind, R.J. and K.B. Katsaros, 1982, A model of Longwave irradiance
    for use with surface observations. J. Appl. Meteor., 21,
    1015-1023.
Lumb, F.E., 1964, The influence of cloud on hourly amounts of total
    solar radiation at the sea surface. Quart. J. Roy. Met. Soc., 90,
    43-56.
Lumley, J.L. and H.A. Panofsky, 1964, The structure of atmospheric
    turbulence. Interscience, London, 239 pp.
McBean, G.A. (ed.), 1979, The planetary boundary layer, Technical
    note no. 165, WMO Geneva, 201 p.
McNaughton, K.G. and T.W. Spriggs, 1986, A mixed-layer model for
    regional evaporation. Boundary-Layer Meteorol., 34, 243-262.
Moeng, C.H, 1984, A large eddy simulation for the study of planetary
    boundary-layer turbulence. J. Atmos. Sci., 41, 2052-2062.
Monteith, J.L., 1963, Dew: Facts and Fallacies, in The water
    relations of plants, A.J. Rulter and F.H. Whitehead, eds.,
    Blackwell, London, 37-56.
Monteith, J.L., 1981, Evaporation and surface temperature. Quart. J.
    Roy. Met. Soc., 107, 1-27.
Monteith, J.L. and G. Szeicz, 1961, The radiation balance of bare
    soil and vegetation. Quart. J. Roy. Met. Soc., 87, 159-170.
Monin, A.S. and A.M. Yaglom, 1971, Statistical Fluid Mechanics:
    mechanics of turbulence. Vol. I, MIT Press, London.
Nichols, S. and C.J. Readings, 1979, Aircraft observations of the
    structure of the lower boundary layer over the sea. Quart. J. R.
    Met. Soc., 105, 785-802.
Nickerson, E.C. and V.E. Smiley, 1975, Surface layer and energy
    budget parameterizations for mesoscale models. J. Appl. Meteorol.
    14, 297-300.
Nielsen, L.B., L.P. Prahm, R. Berkowicz and K. Conradsen, 1981, Net
    incoming radiation estimated from hourly global radiation and/or
    cloud observations. J. Clim., 1, 255-272.
Nieuwstadt, F.T.M., 1978, The computation of the friction velocity u_*
    and the temperature scale T_* from temperature and wind velocity
    profiles by least-square methods. Boundary-Layer Meteorol., 14,
    235-246.
Nieuwstadt, F.T.M., 1980, Application of mixed-layer similarity to
    the observed dispersion from a ground-level source. J. Appl.
    Meteorol., 19, 157-162.
Nieuwstadt, F.T.M, 1981, The nocturnal boundary layer: Theory and
    Experiments. Scientific Report 81-1, Royal Netherlands
    Meteorological Institute, De Bilt.
Nieuwstadt, F.T.M., 1984a, The turbulent structure of the stable,
    nocturnal boundary layer. J. Atm. Sci., 41, 2202-2216.

Nieuwstadt, F.T.M., 1984b, Some aspects of the turbulent stable boundary layer. Boundary-Layer Meteorol., 30, 31-55.

Nieuwstadt, F.T.M. and A.P. van Ulden, 1978, A numerical study on the vertical dispersion of passive contaminants from a continuous source in the atmospheric surface layer. Atmospheric Environment, 12, 2119-2124.

Nieuwstadt, F.T.M. and H. van Duuren, 1979, Dispersion experiments with SF_6 from the 213 m high meteorological mast at Cabauw in The Netherlands. Proceedings of the fourth Symposium on Turbulence, Diffusion and Air Pollution, Reno, Nevada, January 15-18, 1979, Amer. Meteor. Soc., 34-40.

Obukhov, A.M., 1946, Turbulence in an atmosphere with a non-uniform temperature. Tr. Akad. Nauk. SSSR Inst. Teorel. Geofis., No. 1 (translation in Bound. Layer Meteor., 2, 1971, 7-29).

Ogawa, Y., P.G. Diosey, K. Uehara and H. Ueda, 1985, Wind tunnel observation of flow and diffusion under stable stratification. Atmospheric Environment, 19, 65-74.

Oke, T.R., 1978, Boundary Layer Climates. Methuen, London, 372. pp.

Olesen, H.R., Larsen. S.E. and Højstrup, J., 1984, Modeling velocity spectra in the lower part of the planetary boundary layer. Boundary-Layer Meteorol, 29, 285-312.

Paltridge, G.W. and C.M.R. Platt, 1976, Radiative processes in meteorology and climatology. Development in Atm. Science, 5, Elsevier, Amsterdam, 318 pp.

Panofsky, H.A., 1978, Matching in the convective planetary boundary layer. J. Atmos. Sci., 35, 272-276.

Panofsky, P.A, H. Tennekes, D.H. Lenshow and J.C. Wyngaard, 1977, The characteristics of turbulent velocity components in the surface layer under convective conditions. Boundary-Layer Meteorol., 11, 355-361.

Pasquill, F. and F.B. Smith, 1983, Atmospheric Diffusion, 3rd edition, Wiley, London, 437 pp.

Paulson, C.A., 1970, The mathematical representation of wind speed and temperature profiles in the unstable atmospheric surface layer. J. Appl. Meteor., 9, 856-861.

Petersen, E.L. and I. Troen, 1986, The European wind atlas. Proceed. European Wind Energy Conference, Rome, October 7-9, 1986.

Poreh, M and J.E. Cermak, 1984, Wind tunnel simulation of diffusion in a convective boundary layer, Boundary-Layer Met., 30, 431-455.

Priestley, C.H. B. and R.J. Taylor, 1972, On the assessment of surface heat flux and evaporation using large scale parameters, Mon. Wea. Rev., 100, 81-92.

Reiff, J., D. Blaauboer, H.A.R. de Bruin, A.P. van Ulden and G. Cats, 1984, An air-mass transformation model for short range weather forecasting. Mon. Wea. Rev., 112, 393-412.

Rijkoort, P.J., 1968, The increase of mean wind speed with height in the surface friction layer, Ph.D. thesis University of Utrecht, 116 pp.

Rijkoort, P.J., 1983, A compound Weibull model for the description of surface wind velocity distribution, Scientific Report WR 83-13, Royal Netherlands Meteorological Institute, De Bilt, 35 pp.

Sedefian, L., 1980, On the vertical extrapolation of mean wind power density. J. Appl. Meteor., 19, 488-493.

Sellers, W.D., 1965, Physical Climatology, University of Chicago press, Chicago, 272 pp.

SethuRaman, S. and R.M. Brown, 1976, Validity of the log-linear profile relationship over a rough terrain during stable conditions, Boundary-Layer Meteorol., 10, 489-501.

Sivertsen, B., 1978, Dispersion parameters determined from measurements of wind fluctuations (σ_θ), temperature and wind profiles. Proceedings of the 9th International Technical Meeting on Air Pollution Modeling and its Application, Toronto, 251-261.

Sivertsen, B. and T. Bøhler, 1985, Verification of dispersion estimates using tracer data. NILU Report TR 19/85. The Norwegian Institute for Air Research, Lillestrøm, Norway.

Sivertsen, B., S.E. Gryning, A.A.M. Holtslag and J. Irwin, 1986, Atmospheric dispersion modeling based upon boundary layer parameterization, in: Air pollution Modeling and its Application V, C. de Wispelaere, ed., Plenum Press, New York, 177-194.

Slatyer, R.O. and I.C. McIlroy, 1961, Practical Microclimatology, CSIRO, Melbourne, 310 pp.

Smith, F.B. and R.M. Blackall, 1979, The application of field experiment data to the parameterization of the dispersion of plumes from ground level and elevated sources, in: Mathematical Modelling of Turbulent Diffusion in the Environment. J. Harris, ed., London, Academic Press, 500 pp.

Swinbank, W.C., 1963, Longwave radiation from clear skies. Quart. J. Roy. Met. Soc., 89, 339-348.

Swinbank, W.C., 1964, Discussion on the 1963 article. Quart. J. Roy. Met. Soc., 90, 488-493.

Taylor, G.I., 1921, Diffusion by continuous movements. Proc. London Math. Soc., 20, 196-202.

Ten Berge, H.F.M., 1986, Heat and water transfer at the bare soil surface: Aspects affecting thermal imagery. Ph.D. thesis Agricultural University of Wageningen, The Netherlands.

Tennekes, H., 1970, Free convection in the turbulent Ekman layer of the atmosphere. J. Atmos. Sci., 27, 1027-1034.

Tennekes, H., 1982, Similarity relations, scaling laws and spectral dynamics, in: Atmospheric Turbulence and Air Pollution Modeling. F.T.M. Nieuwstadt and H. van Dop, (eds.), Reidel, Dordrecht, 37-68.

Thom, A.S. and H.R. Oliver, 1977, On Penman's equation for estimating regional evaporation. Quart. J. Roy. Met. Soc., 103, 345-357.

Turner, D.B., 1970, Workbook on atmospheric dispersion estimates. HPS Pub. 999-Ap-26, 88 pp.

Turner, J.S., 1973, Buoyancy effects in fluids, Cambridge University press, Cambridge, 368 pp.

Van Dop, H. , B.J. de Haan, G.J. Cats, 1980, Meteorological input for a three dimensional medium range air quality model. Proceed. of the 5th International Clean Air Congress, Rio de Janeiro, 481-484.

Van Dop, H., B.J. de Haan and C.A. Engeldal, 1982, The KNMI mesoscale air pollution transport model. Scientific Report WR 82-6, KNMI, De Bilt, 76 pp.

Van Dop, H., F.T.M. Nieuwstadt and J.C.R. Hunt, 1985, Random walk models for particle displacements in inhomogeneous unsteady turbulent flows, Physics of Fluids, 28, 1639-1653.

Van Ulden, A.P., 1978, Simple estimates for vertical diffusion from sources near the ground, Atmospheric Environment, 12, 2125-2129.

Van Ulden, A.P. and A.A.M. Holtslag, 1980, The wind at heights
between 10 and 200 m in comparison with the geostrophic wind,
Proceed. Seminar on Radioactive releases, Risø, 22-25 april 1980,
Commission E.C., Luxembourg, Vol. I, 83-92.

Van Ulden, A.P. and A.A.M. Holtslag, 1983, The stability of the
atmospheric surface layer during nighttime, Sixth Symp. on
Turbulence and Diffusion, March 22-25, 1983, 257-260. Amer.
Meteor. Soc., Boston, Mass.

Van Ulden, A.P. and A.A.M. Holtslag, 1985, Estimation of atmospheric
boundary layer parameters for diffusion applications. J. Climate
Appl. Meteor., 24, 1196-1207.

Van Wijk, W.R. and W.J. Derksen, 1963, Sinusoidal temperature
variation in a layered soil, in: Physics of plant environment,
W.R. van Wijk, ed., North-Holland Publ. Comp., Amsterdam.

Van Wijk, A.J.M., A.A.M. Holtslag and W.C. Turkenburg, 1985, Wind
profile stability corrections: Their influence on wind energy
assessment studies. Proceed. European Wind Energy Conference,
Hamburg, 22-26 October 1984. Stephens, Bedford, 96-101.

Venkatram, A., 1980, Estimating the Monin-Obukhov length in the
stable boundary layer for dispersion calculations. Boundary-Layer
Meteorol., 19, 481-485.

Venkatram, A., D. Strimaitis and D. Discristofaro, 1984, A semi-
empirical model to estimate vertical dispersion of elevated
releases in the stable boundary layer, Atmospheric Environment,
18, 923-928.

Webb, E.K., 1970, Profile relationships: The logt-linear range and
extension to strong stability. Quart. J. Roy. Meteor. Soc., 96,
67-90.

Weil, J.C., 1983, Application of advances in planetary boundary layer
understanding to diffusion modeling. Proceedings from the sixth
symposium on turbulence, diffusion and air pollution,
March 22-25, 1983, Boston, Am. Met. Soc., 42-46.

Wessels, H.R.A., 1983, Distortion of the wind field by the Cabauw
meteorological tower. Scientific Report 83-15, Royal Netherlands
Meteorological Institute, De Bilt.

Wessels, H.R.A., 1984, Cabauw meteorological data tapes 1973-1984;
description of instrumentation and data processing for the
continuous measurements. Scientific Report 84-6, Royal
Netherlands Meteorological Institute, De Bilt.

Wieringa, J., 1976, An objective exposure correction method for
average wind speeds measured at a sheltered location. Quart. J.
Roy. Met. Soc., 102, 241-253.

Wieringa, J., 1980, Representativeness of wind observations at
airports. Bull. Amer. Meteor. Soc., 61, 962-971.

Wieringa, J., 1981, Estimation of mesoscale and local-scale roughness
for atmospheric transport modeling. Air Pollution Modeling and
its Application, Plenum, New York, 297-295.

Wieringa, J., 1983, Description requirements for assessment of non-
ideal wind stations - for example Aachen. J. Wind. Eng. Industr.
Aerod., 11, 121-131.

Wieringa, J., 1986, Roughness-dependent geographical interpolation of
surface wind speed averages. Quart. J. R. Met. Soc., 112,
867-889.

Wilczak, J.M. and M.S. Phillips, 1984, An indirect estimation of convective boundary layer structure for use in routine dispersion models. Proceed. of fourth Joint Conference on Application of Air Pollution Meteorology, 16-19 October 1984, Portland, Oregon. Amer. Meteor. Soc., Boston, Mass.

Willis, G.E. and J.W. Deardorff, 1978, A laboratory study of dispersion from an elevated source within a modeled convective planetary boundary layer. Atmospheric Environment, 12, 1305-1311.

Wyngaard, J.C., 1973, On surface layer turbulence, Workshop on Micrometeorology, D.A. Haugen (ed.), Amer. Meteor. Soc., Boston, Mass., 101-149.

Yaglom, A.M., 1977, Comments on wind and temperature flux-profile relationships. Boundary-Layer Meteorol., 11, 89-102.

Zilitinkevich, S.S., 1972, On the determination of the height of the Ekman boundary layer. Boundary-Layer Met., 3, 141-145.

CURRICULUM VITAE

Bert Holtslag werd op 18 juni 1953 geboren te Laren (nu gemeente Lochem). Hij volgde technische beroepsopleidingen, voordat hij in 1972 begon met de studie Fysische Techniek aan de Hogere Technische School te Enschede. Binnen deze studie ontwikkelde hij zijn belangstelling voor fysische transportverschijnselen.

In het stagejaar van de HTS (1974-1975) was hij verbonden aan twee vakgroepen van de Universiteit te Groningen. Hier hield hij zich bezig met praktisch gericht milieuonderzoek. Het afstudeeronderwerp van de HTS-opleiding werd besteed aan het ontwerpen van een meetregeltechnische opstelling voor onderwijsdoeleinden (1976). Na de HTS deed hij in 1977 het staatsexamen VWO (Atheneum).

Van 1 oktober 1977 tot 1 mei 1979 vervulde hij vervangende militaire dienst bij het KNMI te De Bilt. Sinds 1 mei 1979 is hij in dienst van het KNMI, waar hij tot 1 december 1985 was aangesteld als assistent-onderzoeker bij de werkgroep Luchtverontreiniging van de afdeling Fysische Meteorologie. Zijn wetenschappelijke vorming werd gestimuleerd door het volgen van cursussen, colleges en het bezoeken van conferenties.

In 1984 was hij verbonden aan de cursus Milieuhygiëne van de Stichting Post Hoger Technisch Onderwijs te Amsterdam, waar hij doceerde in Meteorologie en Luchtverontreiniging. In de zomer van 1985 werkte hij bij het Deense onderzoeksinstituut "Risø".

Vanaf 1 december 1985 is hij werkzaam als wetenschappelijk medewerker bij de afdeling Dynamische Meteorologie van het KNMI. In deze afdeling is hij belast met de ontwikkeling van een "luchtmassatransformatie"-model, voor de korte termijn weersverwachting van bewolking in de grenslaag.